Fakultät für Medizin

Institut für Diabetes und Adipositas

Energy deprivation induces a specific secretome in skeletal muscle

Ellen Walheim

Vollständiger Abdruck der von der Fakultät für Medizin der Technischen Universität München zur Erlangung des akademischen Grades eines

Doktors der Naturwissenschaften

genehmigten Dissertation.

Vorsitzender:	Prof. Dr. Percy A. Knolle
Prüfer der Dissertation:	1. Prof. Dr. Matthias Tschöp
	2. Prof. Dr. Martin Klingenspor

Die Dissertation wurde am 11.01.2017 bei der Technischen Universität München eingereicht und durch die Fakultät für Medizin am 17.05.2017 angenommen.

Table of Contents

Abbreviations

°C	Degree Celsius
µ	Micro
ABC	Ammoniumbicarbonate
aCSF	Artificial cerebrospinal fluid
Agrp	Agouti related neuropeptide
Ahnak	AHNAK nucleoprotein (desmoyokin)
Angpt1	Angiopoietin 1
Anx	Annexin
ATP	Adenosine triphosphate
BAT	Brown adipose tissue
BDNF	Brain derived neurotrophic factor
Btf3	Basic transcription factor 3
Btf3l4	Basic transcription factor 3-like 4
C. elegans	*Caenorhabditis elegans*
Casq	Calsequestrin
CHO	Chinese hamster ovary
CNS	Central nervous system
Coa6	Cytochrome c oxidase assembly factor 6
Col12a1	Collagen, type XII, alpha 1
Col6a3	Collagen, type VI, alpha 3
Cox	Cytochrome c oxidase
Cox6b1	Cytochrome c oxidase, subunit VIb polypeptide 1
Cpt1a	Carnitine palmitoyltransferase 1A
Cyc1	Cytochrome c1
Cyr61	Cysteine rich protein 61
DAPI	4',6-diamidino-2-phenylindole
DMEM	Dulbecco's Modified Eagle Medium
Dnaja2	DnaJ (Hsp40) homolog, subfamily A, member 2
DTT	Dithiothreitol
ECAR	Extracellular acidification rate
e.g.	*Exemplum gratii,* for example
EDTA	Ethylenediaminetetraacetic acid
ELISA	Enzyme-Linked Immunosorbent Assay
Eprs	Glutamyl-prolyl-tRNA synthetase
et al.	*Et alii*, and others
Fasn	Fatty acid synthase
FBS	Fetal bovine serum
FCCP	Carbonyl cyanide-4-(trifluoromethoxy)phenylhydrazone
Fgf	Fibroblast growth factor

Fgfr	Fgf receptor
FI	Fluorescence Intensity
Fn1	Fibronectin 1
FNDC5	Fibronectin type III domain-containing protein 5
Fpr1	Formyl peptide receptor 1
FSTL-1	Follistatin-like 1
G6pc	Glucose-6-phosphatase, catalytic
GO	Gene Ontology
GSEA	Gene Set Enrichment Analysis
h	Hour
HEPES	4-(2-hydroxyethyl)-1-piperazineethanesulfonic acid
HG	High glucose
HnRNP A3/	Heterogeneous nuclear ribonucleoprotein A3 (Gm8991)
Hspg2	Perlecan/heparan sulfate proteoglycan 2
Htra1	HtrA serine peptidase 1
Huwe1	HECT, UBA and WWE domain containing 1
i.e.	*Id est*, that is
IBMX	3-isobutyl-1-methylxanthine
Igf1	Insulin-like growth factor 1
Il	Interleukin
Il5ra	Interleukin 5 receptor alpha
KEGG	Kyoto Encyclopedia of Genes and Genomes
Klb	Klotho beta
Lamc1	Laminin, gamma 1
LC	Liquid chromatography
Ldlr	Low density lipoprotein receptor
LG	Low glucose
Ltbp3	Latent transforming growth factor beta binding protein 3
m	Milli
M	Molar
MOTS-c	Mitochondrial ORF of the twelfe S c
mRNA	Messenger ribonucleic acid
MS	Mass spectrometry
n	Nano
Nduf	NADH:ubiquinone oxidoreductase subunits
Npnt	Nephronectin
OCR	Oxygen consumption rate
Olfr532	Olfactory receptor 532
ORF	Open reading frame
PBS	Phosphate buffered saline
Pdlim1	PDZ and LIM domain protein 1

Pepck	Phosphoenolpyruvate carboxykinase 1, cytosolic
Pfkl	Phosphofructokinase, liver, B-type
Pgc1α	PPARG coactivator 1 alpha
Pklr	Pyruvate kinase, liver and red blood cells
Plau	Plasminogen activator, urokinase
Ppara	Peroxisome proliferator activated receptor alpha
Pparg	Peroxisome proliferator activated receptor gamma
Rp	Ribosomal protein
Rps5	Ribosomal protein S 5
rRNA	Ribosomal ribonucleic acid
Rsu1	Ras suppressor protein 1
Sdh	Succinate dehydrogenase
SGBS	Simpson Golabi Behmel Syndrome
Sirt1	Sirtuin 1
Sp3	Trans-acting transcription factor 3
Srebf	Sterol regulatory element binding transcription factor
TFA	Trifluoroacetic acid
Tgfb2	Transforming growth factor, beta 2
Tgfβ	Transforming growth factor beta
Ucp1	Uncoupling protein 1
UQCR	ubiquinol-cytochrome c reductase complex subunits
Vbp1	Von Hippel-Lindau binding protein 1
vs.	Versus
WAT	White adipose tissue

Summary

Skeletal muscle is an important player in whole body energy homeostasis. It is not only one of the major energy consumers in the body but also an endocrine organ releasing hormones, so-called “myokines”, which can influence metabolism in various target organs. Some of these myokines, e.g. Fgf21 and Irisin, have been reported to increase energy expenditure by inducing browning of white adipose tissue. Thus, they represent a promising opportunity to prevent or combat diabetes and obesity. Irisin is supposed to be induced by exercise, whereas Fgf21 is induced by different conditions that collectively represent a state of low cellular energy.

This work started by evaluating the effects of synthesized irisin on human white adipocytes, showing no profound effects on adipocyte energy metabolism in contrast to previous publications. Given the well-established conditions stimulating Fgf21 secretion from muscle, it was hypothesized that skeletal muscle may respond to the shortage of energy by inducing a complex signaling program that includes various myokines. Those myokines may coordinate metabolism in other parts of the body. Therefore, C2C12 myotubes and intact primary muscle fibers were deprived of energy in two different approaches: C2C12 myotubes were nutrient-deprived, whereas primary muscle fibers were treated with an inhibitor of the mitochondrial electron transport chain. Both treatments compromised respiratory flux and robustly induced *Fgf21* expression.

In order to reveal new myokines, unbiased mass spectrometric analysis was applied to reveal the secretomes of nutrient-deprived C2C12 myotubes and energy-deprived primary muscle fibers. In total, 1960 proteins were identified by the two approaches. This thesis focuses on the comprehensive analysis of those proteomic datasets including the use of an array of bioinformatics tools to predict high-confidence candidates. Combining bioinformatics analyses and the comparison with a previously published secretome analysis predicted the secretion of 1077 proteins as putative myokines. Overlapping the C2C12 and the primary muscle fiber approach narrowed down the number of secretory proteins to 274. Of those proteins, only five were induced by the treatments in both experimental setups and only one correlated with Fgf21 protein abundance: Cox6b1, a subunit of respiratory complex IV. Cox6b1 has previously been described to be shuttled out of mitochondria to the cytoplasm. However, to the best of my knowledge, its secretion from muscle as a “mitokine” is observed in this study for the first time.

Besides this lead compound, a set of potential myokines was chosen to examine their effects on *Ucp1* mRNA expression in white and brown adipocytes, mRNA expression of several metabolic genes in liver cells, and the mRNA expression of *Agrp* in hypothalamic cells. However, in the tested concentrations, they did not show reproducible effects on those genes *in vitro*. The physiological role of the putative myokines with regard to energy metabolism therefore requires further investigation in future studies, in particular *in vivo*.

This thesis provides the identification of secreted muscle proteins *in vitro*, a comprehensive analysis allowing classification and prediction of potential myokines and thus, an important basis for future studies investigating the signaling and hormonal role of energy-challenged muscle and consolidating the proposed candidates of this thesis *in vivo*.

Zusammenfassung

Der Skelettmuskel ist ein Organ mit hoher Relevanz für die Aufrechterhaltung des systemischen energetischen Gleichgewichts. Er ist nicht nur der größte Energieverbraucher des Körpers, sondern auch ein endokrines Organ, das sogenannte „Myokine“ sezerniert, die den Stoffwechsel in verschiedenen Organen beeinflussen können. Einige dieser Myokine, beispielsweise Fgf21 oder Irisin, scheinen laut verschiedener Publikationen den Energieverbrauch des Körpers erhöhen zu können, indem sie eine „Bräunung“ des weißen Fettgewebes hervorrufen. Dies wird als vielversprechende Möglichkeit angesehen, Diabetes und Adipositas zu behandeln und vorzubeugen. Während die Sekretion von Irisin angeblich durch sportliche Aktivität erhöht wird, wird die Expression und Sekretion von Fgf21 unter verschiedenen Bedingungen angeregt, unter denen Zellen und Gewebe wenig Energie zur Verfügung haben.

Diese Arbeit begann mit der Evaluierung der Effekte von Irisin auf humane weiße Adipozyten, ohne jedoch deutliche Effekte auf den Energiestoffwechsel der Fettzellen zu zeigen. In Anbetracht der bekannten Konditionen, welche die Sekretion von Fgf21 aus dem Skeletmuskel anregen, stellte ich die Hypothese auf, dass der Skelettmuskel auf Energiemangel reagiert, indem er ein komplexes Signalprogramm einleitet, das die Sekretion verschiedener Myokine umfasst. Diese Myokine beeinflussen womöglich den Stoffwechsel in anderen Organen. Daher wurde Energiemangel in Muskelzellen in zwei experimentellen Ansätzen herbeigeführt: C2C12 Muskelzellen wurden Nährstoffe entzogen sowie die mitochondriale Atmungskette in primären Maus-Muskelfasern inhibiert. Beide Behandlungen führten zu einer Abnahme der zellulären Atmungsraten und einem Anstieg der *Fgf21* Expression.

Um neue Myokine zu identifizieren, wurde das Sekretom von C2C12 Muskelzellen mit Nährstoffmangel sowie von primären Muskelfasern mit inhibierter Atmungskette massenspektrometrisch untersucht. Insgesamt wurden mit diesen beiden Ansätzen 1960 Proteine identifiziert. Diese Arbeit konzentriert sich auf die umfassende Analyse dieser Proteom-Datensätze mit Hilfe verschiedener bioinformatischer Programme, um zuverlässig Kandidaten vorherzusagen. Bioinformatische Analysen und der Vergleich mit einem veröffentlichten Sekretom prognostizierten die Sekretion von 1077 Proteinen als Myokine. Die Schnittmenge des C2C12 Sekretoms und des Sekretoms primärer Muskelfasern beinhaltete 274 sekretorische Proteine. Nur fünf dieser Proteine wurden sowohl durch Entzug von Nährstoffen in C2C12

Muskelzellen als auch durch Inhibierung der Atmungskette in primären Maus-Muskelfasern induziert. Darüber hinaus korrelierten die Mengen von nur einem dieser Proteine im C2C12 Sekretom mit den Mengen an Fgf21. Bei diesem Protein handelte es sich um Cox6b1, eine Untereinheit von Komplex IV der mitochondrialen Atmungskette. Der Transport von Cox6b1 aus Mitochondrien ins Zytoplasma wurde bereits beschrieben. Nach meinem besten Wissen zeigt diese Studie jedoch zum ersten Mal, dass Cox6b1 als „Mitokin“ vom Muskel sezerniert wird.

Neben diesem Hauptkandidaten wurde eine Reihe möglicher Myokine ausgewählt um ihre Wirkung auf die mRNA Expression von *Ucp1* in weißen und braunen Fettzellen sowie auf die mRNA Expression verschiedener Gene des Zellstoffwechsels in Leberzellen und von *Agrp* in hypothalamischen Zellen zu untersuchen. Auf die untersuchten Gene zeigten sie in den getesteten Konzentrationen jedoch keine reproduzierbaren signifikanten Effekte. Um die physiologische Rolle dieser möglichen Myokine bezüglich des Energiestoffwechsels zu klären, sind daher weitere Studien, insbesondere *in vivo*, notwendig.

Diese Arbeit beinhaltet die Identifikation vom Muskel *in vitro* sezernierter Proteine, eine umfassende Analyse, die die Klassifizierung und Vorhersage potenzieller Myokine erlaubt, und dadurch eine wichtige Grundlage, um in weiteren Studien *in vivo* die Rolle des Muskels und der genannten Kandidaten in der hormonellen Signalübertragung unter Bedingungen des Energiemangels zu untersuchen.

1. Introduction

1.1 Skeletal muscle in whole body energy metabolism

Skeletal muscle is a crucial player in whole body energy homeostasis. It is not only the biggest consumer of substrates and energy but also acts as an endocrine organ affecting other metabolically crucial organs.

Being the largest organ in the human body [1], skeletal muscle accounts for approximately 40% of total body mass in lean subjects and 20-30% of basal metabolic rate [2]. It is essential for the generation of force and movement, but also stabilizes the body during upright standing. Therefore, it has to provide substrates and energy during short bursts of highly increased as well as long periods of moderately increased energy demand. In accordance with its broad spectrum of tasks, skeletal muscle is able to quickly remodel and adapt to different needs and stresses, e.g. different forms of exercise [1, 3]. Adaption to different tasks and requirements is enabled by the presence of different fiber types with distinct contractile speed and oxidative capacity as well as the availability of aerobic and anaerobic metabolic pathways [reviewed in 3].

Skeletal muscle is crucial for systemic metabolism. It serves as a major reservoir for amino acids and ensures stable plasma amino acid levels during fasting. It thus enables protein synthesis in peripheral organs and provides precursors for hepatic gluconeogenesis during fasting [4-6]. Thereby, it warrants maintenance of the protein mass of other tissues and of plasma glucose levels [4]. In fed states, on the other hand, the skeletal muscle incorporates ingested amino acids into muscle protein to balance the loss of amino acids during fasting [4]. Further, it is the major site of insulin-dependent glucose uptake in the postprandial state and insulin resistance in skeletal muscle is considered to be the initiating defect that precedes systemic insulin resistance and type-2-diabetes [7]. Moreover, exercise, i.e. the working skeletal muscle, has many beneficial effects on systemic metabolism and general health [reviewed in e.g. 8, 9].

1.1.1 Energy deprivation has beneficial effects on general health

Energy deprivation, either by withdrawal of sufficient amounts of nutrients like in caloric restriction [10] or by increasing demand as in exercise [8, 9], has beneficial effects on general health and attenuates age-related damage.

Caloric restriction without essential nutrient deficiency has been shown to protect against aging-related pathologies like diabetes, cancer, cardiovascular disease, and brain atrophy. Thus, caloric restriction delays aging and increases life span in multiple species [11]. It does so by affecting behavior, learning, immune response, gene expression, enzyme activities, hormonal action, glucose tolerance, DNA repair, protein synthesis, locomotor activity, muscle mass and function, body temperature, and mitochondrial biogenesis [12-16].

Exercise was shown to protect against neurodegenerative diseases, type 2 diabetes, obesity, cardiovascular disease, and different types of cancer [17]. In the muscle, endurance training increases muscular oxidative capacity by increasing mitochondrial biogenesis, enhances glucose uptake and insulin sensitivity, increases lipid metabolism, and enhances angiogenesis [3]. In the brain, it improves memory function and cognitive performance, affects neuronal plasticity by increasing synapse density, neuronal complexity, and induces neurogenesis [17]. Further it affects the immune system, improves systemic glucose tolerance, decreases serum triglycerides, lowers blood pressure, reduces cardiovascular events, and – like caloric restriction – attenuates aging induced damage [9]. Those beneficial effects of exercise are under suspicion to be caused by one or several "exercise factors". Indeed, skeletal muscle has been shown to release hormone-like factors, so-called myokines, several of which have beneficial effects on general health [18] and may also play a role in caloric restriction [19, 20].

1.2 Skeletal muscle as an endocrine organ

Skeletal muscle has been recognized as an endocrine organ secreting so-called myokines upon muscle contraction [18, 21, 22] and other stimuli. Those include induction during myogenesis or muscle remodeling [9] as well as stressors like autophagy deficiency or uncoupling [23, 24]. Myokines can act in an autocrine, paracrine or endocrine manner and contribute to inter-organ communication [21]. They are generally believed to mediate at least parts of the beneficial effects of exercise on general health and also have been suspected to play a role during caloric restriction [19, 20]. Therefore, it is suggested that some of them are promising therapeutic targets for the treatment of numerous diseases including metabolic syndrome, cardiovascular disease, or neurodegeneration [18, 21, 22, 25, 26].

1.2.1 Myokines

In recent years, many potential novel myokines have been identified in proteomic studies [e.g. 27, 28, 29]. In most cases, their physiological role is still unknown. However, there are also a number of well-examined myokines, e.g. Interleukin 6 (Il6) or Fibroblast growth factor 21 (Fgf21), and several myokines have been shown to affect glucose and lipid metabolism in muscle, liver, and adipose tissue, e.g. Il6, Il13, Il15, and Fgf21 [reviewed e.g. in 30].

Endocrine effects of myokines

Myokines are factors that act in an autocrine, paracrine or endocrine way on skeletal muscle itself as well as on various other organs (Fig. 1).

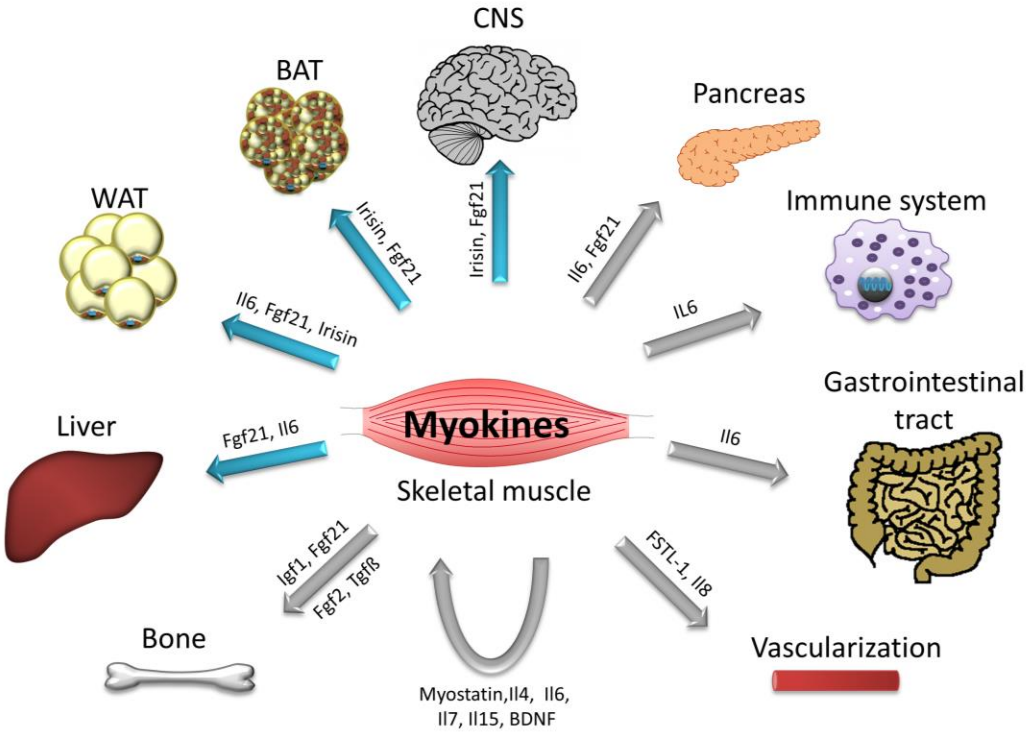

Figure 1: Myokines can exert autocrine, paracrine or endocrine effects on various organs. Myokines are secreted from skeletal muscle and can either have autocrine and paracrine effects on skeletal muscle itself or enter the circulation to exert endocrine effects on a variety of organs. For each target organ at least one example myokine is given. Arrows in blue indicate target organs that play a role for the experimental part of this thesis. BAT: Brown adipose tissue; BDNF: Brain derived neurotrophic factor; CNS: Central nervous system; Fgf: Fibroblast growth factor; FSTL-1: Follistatin-like 1; Il: Interleukin; Igf1: Insulin-like growth factor 1; Tgfβ: Transforming growth factor beta; WAT: White adipose tissue

Several myokines primarily affect skeletal muscle itself, e.g. myostatin, which inhibits muscle growth and whose expression is reduced by exercise [31]. Leukemia inhibitory factor, on the other hand, stimulates muscle growth and regeneration as a myokine [32]. Further examples are Il4, Il7, Il8, and Il13 which affect muscle development, growth, and angiogenesis [9]. However,

many myokines have been shown to have endocrine effects on other organs, e.g. adipose tissue, liver, or brain [9]. Secretion of the prototype myokine Il 6 from muscle upon exercise was first reported by Pedersen and colleagues [33]. It has since been shown to have multiple effects on different organs and was suggested to be an energy sensor aiming to maintain energy status during exercise as it is induced in response to exercise but also dependent on substrate availability [34]. It stimulates muscle growth, angiogenesis, hepatic gluconeogenesis, lipolysis and lipid oxidation and glucose uptake in skeletal muscle and adipose tissue, affects pancreatic function, and stimulates GLP-1 secretion from intestinal L cell as well as pancreatic α cells, and suppresses inflammation [9, 34-36]. In addition to its direct effects on peripheral organs, Il6 can cross the blood-brain barrier and may exert some of its effects via central pathways [37, 38] like other myokines, e.g. Fgf21 and irisin [39-41].

Many myokines have been shown to affect adipose tissue directly or indirectly, e.g. influencing glucose uptake or lipolysis [35]. As obesity has become a major threat to public health in the industrialized world, one aspect of myokines that gained particular interest in the recent years is the ability of some myokines, especially Fgf21 and irisin, to activate brown adipose tissue (BAT) and/or induce browning of white adipose tissue (WAT) [30]. This means that skeletal muscle can increase energy expenditure through its own increased energy demand, e.g. during exercise, and via endocrine induction of uncoupling of the electron transport chain in brown or beige adipocytes [42-44].

Browning of white adipose tissue

Browning of WAT or induction of BAT was suggested as a potential treatment of metabolic disease since it is a powerful mechanism to increase energy expenditure [42, 45-48]. It is generally understood as the appearance of so-called “recruitable”, “brite” (brown in white) or “beige” adipocytes within WAT and an induction of Uncoupling protein 1 (Ucp1) expression and mitochondrial biogenesis in these cells [44]. Beige adipocytes are interspersed in white adipocytes and functionally resemble brown adipocytes [49]. Due to their distinct gene expression signature they are generally regarded a distinct class of adipocytes [50-53]. While white adipocytes store lipids [54, 55] and are morphologically characterized by one big unilocular lipid droplet (Fig. 2) [56-58], brown adipocytes are characterized by a large number of mitochondria and multilocular lipid droplets (Fig. 2) [58] and do not store but dissipate energy as

heat [59, 60]. This is enabled by uncoupling of the electron transport chain via Ucp1, whose expression is a hallmark of brown and beige adipocytes [61-67]. Ucp1 is a proton channel located in the mitochondrial inner membrane dissipating proton motive force, which is built by substrate oxidation via the mitochondrial electron transport chain and is normally used for ATP production, as heat allowing non-shivering thermogenesis [62, 68, 69]. In addition to its role in thermoregulation in small rodents and human infants [42, 43, 59, 60], increasing dissipation of energy as heat by BAT or beige adipocytes can prevent diet-induced obesity. It is therefore regarded a potentially powerful therapeutic target to combat metabolic disease [42, 45-48]. However, in many models, browning of WAT markedly improves glucose tolerance and insulin resistance despite only moderate weight loss, i.e. the improvements in glucose metabolism exceed the effect of the observed increase in energy expenditure [70, 71]. Together with the fact that browning also occurs in energy deficient states like exercise or cachexia [70, 72, 73], this implies that brown and beige adipocytes exert functions apart from thermogenesis. Beige and brown fat were suggested to modulate glucose homeostasis and insulin sensitivity via non-thermogenic mechanisms, e.g. by influencing the secretion of adipokines [74, 75]. Furthermore, beige and brown adipose tissue appear to influence WAT physiology, blood lipids, liver steatosis, cardiovascular system, immune system, skeletal muscle mass, bone morphology, circadian rhythm, and sleep regulation [76-81].

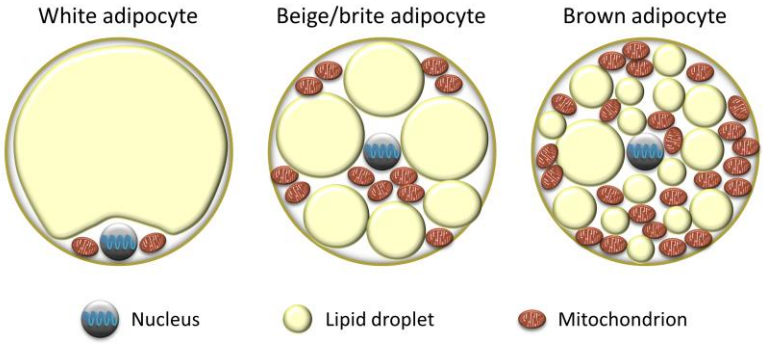

Figure 2: White, beige, and brown adipocytes. White adipocytes are characterized by one big lipid droplet ("unilocular") and only few mitochondria, whereas brown adipocytes contain several small lipid droplets ("multilocular") and a high number of mitochondria. Beige adipocytes are interspersed in white adipose tissue and functionally resemble brown adipocytes. Both brown and beige adipocytes are characterized by the expression of uncoupling protein 1 (Ucp1) which allows the dissipation of proton motive force as heat instead of generating ATP.

Browning of WAT can be induced by different stimuli including chemical compounds, hormones, genetic modifications, and food components [44, 51], e.g. beta-adrenergic receptor agonists, peroxisome proliferator-activated receptor (PPAR) alpha or gamma agonists, retinoids,

thyroid hormones, or capsaicin [56, 82-107]. More recently, myokines have been added to the list of browning agents. In particular, Fgf21 and irisin have been reported to be secreted by skeletal muscle and induce browning of WAT [23, 70, 108].

Irisin

Irisin is the proteolytically cleaved and secreted part of the type I membrane protein FNDC5 (Fibronectin type III domain-containing protein 5) and was found to be induced in muscle by Peroxisome proliferator-activated receptor gamma coactivator 1-alpha (PGC1α) overexpression or exercise by Boström and colleagues [70]. They claimed that this newly identified myokine mediates the browning of WAT and thereby induces thermogenesis and elevates energy expenditure [70].

Irisin is a 112 amino acid peptide with 100% identity in mouse and human according to Boström and colleagues [70]. Surprisingly, a study by Raschke and colleagues stated that the start codon of human *FNDC5* is mutated resulting in a strongly reduced translation efficiency [109]. Nevertheless, circulating irisin was detected and quantified in humans by several groups most of which used Enzyme-Linked Immunosorbent Assay (ELISA) kits [110-115] whose specificity for irisin was doubted by Raschke *et al.* [109]. Not only the quantification methods, but also the physiological induction of irisin is under debate [e.g. 109, 111, 116, 117-121].

Boström and colleagues reported increased *FNDC5* expression in muscle and elevated irisin plasma levels after exercise in mice and humans [70]. In humans, an acute bout of exercise induced serum irisin in some but not all studies, while prolongued aerobic, resistance, or strength training schedules do not seem to alter serum irisin levels or even lower them [109, 111, 116-118, 122-126]. Furthermore, in studies that observed an induction of irisin expression or serum levels, this often applied only for a very specific group of subjects, e.g. depending on their age or a specific health status [119-121]. The relevance of muscle-derived irisin was further weakened by studies showing irisin to also be an adipokine [127-130]. In accordance with irisin secretion from adipose tissue, several studies reported positive correlation of irisin with obesity [111-113, 121, 131-133]. Other studies found a negative association of irisin levels with body-mass-index [115, 128, 134-136], which is in line with the initial irisin study reporting irisin to have beneficial effects on whole body metabolism [70]. However, it has also been reported that there is no association between irisin and obesity [120]. Equally confusing, there is evidence for a

negative [112, 122, 128, 133, 135], positive [132, 137], or no association [120, 121, 138] between irisin and type 2 diabetes or metabolic syndrome.

After publication of the initial irisin study [70], several studies confirmed irisin to increase *Ucp1* expression in different adipocyte cell lines and primary adipocytes of rodent origin [51, 139-141]. Further, Myostatin-knockout mice with increased muscle mass and leaner body composition than wild type mice show browning of WAT which Shan and colleagues claim to be mediated by increased expression and secretion of irisin [142]. However, at the beginning of this study it was still not clear whether browning of WAT by irisin as observed in rodents/rodent cells is transferable to human WAT.

Fibroblast growth factor 21 (Fgf21)

Fgf21 is a hormone-like member of the fibroblast growth factor-family. In recent years, it gained increasing interest as a systemic metabolic regulator secreted by the liver as a hepatokine, by adipose tissue as an adipokine, and by skeletal muscle as a myokine [23, 24, 143].

Initially, it was described to be highly expressed in murine liver [144], where it was strongly upregulated via PPARalpha by fasting [145-147], in response to a ketogenic, i.e. high-fat, low-carbohydrate diet [145], as well as in suckling pubs [148]. Later, Fgf21 was shown to be induced in adipose tissues by cold exposure [108, 149, 150]. Its secretion from muscle was observed upon skeletal muscle-specific Akt1-overexpression, fasting [143], mitochondrial dysfunction caused by autophagy deficiency [23], and muscle-specific uncoupling of the mitochondrial respiratory chain [24]. Expression of *Fgf21* was also induced in C2C12 cells upon treatment with rotenone or antimycin A, which inhibit mitochondrial respiratory complexes I and III, respectively [23]. These data imply that mitochondrial dysfunction contributes to secretion of Fgf21, which is corroborated by Fgf21 being a biomarker for muscle-manifesting mitochondrial disorders in humans [151].

In order to exert its functions, Fgf21 binds to a complex of one of the Fgf-Receptors (Fgfr1c, 2c, 3c, 4) and the co-receptor beta-Klotho [152, 153] and seems to exert at least some of its effects in synergy with or via PPARgamma [154, 155].

Fgf21 was first revealed to play a role in regulation of systemic metabolism, when *Fgf21*-transgenic mice were observed to be resistant to diet-induced obesity and treatment with

recombinant Fgf21 was shown to lower plasma glucose and triglycerides to nearly normal levels in mouse models of diabetes and obesity [156]. Since then, Fgf21 has been shown to affect carbohydrate and lipid metabolism in several tissues, to increase fat utilization and lipid excretion, to enhance insulin sensitivity, to induce browning of white adipose tissue, to increase energy expenditure, to reduce hepatosteatosis, and to cause weight loss [157-159]. More specific, in the liver, Fgf21 regulates hepatic fatty acid oxidation, gluconeogenesis and ketogenesis in response to fasting [160]. In adipocytes, Fgf21 enhances glucose-uptake and decreases lipolysis *in vitro* [156]. *In vivo*, Fgf21 seems to increase lipolysis in adipocytes in fed states and decrease lipolysis in adipocytes in fasted states [161]. Furthermore, Fgf21 increases the expression and secretion of adiponectin from WAT, which in turn affects energy metabolism and insulin sensitivity in liver and muscle [162, 163]. Strikingly, Fgf21 also induces browning of white adipose tissue and activation of brown adipose tissue [108].

1.3 Aim of the study

The aim of this thesis comprises the identification and characterization of known and novel myokines.

The first aim of this study was to consolidate the published browning effects of irisin in a human white adipocyte strain, namely Simpson Golabi Behmel Syndrome (SGBS) adipocytes.

Based on the results, it was moved to consolidate the induction of Fgf21 in muscle cells. Fgf21 secretion has previously been shown to be increased by different conditions causing a state of low cellular energy [23, 24, 146, 164], showing that skeletal muscle communicates the lack of substrate or energy to other organs. Assuming that maintenance of the muscular energy status requires not only the secretion of Fgf21 but of a whole program of secreted factors, this study, aimed to characterize the secretome of energy deprived skeletal muscle. Herein, Fgf21 induction was used as a positive control to verify the induction of nutrient stress programs. Secretome analysis with different bioinformatics tools aimed to identify putative myokines that may exert beneficial effects on whole body metabolism in collaboration or independent of Fgf21. Pilot experiments investigating effects of chosen candidate proteins *in vitro* aimed to unravel the metabolic effects of these new myokines.

2. Material and methods

2.1 Materials

2.1.1 Mouse strains

For isolation of primary muscle fibers and primary adipocytes, C57BL/6J mice bred within the animal facilities of the Helmholtz Zentrum München, Germany, were used.

2.1.2 Cell lines

Table 1: Cell lines

Cell line	Supplier
C2C12 murine myoblasts	Leibniz Institute DSMZ-German Collection of Microorganisms and Cell Cultures, Braunschweig, Germany; DSMZ no. ACC 565
HepG2 human hepatoma cells	Leibniz Institute DSMZ-German Collection of Microorganisms and Cell Cultures, Braunschweig, Germany; DSMZ no. ACC 180
Embryonic mouse hypo-thalamic cell line N41	Cedarlane, CLU 121, Burlington, Ontario, Canada; ordered via Biozol, Eching, Germany
SGBS preadipocyte cell strain	Prof. Dr. Wabitsch / Prof. Dr. Fischer-Posovszky, University clinics, Ulm, Germany

2.1.3 Culture media, buffers, and solutions

Table 2: Culture media, buffers, and solutions

Product	Supplier
DMEM, high glucose, HEPES, no Phenol Red	Gibco/ Life Technologies/Thermo Fisher Scientific Inc., Waltham, Massachusetts MA 02451, USA
DMEM, high glucose, no pyruvate	Gibco/ Life Technologies/Thermo Fisher Scientific Inc., Waltham, Massachusetts MA 02451, USA
DMEM, high glucose, pyruvate	Gibco/ Life Technologies/Thermo Fisher Scientific Inc., Waltham, Massachusetts MA 02451, USA
DMEM, low Glucose, Pyruvate	Gibco/ Life Technologies/Thermo Fisher Scientific Inc., Waltham, Massachusetts MA 02451, USA
DMEM, no glucose	Gibco/ Life Technologies/Thermo Fisher Scientific Inc., Waltham, Massachusetts MA 02451, USA
DMEM, no Glucose, no Glutamine, no Phenol Red	Gibco/ Life Technologies/Thermo Fisher Scientific Inc., Waltham, Massachusetts MA 02451, USA
DMEM/F-12 (1:1) (1x) liquid	Gibco/ Life Technologies/Thermo Fisher Scientific Inc., Waltham, Massachusetts MA 02451, USA
Fetal bovine serum	Gibco/Life Technologies/Thermo Fisher Scientific Inc., Waltham, Massachusetts MA 02451, USA
Horse serum, heat inactivated	Sigma-Aldrich Chemie GmbH, Taufkirchen, 82024 Germany
PBS – Phosphate Buffered Saline	Gibco/Life Technologies/Thermo Fisher Scientific Inc., Waltham, Massachusetts MA 02451, USA
Penicillin-Streptomycin (10,000 U/mL)	Gibco/ Life Technologies/Thermo Fisher Scientific Inc., Waltham, Massachusetts MA 02451, USA
Trypsin-EDTA (0.05%), phenol red	Gibco/ Life Technologies/Thermo Fisher Scientific Inc., Waltham, Massachusetts MA 02451, USA

2.1.4 Chemicals

Table 3: Chemicals

Chemical	Supplier
2-Deoxy-D-Glucose	Sigma-Aldrich Chemie GmbH, 82024 Taufkirchen, Germany
2-Propanol/ Isopropanol	Carl Roth GmbH + Co. KG, 76185 Karlsruhe, Germany
3,3',5-Triiodo-l-thyronine free acid	Sigma-Aldrich Chemie GmbH, 82024 Taufkirchen, Germany
3-Isobutyl-1-methylxanthine	Sigma-Aldrich Chemie GmbH, 82024 Taufkirchen, Germany
Albumin bovine Fraction V, Protease-free	SERVA Electrophoresis GmbH, 69115 Heidelberg, Germany
Ammonium chloride	Carl Roth GmbH + Co. KG, 76185 Karlsruhe, Germany
Antimycin A	Sigma-Aldrich Chemie GmbH, 82024 Taufkirchen, Germany
Apo-Transferrin human	Sigma-Aldrich Chemie GmbH, 82024 Taufkirchen, Germany
BSA lyophilized powder, essentially fatty acid free	Sigma-Aldrich Chemie GmbH, 82024 Taufkirchen, Germany
Calcium chloride	Carl Roth GmbH + Co. KG, 76185 Karlsruhe, Germany
Chloroform	Applichem GmbH, 64291 Darmstadt, Germany
CL-316,243	Sigma-Aldrich Chemie GmbH, 82024 Taufkirchen, Germany
Collagen A	VWR International GmbH, 64295 Darmstadt, Germany
Collagenase type II	Worthington Biochemical Corporation, Lakewood, NJ 08701, USA
Collagenase type IV	Life Technologies/Thermo Fisher Scientific Inc., Waltham, Massachusetts MA 02451, USA
D-(+)-Glucose	Carl Roth GmbH + Co. KG, 76185 Karlsruhe, Germany
DAPI	Sigma-Aldrich Chemie GmbH, 82024 Taufkirchen, Germany
Dexamethasone	Sigma-Aldrich Chemie GmbH, 82024 Taufkirchen, Germany
Dimethylsulfoxid	Carl Roth GmbH + Co. KG, 76185 Karlsruhe, Germany
EDTA	Carl Roth GmbH + Co. KG, 76185 Karlsruhe, Germany
Ethanol, absolute	Merck KGaA, 64271 Darmstadt, Germany
FCCP	R&D Systems, Minneapolis, MN 55413, USA
HEPES	Carl Roth GmbH + Co. KG, 76185 Karlsruhe, Germany
Hydrochloric acid	Carl Roth GmbH + Co. KG, 76185 Karlsruhe, Germany
Hydrocortisone	Sigma-Aldrich Chemie GmbH, 82024 Taufkirchen, Germany
Insulin solution human	Sigma-Aldrich Chemie GmbH, 82024 Taufkirchen, Germany
Magnesium chloride	Carl Roth GmbH + Co. KG, 76185 Karlsruhe, Germany
Monopotassium phosphate	Carl Roth GmbH + Co. KG, 76185 Karlsruhe, Germany
Myxothiazol	Sigma-Aldrich Chemie GmbH, 82024 Taufkirchen, Germany
Nile Red	Life Technologies/Thermo Fisher Scientific Inc., Waltham, Massachusetts MA 02451, USA
Nuclease free water	Carl Roth GmbH + Co. KG, 76185 Karlsruhe, Germany
Oligomycin	Sigma-Aldrich Chemie GmbH, 82024 Taufkirchen, Germany
Potassium bicarbonat	Carl Roth GmbH + Co. KG, 76185 Karlsruhe, Germany
Potassium chloride	Carl Roth GmbH + Co. KG, 76185 Karlsruhe, Germany
Qiazol	Qiagen GmbH, Hilden, 40724, Germany
Rosiglitazone	Sigma-Aldrich Chemie GmbH, 82024 Taufkirchen, Germany
Rotenone	Sigma-Aldrich Chemie GmbH, 82024 Taufkirchen, Germany

Roti nanoquant	Carl Roth GmbH + Co. KG, 76185 Karlsruhe, Germany
Sodium chloride	Carl Roth GmbH + Co. KG, 76185 Karlsruhe, Germany
Sodium oxamate	Th. Geyer GmbH & Co. KG, 71272 Renningen, Germany
Sodium Pyruvate	Sigma-Aldrich Chemie GmbH, 82024 Taufkirchen, Germany
TRIS	Carl Roth GmbH + Co. KG, 76185 Karlsruhe, Germany
TRIS HCL	Carl Roth GmbH + Co. KG, 76185 Karlsruhe, Germany
Tunicamycin	Sigma-Aldrich Chemie GmbH, 82024 Taufkirchen, Germany

2.1.5 Recombinant proteins and synthesized proteins

Synthesized irisin and Cox6b1 (FZ-4-816) were synthesized and folded by Richard DiMarchi's team at Indiana University Bloomington, USA based on the published sequences. Glycosylated irisin was designed, cloned, expressed in Chinese hamster ovary (CHO) cells, and purified by evitria AG, Schlieren, 8952, Switzerland. All other proteins used in this study were purchased from Abcam, R&D Systems or Thermo Fisher Scientific.

Table 4: Recombinant proteins and synthesized proteins

Protein	Supplier
human Ang-1	923-AN-025, R&D Systems, Minneapolis, MN 55413, USA
human Casq1	ab112257, Abcam plc, Cambridge, CB4 0FL, UK
human Cox6b1	ab114917, Abcam plc, Cambridge, CB4 0FL, UK
human Cox6b2	ab165239-10ug, Abcam plc, Cambridge, CB4 0FL, UK
human FN1	4305-FN-200, R&D Systems, Minneapolis, MN 55413, USA
human Il5Ra	ab85983, Abcam plc, Cambridge, CB4 0FL, UK
human Pdlim	ab132184, Abcam plc, Cambridge, CB4 0FL, UK
human PLAU	10815-H08H-25, Life Technologies/ Thermo Fisher Scientific Inc., Waltham, Massachusetts MA 02451, USA
human Rps5	89010586, Thermo Fisher Scientific Inc., Waltham, Massachusetts MA 02451, USA
human Rsu1	ab132332, Abcam plc, Cambridge, CB4 0FL, UK
murine NPNT	4298-NP-050, R&D Systems, Minneapolis, MN 55413, USA
murine PLAU	ab92641, Abcam plc, Cambridge, CB4 0FL, UK

2.1.6 Synthetical oligonucleotides and TaqMan probes and other supplies for qPCR

SYBR Green PCR Master Mix and Taqman Universal Master Mix II, no UNG as well as Taqman probes for murine Fgf21 (Mm00840165_g1) and murine Hprt (Mm01545399_m1) were purchased from Life Technologies / Thermo Fisher Scientific Inc., Waltham, Massachusetts MA 02451, USA. Primers for qPCRs using SybrGreen were purchased from Sigma-Aldrich Chemie GmbH, Taufkirchen, 82024 Germany. The respective primer sequences are given in Table 5.

Table 5: Primer sequences used for qPCRs with SybRGreen

Gene	Forward primer	Reverse primer
Human Cpt1a	ATGCGCTACTCCCTGAAAGTG	GTGGCACGACTCATCTTGC
Human Fasn	TCTCCGACTCTGGCAGCTT	GCTCCAGCCTCGCTCTC
Human Fgf21	AGGCCTCAGGGTCAAAGTG	CCTTGAAGCCGGGAGTTATT
Human G6pc	ACTGGCTCAACCTCGTCTTTA	CGGAAGTGTTGCTGTAGTAGTCA
Human Hprt	CCTGGCGTCGTGATTAGTGAT	AGACGTTCAGTCCTGTCCATAA
Human Il8	AAATTTGGGGTGGAAAGGTT	TCCTGATTTCTGCAGCTCTGT
Human Klb	TTCTGGGGTATTGGGACTGGA	CCATTCGTGCTGCTGACATTTT
Human Ldlr	GTCTTGGCACTGGAACTCGT	CTGGAAATTGCGCTGGAC
Human Pck1	AAAACGGCCTGAACCTCTCG	ACACAGCTCAGCGTTATTCTC
Human Pfkl	GATGATGTTGGAGACGCTCA	GGTGCCAAAGTCTTCCTCAT
Human Pklr	GAGAAGTTGAGTCGCGCAAT	CAGTACCAGCATCATTGCCA
Human Ppara	CGGTGACTTATCCTGTGGTCC	CCGCAGATTCTACATTCGATGTT
Human Sirt1	AGAGATGGCTGGAATTGTCC	CCAGATCCTCAAGCGATGTT
Human Srebf1	GCCCCTGTAACGACCACTG	CAGCGAGTCTGCCTTGATG
Human Srebf2	TCAGGGAACTCTCCCACTTG	GAGACCATGGAGACCCTCAC
Murine Agrp	GGCCTCAAGAAGACAACTGC	GCAAAAGGCATTGAAGAAGC
Murine CypA	ATGGTCAACCCCACCGTGT	TTTCTGCTGTCTTTGGAACTTTGTC
Murine Fabp4	AAGGTGAAGAGCATCATAACCCT	TCACGCCTTTCATAACACATTCC
Murine Hprt	CAGTCCCAGCGTCGTGATTA	AGCAAGTCTTTCAGTCCTGTC
Murine Npy	TGGACTGACCCTCGCTCTAT	TGTCTCAGGGCTGGATCTCT
Murine Ucp1	GGCCTCTACGACTCAGTCCA	TAAGCCGGCTGAGATCTTGT

2.1.7 Kits

Table 6: Kits

Kit	Supplier
Fgf21 Elisa KIT	R&D Systems, Minneapolis, MN 55413, USA
QuantiTect Reverse Transcription Kit	Qiagen GmbH, Hilden, 40724, Germany
RNeasy Lipid Tissue Kit	Qiagen GmbH, Hilden, 40724, Germany
RNeasy Mini Kit	Qiagen GmbH, Hilden, 40724, Germany

2.1.8 Consumables for respirometry

All consumables for respirometry, i.e Xf24 FluxPaks, XF24 PS Cell Culture Microplates, XFe96 Flux Paks, XF96 PS Cell Culture Microplates, and XF Assay Medium were purchased from Seahorse Bioscience/Agilent Technologies, Santa Clara, CA 95951, USA

2.1.9 Machines and software

Machines and software used are indicated for each method in its respective description.

2.2 Methods

2.2.1 Cell culture

Cultivation and treatment of cell lines/strains

C2C12

C2C12 myoblasts were grown in Dulbecco's Modified Eagle Medium (DMEM) containing 25 mM glucose, 4 mM l-glutamine, 10% FBS, 100 U/ml Penicillin, and 100 µg/ml Streptomycin. Confluent myoblasts were washed with PBS two times and differentiated in DMEM containing 25 mM glucose, 4 mM l-glutamine, 2% horse serum, 100 U/ml Penicillin, and 100 µg/ml Streptomycin for five days.

All experiments with C2C12 myotubes were performed under serum-free conditions if not indicated otherwise. If samples were further processed for LC-MS/MS analysis, DMEM without phenol red was used for treatments.

HepG2 cells

HepG2 cells were grown and treated in DMEM with either high (4.5 g/l) or low (1 g/l) glucose supplemented with 10% FBS and 100 U/ml Penicillin, and 100 µg/ml Streptomycin.

N41 hypothalamic cells

N41 hypothalamic cells were grown and treated in DMEM (25 mM glucose, 4 mM l-glutamine, HEPES, without pyruvate) supplemented with 10% FBS and 100 U/ml Penicillin, and 100 µg/ml Streptomycin.

SGBS preadipocyte cell strain

As previously described [165], human SGBS preadipocytes were grown in DMEM/F-12 supplemented with 33 µM biotin, 17 µM pantothenat, 10% FBS and 100 U/ml Penicillin, and 100 µg/ml Streptomycin. For experiments, they were grown to confluency, washed with PBS, and differentiated in serum-free DMEM/F-12 supplemented with 33 µM biotin, 17 µM panthotenat, and 100 U/ml Penicillin, and 100 µg/ml Streptomycin. Differentiation was induced by adding 0.01 mg/ml transferrin, 20 nM insulin, 100 nM cortisol, 0.2 nM T3, 25 nM dexamethasone, 250 µM 3-isobutyl-1-methylxanthine (IBMX), and 2 µM rosiglitazone. After

four days, the medium was changed and only 0.01 mg/ml transferrin, 20 nM insulin, 100 nM cortisol, and 0.2 nM T3 were added. Cells were harvested after 10-11 days of differentiation.

Primary cells

Primary adipocytes

For the isolation of white primary adipocytes, subcutaneous white adipose tissue was harvested from C57BL/6J mice aged six to eight weeks. The tissue was minced and digested in 6 ml digestion buffer (DMEM with 0.15% collagenase Type IV and 2% BSA) per gram of adipose tissue for 50 min at 37°C shaking at 100 rpm. The digest was filtered through a 100 µm cell strainer and centrifuged at 400 g for 10 min at room temperature. The pellet was resuspended in Erythrocyte-lysis buffer (154 mM NH4Cl, 10 mM KHCO3, 0.1 mM EDTA) and incubated at room temperature for 10 min. After centrifugation at 400 g for 10 min at room temperature, the pellet was resuspended in DMEM containing 10% FBS, 100 U/ml Penicillin, and 100 µg/ml Streptomycin and filtered through a 40 µm cell strainer. Cells were grown in DMEM/F12 containing 10% FBS, 100 U/ml Penicillin, and 100 µg/ml Streptomycin. For experiments, they were grown to 90-100% confluency and differentiated with induction medium (growth medium with 1 µm Dexamethasone, 0.5 mM IBMX, 1 µm Rosiglitazone, 5 µg/ml Insulin) for two days, followed by differentiation medium (growth medium with 5 µg/ml Insulin) for five days.

Primary muscle fibers

Isolation of primary muscle fibers was performed by Daniel Lamp as follows: Intact interossei muscles of C57BL/6J mice were isolated and put in DMEM containing 1 g/l glucose. The muscle was digested with 4 mg/ml collagenase type II in DMEM containing 1 g/l glucose for about three hours at 37°C while mixing the digest roughly every 20 min by pipetting up and down with a cut 1 ml pipette tip. After digestion, tendons, connective tissues and other debris were removed from the muscle fiber suspension under a stereo microscope. The muscle fibers were washed three times with DMEM containing 1 g/l glucose and 10% heat inactivated FBS, seeded to plates that were previously coated with at least 3.5 mg/ml BD Matrigel in aCSF buffer (120 mM NaCl, 3.5 mM KCl, 1.3 mM CaCl2, 0.4 mM KH2PO4, 1 mM MgCl2, 5 mM HEPES, pH 7.4) and allowed to attach for one to two hours before they were used for further experiments. All experiments were performed in serum-free media.

2.2.2 Respirometry (Seahorse technology)

C2C12 myotubes:

For respirometry in a Seahorse XF24 extracellular flux analyzer (Seahorse Bioscience/Agilent technologies, Santa Clara, CA 95051, USA), C2C12 myoblasts were grown and differentiated in XF24 plates. On day five of differentiation, C2C12 myotubes were deprived of glucose and l-glutamine, i.e. nutrient deprived, for 4 h, 8 h, 12 h, or 24 h. Prior to measurement, they were washed twice with DMEM containing 25 mM glucose and 4 mM l-glutamine (Control) or DMEM without glucose and l-glutamine (nutrient deprivation). After 30 min incubation in the same media at 37°C in a XF Prep station (Seahorse Bioscience/Agilent technologies, Santa Clara, CA 95051, USA), the plate was transferred into the XF24 extracellular flux analyzer. Following equilibration, basal respiration was recorded over three measuring cycles. 1 µg/ml oligomycin was injected to inhibit ATP synthase and calculate ATP-linked and proton leak-linked respiration. After three measuring cycles, 1.1 µM of Carbonyl cyanide-4-(trifluoromethoxy)phenylhydrazone (FCCP) were injected uncoupling respiratory chain activity from ATP synthesis and maximal respiration rates were measured over three cycles. Last, 0.1 µM rotenone and 2 µM antimycin A were injected to inhibit respiratory complexes I and III to measure non-mitochondrial respiration over three cycles. Along with the mitochondrial inhibitors, 100 mM 2-deoxy-glucose was injected to inhibit glycolysis. Each measuring cycle consisted of 1 min mixing, 2 min waiting, and 3 min measuring.

Primary muscle fibers:

Primary muscle fibers were seeded in matrigel-coated 96-well Seahorse plates. After one to two hours at 37°C in a 5% CO2-atmosphere to allow attachment, the incubation media was exchanged with 180 µl aCSF. Control fibers were incubated in aCSF containing 15 mM glucose and 2 mM pyruvate, nutrient deprived fibers were incubated in aCSF. Myxothiazol treated fibers were incubated in aCSF containing 15 mM glucose and 2 mM pyruvate and 100 nM myxothiazol.

Prior to respiratory flux analysis in a Seahorse XF96 extracellular flux analyzer (Seahorse Bioscience/Agilent technologies, Santa Clara, CA 95051, USA), the plates were incubated at 37°C in a XF Prep Station (Seahorse Bioscience/Agilent technologies, Santa Clara, CA 95051, USA) for 1 h. Following equilibration, basal respiration was recorded over four measuring

cycles. 2 µg/ml oligomycin was injected to inhibit ATP synthase and calculate ATP-linked and proton leak-linked respiration. After three measuring cycles, 4 µM of FCCP were injected uncoupling respiratory chain activity from ATP synthesis and maximal respiration rates were measured over three cycles. Next, 2.5 µM Rotenone and 2.5 µM Antimycin A were injected to inhibit respiratory complexes I and III to measure non-mitochondrial respiration over four cycles. Last, 100 mM 2-deoxy-glucose was injected to inhibit glycolysis and measure non-glycolytic extracellular acidification rate (ECAR) over four cycles. Each measuring cycle consisted of 1 min mixing, 2 min waiting, and 3 min measuring.

SGBS adipocytes

For analysis in a XF96 extracellular flux analyzer, SGBS preadipocytes were seeded in XF96-PS plates (Seahorse Bioscience/Agilent technologies, Santa Clara, CA 95051, USA) and differentiated for 10 days. Prior to measurement, the cells were washed twice with XF DMEM (Seahorse Bioscience/Agilent technologies, Santa Clara, CA 95051, USA) containing 25 mM glucose and 5 mM sodium pyruvate. After 1 h incubation at 37°C in a XF Prep Station (Seahorse Bioscience/Agilent technologies, Santa Clara, CA 95051, USA), the plate was transferred to the XF96 extracellular flux analyzer. Following equilibration, basal respiration was recorded over three measuring cycles. 1 µg/ml oligomycin was injected to inhibit ATP synthase and calculate ATP-linked and proton leak-linked respiration. After three measuring cycles, 0.5 µM of FCCP were injected uncoupling respiratory chain activity from ATP synthesis and maximal respiration rates were measured over three cycles. Last, 4 µM Rotenone and 2 uM Antimycin A were injected to inhibit respiratory complexes I and III to measure non-mitochondrial respiration over three cycles. Along with the mitochondrial inhibitors, 100 mM 2-deoxy-glucose was injected to inhibit glycolysis. Each measuring cycle consisted of 1 min mixing, 2 min waiting, and 3 min measuring.

Assessment of SGBS differentiation rate

After respirometry analysis, cells were fixated with 4% paraformaldehyde for 10-20 min at room temperature. They were stained with 1 µg/ml 4',6-diamidino-2-phenylindole (DAPI) and lipids were stained with 4 µg/ml Nile red at 37°C for 2 h. After washing them once in PBS, the fluorescence intensity was measured on a PHERAstar FS (BMG Labtech, 77799 Ortenberg, Germany) using the FI 340 460 filter for DAPI signal and the FI 485 520 filter to measure Nile

Red signal. The Nile Red signal was normalized with the DAPI signal to compare the degree of differentiation.

Data analysis:

Basal mitochondrial respiration was calculated by subtracting non-mitochondrial respiration from basal respiration rates. Proton leak-linked respiration was calculated by subtracting non-mitochondrial respiration from oligomycin-insensitive respiration. For ATP-linked respiration, proton leak-linked respiration was subtracted from basal respiration. ATP production was calculated from ATP-linked respiration assuming a stoichiometry of 5 mol ATP per mol O2 [166]. Maximal respiration was calculated by subtracting non-mitochondrial respiration from the maximal respiration after FCCP injection.

2.2.3 Gene expression analysis

RNA isolation and quantification

The RNeasy Mini Kit was used for isolation of mRNA from C2C12, HepG2 and N41 cells, whereas mRNA from primary muscle fibers and SGBS adipocytes was isolated using the RNeasy Lipid Tissue Kit according to the manufacturer's instructions. Primary adipocyte mRNA was isolated as follows. Cells were collected and homogenized in 1 ml Qiazol per sample. 200 µl chloroform were added and the samples were vortexed 4 times within 10 min of incubation. After centrifugation at 18,400 g at 4°C for 30 min, the upper phase was transferred to a new tube containing 0.5 ml of isopropanol. After mixing by inversion, samples were left on ice for 10 min and centrifuged at 18,400 g at 4°C for 30 min. The supernatant was discarded and the pellet was washed two times with 1 ml 75% ethanol and centrifuged at 12,000 g, 4°C for 10 min. After drying the pellet, it was dissolved in nuclease free water. mRNA concentrations were determined on a Nanodrop 2000 UV-Vis spectrophotometer (Thermo Fisher Scientific Inc., Waltham, Massachusetts MA 02451, USA).

Reverse transcription

All mRNA was reverse transcribed with the Quantitect Reverse Transcription Kit according to the manufacturer's instructions.

Quantitative polymerase chain reaction

Fgf21 mRNA expression in C2C12 cells and primary muscle fibers was determined by qPCR on a Viia7 cycler (Applied Biosystems / Thermo Fisher Scientific Inc., Waltham, Massachusetts MA 02451, USA) using Taqman MasterMix and Taqman probes for *Fgf21* and *Hprt*. In all other cases, mRNA expression was measured with the same machine using SybRGreen Master Mix and the respective primers (10 µM) as listed in Table 5. Target gene expression was normalized to *Hprt* expression unless otherwise stated and mRNA fold induction compared to the respective control conditions was calculated with the delta delta Ct method.

2.2.4 Immunological detection of Fgf21 in conditioned media

The amount of Fgf21 secreted to culture media was determined with an Fgf21 ELISA Kit according to the manufacturer's instructions.

2.2.5 Mass spectrometric analysis

Collection of samples:

Conditioned media were collected after 8 h (C2C12 myotubes) or 16 h (primary muscle fibers) of treatment and centrifuged at 500 g for 5 min in order to spin down any floating cells. In case of the primary muscle fibers, the conditioned medium was furthermore centrifuged at 10,000 g for 10 min at 4°C. The supernatant was collected as conditioned media and the lower phase was collected as the vesicle enriched fraction. The protein concentration of all samples was determined with Roti nanoquant according to the manufacturer's instructions.

Sample preparation and LC-MS/MS analysis were performed by Dr. Stefanie Hauck and Dr. Christine von Törne from the Research Unit Protein Science at Helmholtz Zentrum München as follows.

MS sample preparation

The supernatants were digested applying a modified FASP procedure. Samples were diluted by adding 400 µl UA buffer (8 M urea in 0.1 M Tris/HCl pH 8.5). For protein reduction, 10 µl of 100 mM DTT were added to the samples and incubated for 30 minutes at 60°C. After cooling, 10 µl of freshly prepared 300 mM iodacetamide solution were added for 30 min at room temperature in the dark. Samples were centrifuged on a 30 kDa cut-off filter device (PALL) and washed thrice with UA buffer and twice with 50 mM ammoniumbicarbonate (ABC). Proteins

were digested in 50 µl of 50 mM ABC for 2 h at room temperature using 1 µg Lys-C (Wako) and subsequently for 16 h at 37°C using 2 µg trypsin (Promega). Peptides were collected by centrifugation and filters were washed with 100 µl 50 mM ABC/2% ACN. Samples were acidified with 0.5% trifluoroacetic acid (TFA) and analyzed on the OrbitrapXL as described.

Mass spectrometry

Before loading, the samples were centrifuged for 5 minutes at 4°C. LC-MS/MS analysis was performed as described previously on a LTQ-Orbitrap XL (Thermo Scientific). Briefly, samples were automatically injected and loaded onto the trap column and after 5 min, the peptides were eluted and separated on the analytical column separation by reversed phase chromatography operated on a nano-HPLC (Ultimate 3000, Dionex). A nano trap column was used (300 µm inner diameter × 5 mm, packed with Acclaim PepMap100 C18. 5 µm, 100 Å; LC Packings, Sunnyvale, CA) before separation by reversed phase chromatography (PepMap, 25 cm, 75 µm ID, 2 µm/100 Å pore size, LC Packings) operated on a RSLC (Ultimate 3000, Dionex, Sunnyvale, CA) using a nonlinear 300 min LC gradient from 3% to 40% of buffer B (98% acetonitrile) at a 300 nl/min flow rate followed by a short gradient from 40 to 95% buffer B in 5 min and an equilibration for 15 min to starting conditions. From the MS prescan, the 10 most abundant peptide ions were selected for fragmentation in the linear ion trap if they exceeded an intensity of at least 200 counts and were at least doubly charged. During fragment analysis a high-resolution (60000 full-width half maximum) MS spectrum was acquired in the Orbitrap with a mass range from 300 to 1500 Da.

Protein identification and label-free relative quantification

The RAW files (Thermo Scientific) were further analyzed using the Progenesis LC-MS (v4.1, Nonlinear Dynamics), as described previously, with the following changes: Spectra were searched using the search engine Mascot (version 2.4, Matrix Science) against the Ensembl mouse database (release 72; 51372 sequences). Search parameters used were: 10 ppm peptide mass tolerance and 0.6 Da fragment mass tolerance, one missed cleavage allowed, carbamidomethylation was set as fixed modification, methionine oxidation and asparagine or glutamine deamidation were allowed as variable modifications. A Mascot-integrated decoy database search using the Percolator algorithm calculated an average peptide false discovery rate of < 1% when searches were performed with a Percolator score cut-off of 13 and a significance

threshold of $p < 0.05$. Peptide assignments were re-imported into Progenesis LC-MS. Normalized abundances of all unique peptides were summed up and allocated to the respective protein.

2.2.6 Analysis of the secretomic datasets

Dr. Stefanie Hauck and Dr. Christine von Törne provided me with the lists of proteins and peptides for further analyses.

Gene set enrichment analysis and generation of heatmaps

Gene set enrichment analysis was performed with GSEA v2.2.1 [167] with standard settings except from the minimum gene set size which was set to 10. Kyoto Encyclopedia of Genes and Genomes (KEGG) pathway [168] and Gene Ontology (GO) term [169] databases were used in version v5.1 that was implemented in the software (c2.cp.kegg.v5.1.symbols.gmt, c5.all.v5.1.symbols.gmt). Enrichment analysis for KEGG pathways and GO terms irrespective of group affiliation or protein concentration was performed with Enrichr [170] with the databases of June 2016.

The heatmaps of the 30 top up- and down-regulated proteins were generated with GenePattern [171] using default settings.

Prediction of classical and non-classical secretion

The browser based tools SignalP [172, 173] and SecretomeP [174] were used to predict whether the proteins are secreted via classical or non-classical secretion based on FASTA-sequences of the respective proteins.

Correlation analysis

Normalized abundances of all proteins contained in the C2C12 secretome were correlated with the normalized abundance of Fgf21 using GraphPad Prism 6. For proteins with significant Pearson correlation (R squared>0.5, $p<0.05$), linear regression analysis was performed using GraphPad Prism 6.

Comparison of the three secretomic datasets

For comparison of the three datasets, the secretomes of C2C12 myotubes and primary muscle fibers as well as the vesicle-enriched fraction of the fiber secretome were merged in Microsoft Excel 2010 using the Ensembl protein ID given for each protein as a common identifier.

Comparison with published datasets

The datasets were compared with a published putative secretome by Eichelbaum and colleagues [175] based on gene symbols using Microsoft Excel 2010.

Further, the secretomes were searched for proteins located in mitochondria using the MitoCarta 2.0, a compendium of proteins that are located in mitochondria [176]. The comparison was based on gene symbols and performed with Microsoft Excel 2010.

For comparison with a set of proteins that was published to be secreted from muscle via microparticles, the "Proteome of muscle-derived Microparticles" [27] was compared with the vesicle-secretome of primary muscle fibers based on gene symbols using Microsoft Excel 2010.

2.2.7 Statistical analysis

Statistical analysis was performed with GraphPad Prism 6. If not stated otherwise, all data that were following a Gaussian distribution were tested for significant differences between two groups by t-test, while experiments with more than two groups were tested for significant differences by ordinary one-way ANOVA and Tukey's multiple comparisons test. If data did not follow a Gaussian distribution, Mann-Whitney test was used to compare two groups and Kruskal-Wallis test combined with Dunn's multiple comparisons test were used to compare more than two groups.

3. Results

3.1 Irisin alters neither cellular respiration nor Ucp1 mRNA expression in human SGBS adipocytes

Irisin was reported to be a myokine capable of browning murine white adipocytes [70]. In order to consolidate whether irisin can induce browning in human white adipocytes, SGBS preadipocytes were differentiated to adipocytes and treated with 20 nM of either synthesized irisin or native irisin for 1 hour, 1 day or 2 days. Neither synthesized nor native irisin altered *Ucp1* mRNA expression as determined by qPCR (Figure 3a).

Further, cellular respiration of SGBS adipocytes that were treated with 20 nM or 100 nM of synthesized or native irisin for 1 hour, 1 day or 2 days was measured in a XF extracellular flux analyzer (Figure 3b-i). Although basal respiration, ATP production-linked respiration, and maximal respiratory capacity trended towards higher rates in irisin-treated cells, the differences did not reach statistical significance and this trend was not seen with longer incubation times (3 e, f, h). Coupling efficiency, which is the proportion of basal respiration that is consumed by ATP synthesis (ATP production related respiration divided by basal respiration), was not altered in any of the irisin-treated groups. Additionally, differentiation rates were determined by staining lipid droplets with Nile Red and normalizing the fluorescence intensity with that of DAPI-stained nuclei. No difference was visible between irisin treated and control groups (Figure 3j).

Although a browning effect of irisin was observed in murine adipocytes [70], it could not be reproduced in human subcutaneous adipocytes in this study. As other factors such as Fgf21 have been shown to induce browning of WAT [108], this study continued with the aim to identify new myokines using alternative approaches.

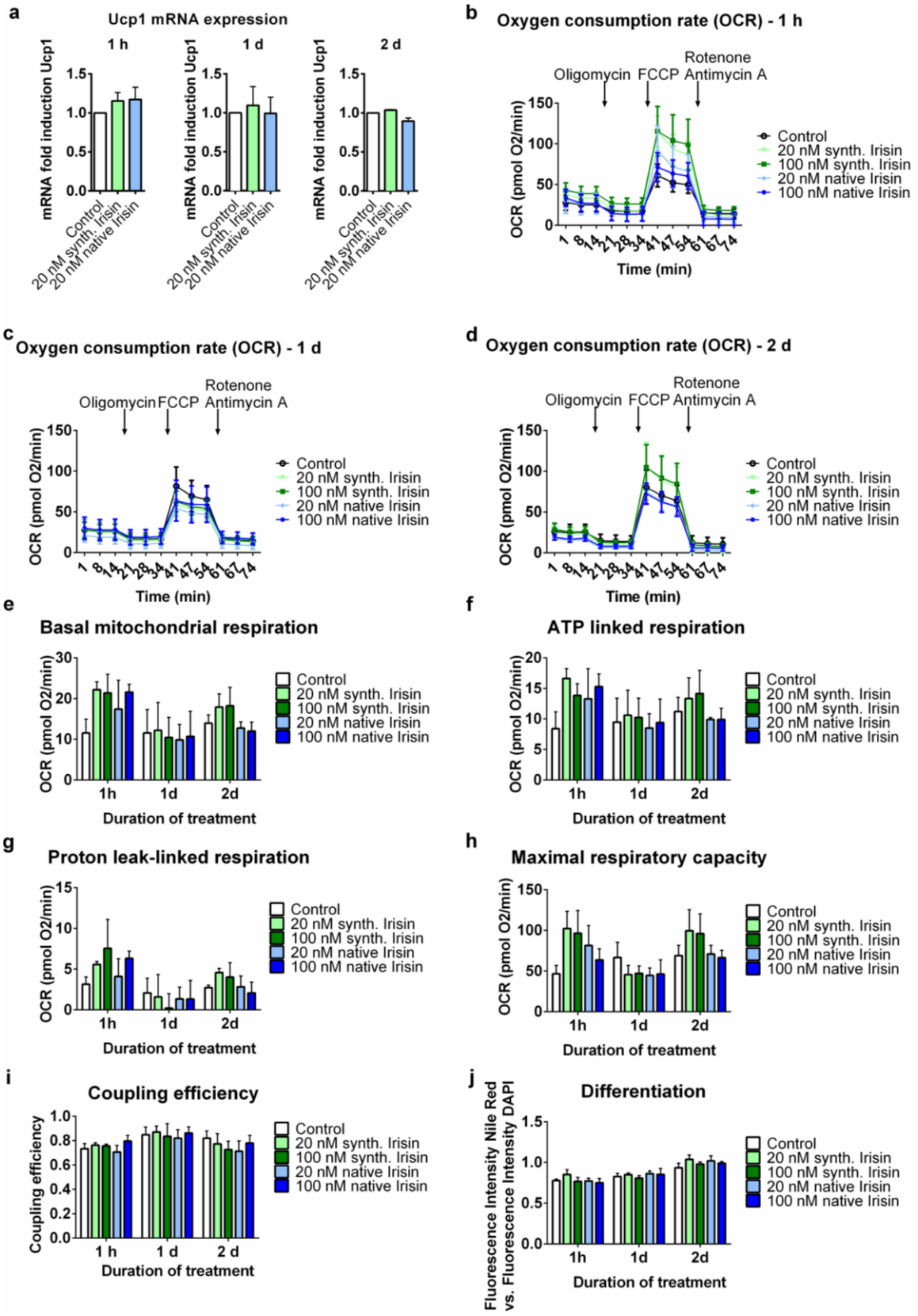

Figure 3: Irisin does not increase *Ucp1* expression or oxygen consumption in human SGBS adipocytes. Human SGBS adipocytes were treated with synthesized or native (glycosylated) Irisin for 1 h, 1 day or 2 days. *Ucp1* mRNA expression was

measured by qPCR and was not significantly altered by irisin treatment (a). Further, respiratory flux was monitored on an XF96 extracellular flux analyzer (b-d). Basal mitochondrial respiration (e), ATP-production linked respiration (f), Proton leak-linked respiration (g), Maximal respiratory capacity (h) and coupling efficiency (i.e. ATP production linked respiration/basal respiration) (i) were calculated based on the oxygen consumption rates measured, but were not altered significantly by irisin treatment. Differentiation of the adipocytes was approximated by normalizing NileRed staining of lipid droplets with DAPI staining for nuclei and was not altered by irisin treatment (j). All data are shown as mean ± standard error of mean representing n=3 independent experiments.

3.2 Nutrient deprivation compromises the energy metabolism of C2C12 myotubes and induces Fgf21 expression and secretion

C2C12 cells were used to achieve conditions of robust Fgf21 expression and secretion. As previously shown Fgf21 is induced in states of low cellular energy. For example, Kim and colleagues showed *Fgf21* mRNA expression to be induced in C2C12 myotubes by 0.5 µM rotenone or 4 µM antimycin A which inhibit complexes I and III of the mitochondrial electron transport chain, respectively [23]. A pilot experiment was aimed at reproducing those results. Additionally, the effects of the following treatments were tested: myxothiazol (4 µM), which is a complex III inhibitor, a combination of antimycin A (4 µM) and rotenone (0.5 µM), and a combination of antimycin A (4 µM) and oxamate (10 mM). Oxamate is an inhibitor of lactate dehydrogenase and therefore glycolysis [177]. All of the aforementioned conditions tended to increase *Fgf21* mRNA levels in C2C12 myotubes after 8 h of treatment (Fig. 4a). In order to decrease off-target effects, the concentration of the mitochondrial inhibitors was lowered to 100 nM. Furthermore, the C2C12 myotubes were treated with 1 µM tunicamycin inducing endoplasmic reticulum stress, which is known to induce *Fgf21* expression [178]. Energy shortage is a known inducer of *Fgf21* expression. Therefore, the myotubes were deprived of glucose and l-glutamine, which are usually contained in their culture medium, to find out whether lack of substrate is sufficient to induce *Fgf21*. Indeed, the highest mRNA induction of *Fgf21* was seen with nutrient deprivation (13-fold, Fig. 4b). Thus, the experiment was repeated comparing only nutrient deprived with control cells and the conditioned culture media were collected after 8 h of treatment. A Fgf21-specific ELISA revealed Fgf21 secretion to be increased 5-fold after 8 h of nutrient deprivation (Fig 4c). In all experiments combined, nutrient deprivation induced *Fgf21* mRNA expression 24-fold (Fig. 4d).

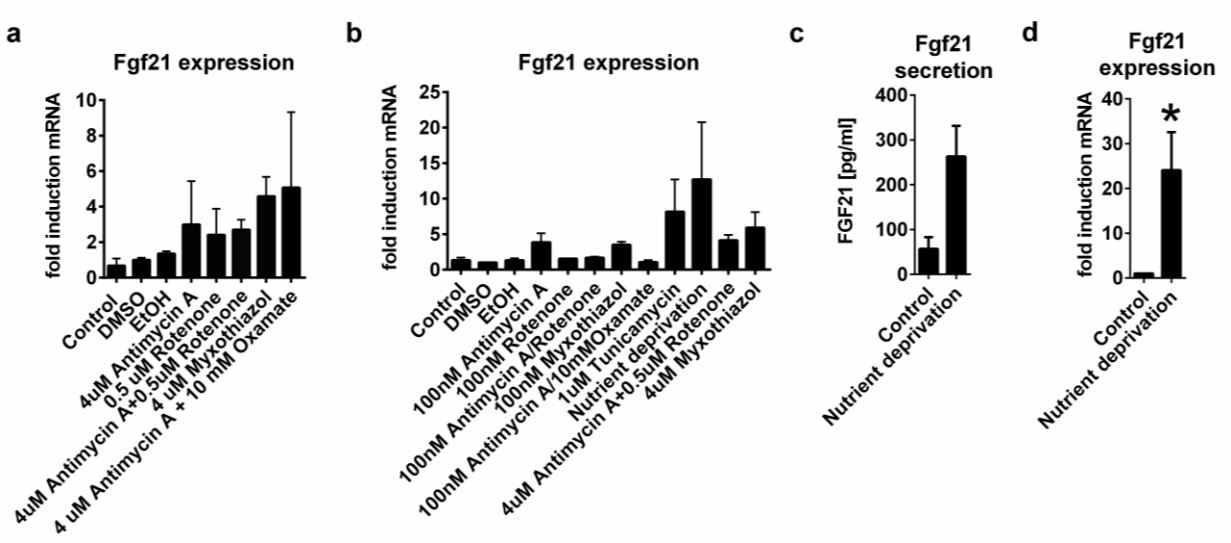

Figure 4: Nutrient deprivation for 8h induces *Fgf21* mRNA expression and secretion from C2C12 myotubes. a) C2C12 myotubes were treated with the mitochondrial inhibitors, 0.5 µM rotenone, 4 µM antimycin A or myxothiazol, or 10 mM oxamate, an inhibitor of glycolysis, in serum-containing culture medium and *Fgf21* mRNA expression was determined by qPCR. b) Under serum-free conditions, C2C12 myotubes were treated with the same mitochondrial inhibitors as in (a) at the same and lower (100 nM) concentrations. Additionally, the cells were treated with 1 µM tunicamycin, which induces endoplasmic reticulum stress, and were deprived of l-glutamine and glucose which are contained in the normal culture medium ("nutrient deprivation"). The highest induction of *Fgf21* mRNA expression was seen with nutrient deprivation and was indicative of increased secretion of Fgf21 from the C2C12 myotubes as determined with an Fgf21-specific ELISA (c). However, it only reached statistical significance when repeated n>3 (d) All treatments were performed for 8 h. All data are shown as mean ± standard error of mean representing n=2 in (a), n=3 in (b), n=3-4 in (c) and n=9-10 in (d). *$p<0.05$ in an unpaired t-test.

In order to find out to which extend nutrient deprivation compromises their bioenergetic status, oxygen consumption rates (OCR) and extracellular acidification rates (ECAR) of C2C12 myotubes were monitored on an XF24 extracellular flux analyzer acutely after 30 min of nutrient deprivation or after prolonged (4 h, 8 h, 12 h, 24 h) nutrient deprivation. Nutrient deprivation induced an immediate decrease in glycolysis represented by ECAR (Fig. 5a). This lack of glycolysis appeared to be first compensated by increased mitochondrial turnover, represented by a tendency of increased OCR (Fig. 5b-c). This observation is consistent with the Crabtree effect describing the inverse relationship of glucose concentration and oxidative phosphorylation [179]. With prolonged nutrient deprivation, however, mitochondrial respiration and ATP production were progressively compromised until reaching levels below reliable detection after 24 h (Fig. 5b-c).

After 8 h of nutrient deprivation, the cells were bioenergetically compromised, but still responded to the compounds used to perform the mitochondrial stress test, which was no longer the case after 12 or 24 h of nutrient deprivation (Fig. 5b). Furthermore, they still showed normal morphology after this time period (Fig. 6). Therefore, the C2C12 myotubes were treated for 8 h in all further experiments.

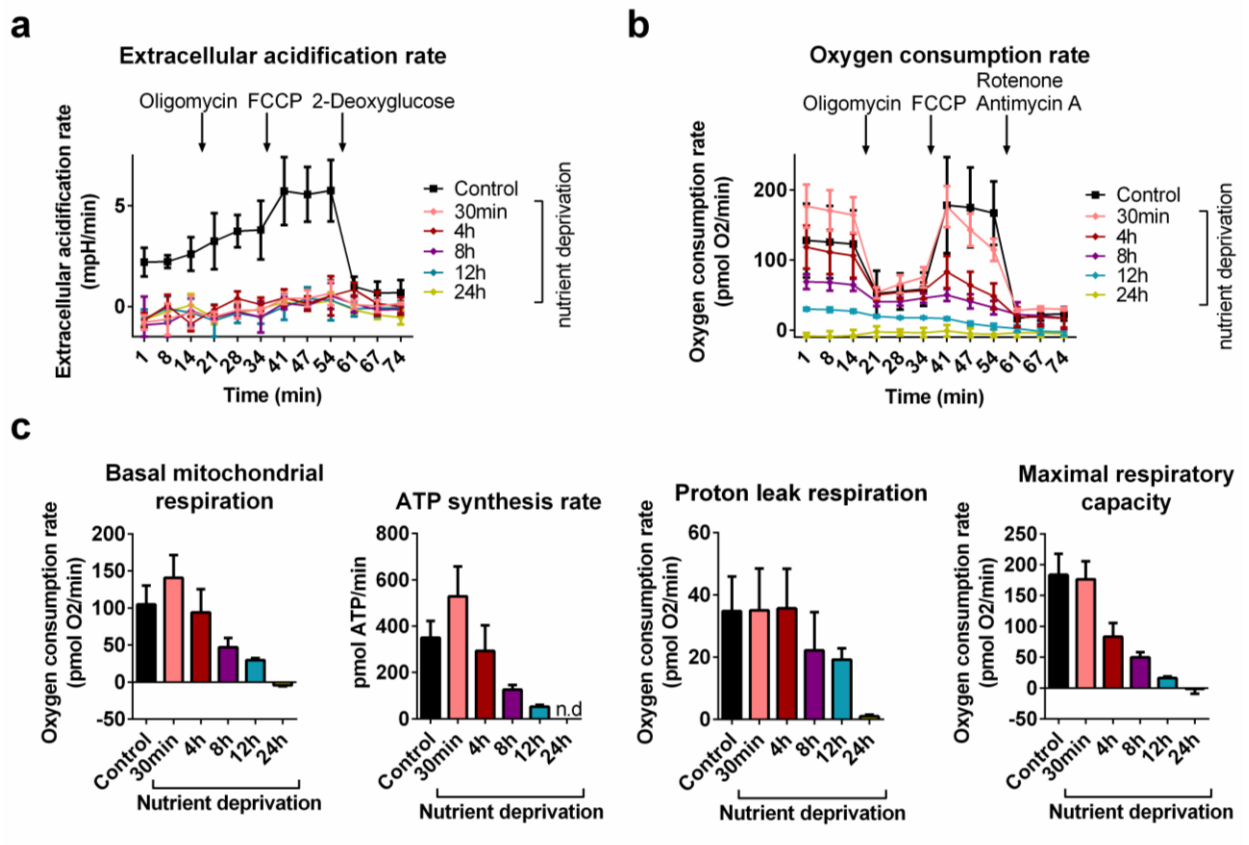

Figure 5: Prolonged nutrient deprivation progressively compromises mitochondrial respiration and ATP production in C2C12 myotubes. C2C12 myotubes were deprived of glucose and l-glutamine for 30 min, 4 h, 8 h, 12 h or 24 h. Respirometry revealed an immediate decrease in glycolysis, represented by the extracellular acidification rate (ECAR, a) which was first compensated by a slight increase in oxidative phosphorylation (b, c). With prolonged nutrient deprivation, basal, proton leak-linked, and maximal respiration as well as ATP production were progressively compromised until reaching levels below reliable detection after 24 h (c). Basal, ATP production-linked, proton leak-linked, and maximal respiration were calculated from oxygen consumption rates (OCR) measured on a XF24 extracellular flux analyzer. ATP production was calculated from the ATP production-linked respiration rates assuming a stoichiometry of 5 mol ATP per mol O2 [166]. All data are shown as mean ± standard error of mean and represent n=3 independent experiments.

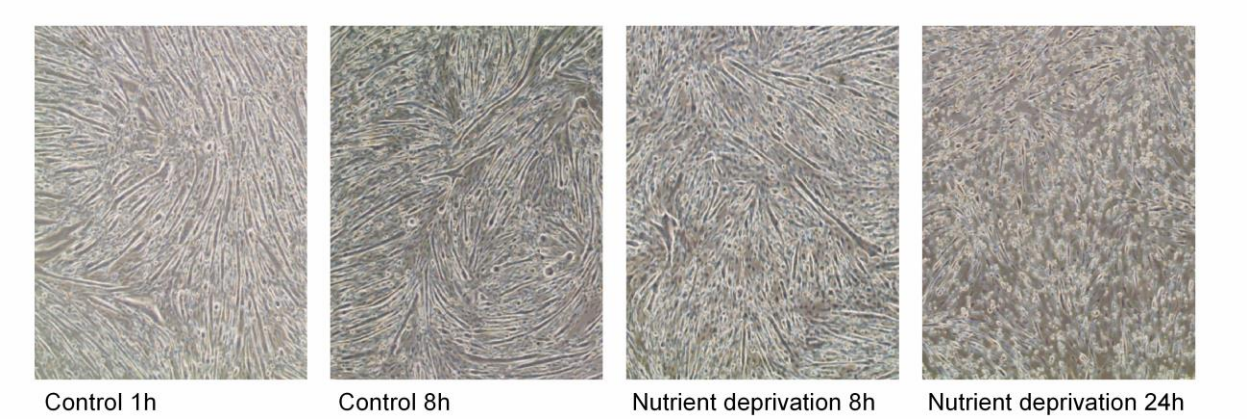

Figure 6: 8h nutrient deprivation does not induce morphological changes or visible cell death in C2C12 myotubes. C2C12 myotubes were incubated in normal culture medium or medium without glucose and l-glutamine for 1h, 8h, or 24h. Representative pictures were chosen for each condition.

3.3 Nutrient deprivation induces a distinct secretome in C2C12 myotubes

Assuming that nutrient deprivation does not only induce Fgf21 expression and secretion but a complex program of secreted factors, conditioned media of C2C12 myotubes that were deprived of nutrients for 8 h and control cells supplied with glucose and l-glutamine were collected for unbiased label-free mass spectrometric analysis. LC-MS/MS analyses were performed by Dr. Stefanie Hauck and Dr. Christine von Törne who provided me with the lists of proteins and peptides for further analyses. 1497 different proteins encoded by 1481 different genes were identified in the conditioned culture media by LC-MS/MS-analysis. The 25 proteins with the strongest significant up- and downregulation, respectively, are shown in a heatmap sorted by fold change (Fig. 7a). Gene Set Enrichment Analysis was performed with GSEA v2.2.1 [167] with default settings and a minimum gene set size of 10 using the Kyoto Encyclopedia of Genes and Genomes (KEGG) pathway [168] and Gene Ontology (GO) term [169] database version 5.1 as implemented in the software. In conditioned media of control cells, the KEGG pathway "Ribosome" as well as the GO terms "Cell surface", "Negative regulation of cell proliferation", "Microtubule associated complex", "Oxidoreductase activity acting on CH OH group of donors", "Carbohydrate metabolic process", "Cellular carbohydrate metabolic process", and "Exopeptidase activity" were significantly enriched. In conditioned media of nutrient deprived cells, the KEGG pathway "Proteasome" as well as the GO terms "Structural molecule activity", "Structural constituent of ribosome", "Positive regulation of catalytic activity", and "Translation" were significantly enriched.

3.3.1 Filtering the secretome by bioinformatic prediction of secretion

In order to exclude proteins that were not secreted but might have originated from disrupted cells, the list of proteins was analyzed with the bioinformatics tools SignalP [172] and SecretomeP [174]. SignalP identifies proteins secreted via the classical pathway requiring an N-terminal signal peptide that targets the protein to the endoplasmic reticulum based on their respective FASTA sequences. SecretomeP identifies proteins that are secreted via non-classical secretion pathways. In addition, the C2C12 secretome was compared to a putative secretome published by Eichelbaum and colleagues [175]. SignalP identified 372 proteins to be secreted via classical secretion and SecretomeP identified 451 proteins to be secreted via non-classical pathways. 363 proteins identified in conditioned media of C2C12 myotubes were also contained in the putative secretome published by Eichelbaum *et al*. [175]. Of those 363 proteins, 320 were also identified by SignalP and 23 were also identified by SecretomeP. In total, 843 of the proteins were predicted and/or published to be secreted, which in the following will be referred to as secretory, while no evidence for secretion was found for 654 proteins (Fig. 7b).

93 (59 secretory, 63%) proteins were significantly upregulated ($p < 0.05$, fold induction > 1.3) by 8 h of nutrient deprivation, while 123 (71 secretory, 58%) proteins were significantly downregulated ($p < 0.05$, fold induction < 0.769). 1280 (712 secretory, 56%) proteins were not significantly altered (Fig. 7c). This indicates that 8 h of nutrient deprivation did not lead to an increased proportion of ruptured cells. Notably, one of the strongly induced secretory proteins was Fgf21, confirming the results of our previous experiments (Fig. 7d).

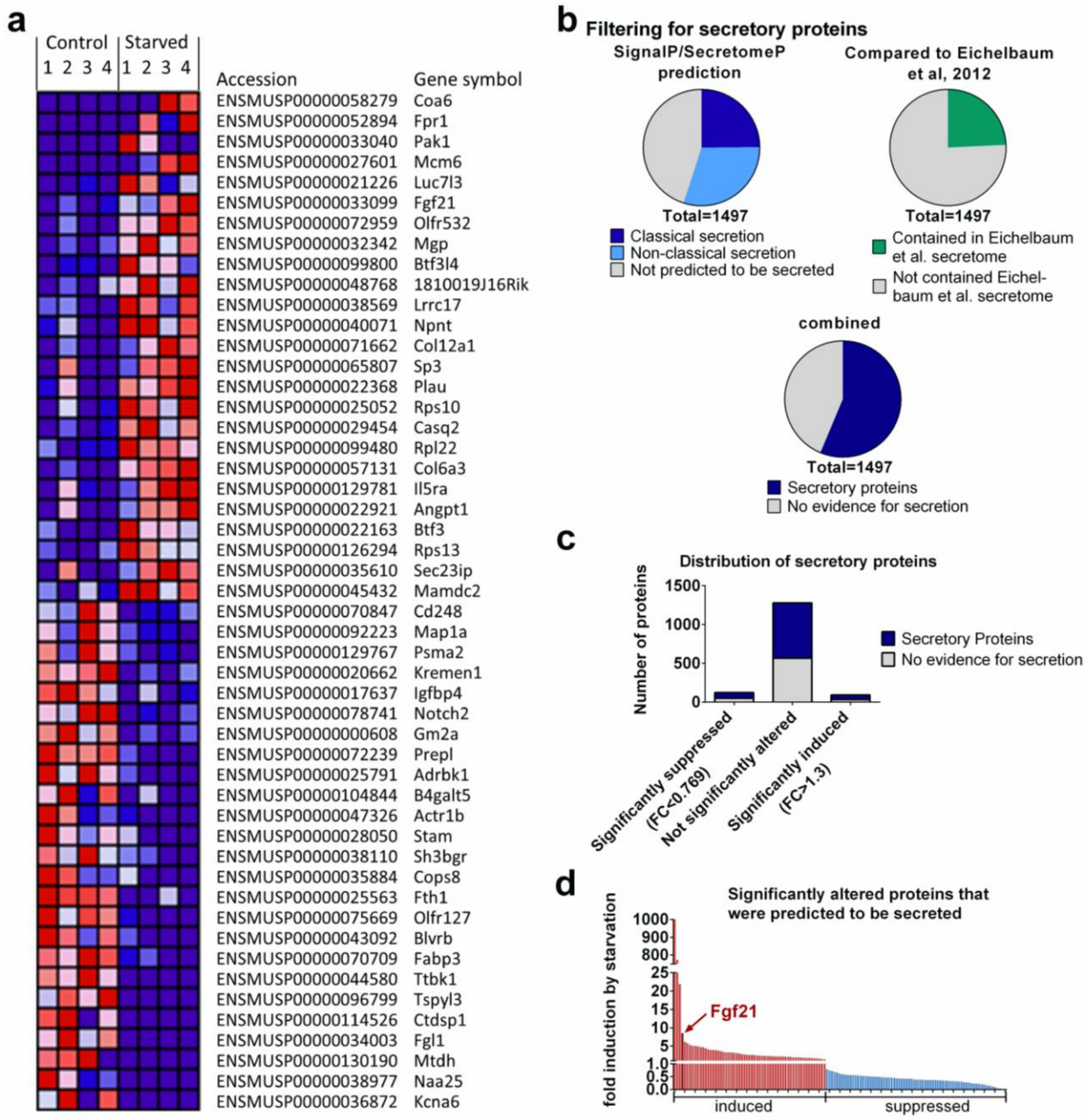

Figure 7: Nutrient deprivation induces the secretion of 843 potential myokines in C2C12 myotubes. Conditioned media of control and nutrient deprived cells were collected after 8 h of treatment and subjected to unbiased proteomic analysis (n=4). In total, 1497 proteins were identified. The top 25 proteins induced and suppressed by 8 h of nutrient deprivation are shown in the heatmap sorted by fold change (a). b) SignalP and SecretomeP were used to predict classical and non-classical secretion of all proteins identified (upper left panel). Furthermore, they were compared to a published putative human secretome [175] (upper right panel). A total of 843 proteins were classified as secretory proteins with both approaches combined (lower panel). The levels of the majority of those proteins are not altered by nutrient deprivation (c) showing that the identified proteins are released via a controlled mechanism rather than from cellular rupture induced by the treatment. In (d) all secretory proteins that were significantly altered by nutrient deprivation for 8 h are shown.

3.3.2 Filtering the secretome by correlation with Fgf21 protein abundance

Based on the hypothesis that along with Fgf21 expression and secretion a whole starvation/hunger signaling program would be induced within the stress-induced secretome, the normalized protein abundance of Fgf21 was correlated with the normalized protein abundance of the other proteins that were identified in the conditioned media of nutrient deprived vs. control C2C12 myoblasts. Secretion levels of 123 proteins significantly correlated with the secretion levels of Fgf21 ($p < 0.05$, R squared > 0.5). Among those proteins, 95 proteins were predicted to be secreted, of which 23 were significantly induced by 8 h of nutrient deprivation (Fig. 8a-f), namely angiopoietin 1 (Angpt1), annexin A1 (Anxa1), annexin A2 (Anxa2), cytochrome c oxidase assembly factor 6 (Coa6), collagen, type XII, alpha 1 (Col12a1), collagen, type VI, alpha 3 (Col6a3), cytochrome c oxidase, subunit VIb polypeptide 1 (Cox6b1), cysteine rich protein 61 (Cyr61), fibronectin 1 (Fn1), formyl peptide receptor 1 (Fpr1), perlecan/heparan sulfate proteoglycan 2 (Hspg2), HtrA serine peptidase 1 (Htra1), interleukin 5 receptor, alpha (Il5ra), laminin, gamma 1 (Lamc1), latent transforming growth factor beta binding protein 3 (Ltbp3), olfactory receptor 532 (Olfr532), plasminogen activator, urokinase (Plau), ribosomal protein L38 (Rpl38), ribosomal protein S12 (Rps12), ribosomal protein S28 (Rps28), trans-acting transcription factor 3 (Sp3), transforming growth factor, beta 2 (Tgfb2), and von Hippel-Lindau binding protein 1 (Vbp1). These proteins might represent potential myokines signaling lack of nutrients in concert with Fgf21.

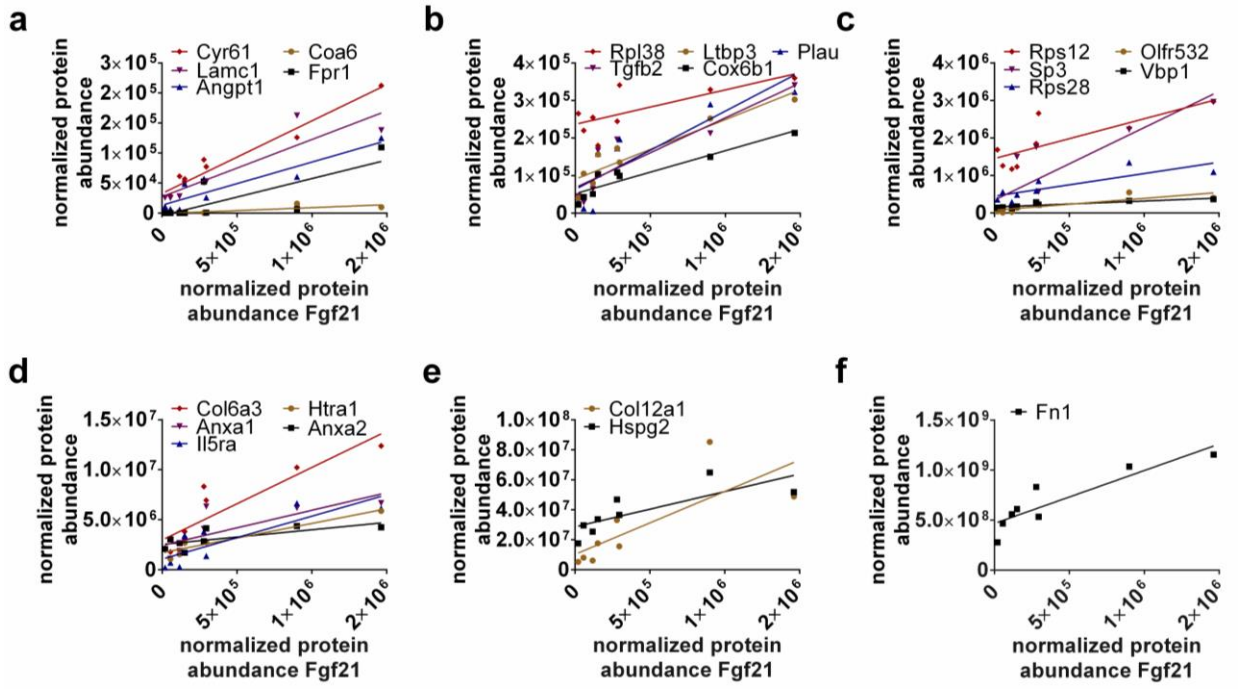

Figure 8: Secretion levels of 23 proteins are induced upon 8h of nutrient deprivation and correlate with Fgf21 secretion levels from C2C12 myotubes. The relative abundances of all proteins contained in the C2C12 secretome were correlated with those of Fgf21. Of the 123 proteins significantly correlating with Fgf21 protein abundance (Pearson R square >0.5, p>0.05), only the 23 secretory proteins that were significantly induced by nutrient deprivation (fold induction > 1.3, p<0.05) are shown and sorted by their normalized protein abundances (a-f).

3.4 Induction of *Fgf21* gene expression in primary muscle fibers by myxothiazol treatment

In order to explore a skeletal muscle secretome that better resembles the physiological state than an immortalized cell line, primary muscle fibers were isolated from the hind limb of C57BL/6J mice. When they were deprived of nutrients extracellular acidification rates (indicative of glycolysis) and oxygen consumption rates after 16 h tended to decrease (Fig. 9a-c). However, this condition was not sufficient to induce *Fgf21* expression on mRNA level (Fig. 9d) and Fgf21 secretion was below detection limit of the ELISA for all conditions. It was hypothesized that ATP production in the fibers is low under normal conditions and small decreases in ATP production by nutrient deprivation did not energy-deplete the fibers causing stress responses including Fgf21 induction. Therefore, primary muscle fibers were deprived of energy by inhibition of complex III of the electron transport chain with 100 nM of myxothiazol. This inhibited extracellular acidification and respiratory flux almost completely (Fig. 9a-c). Furthermore, 16 h of myxothiazol treatment induced *Fgf21* mRNA expression by 3-fold (Fig. 9d). However, no Fgf21 secretion was detected by ELISA from control or treated muscle fibers.

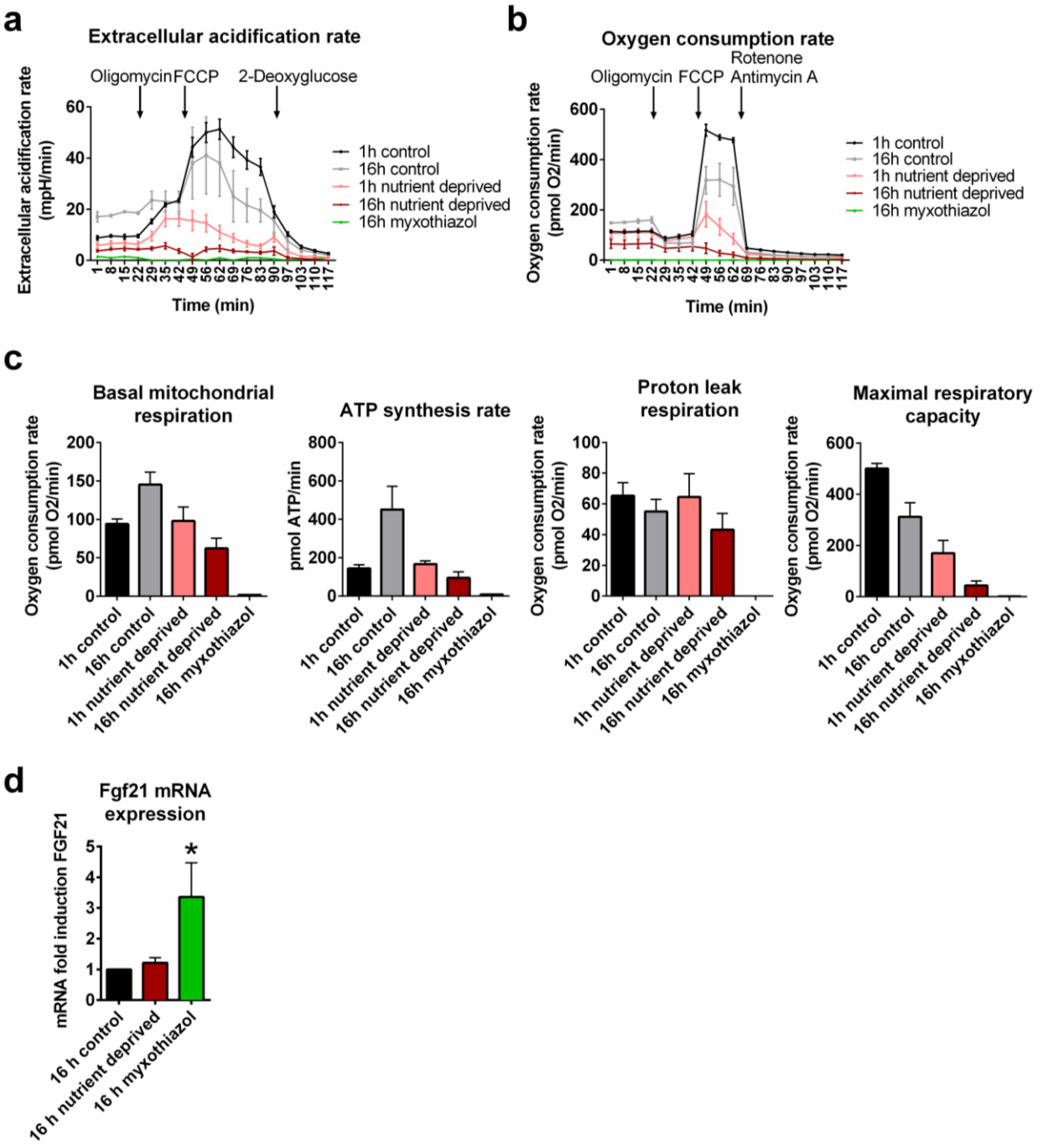

Figure 9: Myxothiazol treatment completely inhibits mitochondrial respiration and induces *Fgf21* mRNA expression in primary muscle fibers. Primary muscle fibers were isolated from the interossei muscle of C57BL/6J mice. Control fibers were incubated in medium containing 2 mM Pyruvate and 15 mM Glucose. For myxothiazol treatment 100 nM myxothiazol were added. Nutrient deprived fibers were deprived of pyruvate and glucose. Extracellular flux analysis was performed after 1 h or 16 h of incubation. Extracellular acidification rates (ECAR, a), and oxygen consumption rates (OCR, b) tended to be decreased by nutrient deprivation and were abolished by myxothiazol treatment. (c) Basal mitochondrial respiration, ATP production-linked respiration, maximal respiration, and proton leak-linked respiration were calculated from the Oxygen consumption rates measured on an XF96 Seahorse Extracellular Flux Analyser. ATP production rates were calculated from the ATP linked respiration rates assuming a stoichiometry of 5 mol ATP per mol O2 (Brand, 2005). (d) Myxothiazol treatment but not nutrient deprivation induces *Fgf21* mRNA expression as determined by qPCR: (a-c) Data are shown as mean ± standard error of mean representing n=2-4, (d) Data are shown as mean ± standard error of mean representing n=5-7. *p<0.05 in a one-way ANOVA with Tukey's multiple comparisons test.

3.5 Myxothiazol treatment induces a distinct secretome in primary muscle fibers

In order to analyze their secretome, primary muscle fibers were incubated in assay medium aCSF containing 15 mM glucose and 2 mM pyruvate for 16 h. Both control and myxothiazol treated fibers appeared to shed vesicles from their surface (Fig. 10). Hypothesizing that the vesicles are released in a targeted way contributing to the secretory machinery of the primary muscle fibers, those vesicles were enriched by differential centrifugation and the supernatant and the vesicle-enriched fraction were subjected to LC-MS/MS separately. Mass spectrometric analysis was again performed by Stefanie Hauck and Christine von Törne who provided me with the lists of proteins and peptides for further analyses.

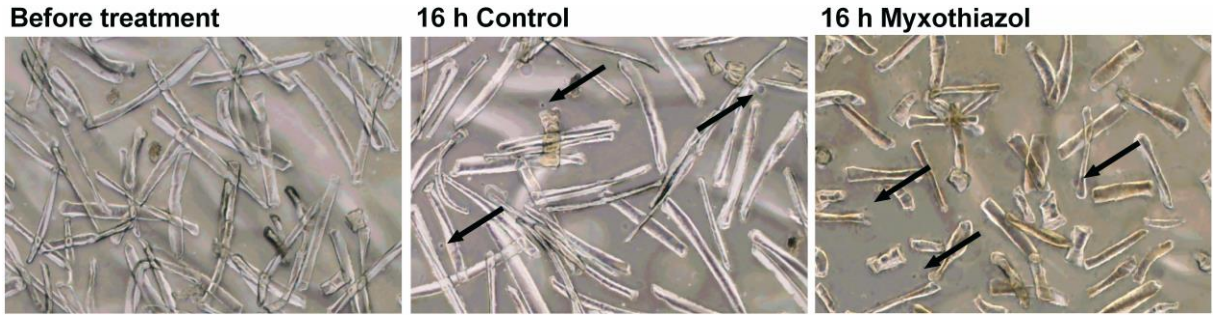

Figure 10: Primary muscle fibers shed vesicles from their surface. After 16 h of incubation, vesicles are visible around primary muscle fibers and in the culture medium (indicated by black arrows). Further, myxothiazol visibly stresses primary muscle fibers and induces shrinking of the fibers. Representative images were chosen for each condition.

3.5.1 The myxothiazol-induced secretome of primary muscle fibers I: medium fraction

Tandem mass spectrometric analysis of conditioned media of primary muscle fibers after 16 h of treatment with 100 nM myxothiazol vs. control fibers identified 646 proteins, of which the top 25 up- and downregulated are shown in the heatmap sorted by fold induction through myxothiazol (Fig. 11a). Fgf21 was not detected which was consistent with the results of the Fgf21 ELISA. Gene set enrichment analysis showed the GO terms for “Response to stress”, “Signal transduction”, “Cell surface receptor linked signal transduction GO 0007166”, “DNA metabolic process”, “Biopolymer metabolic process”, “Post translational protein modification”, “Biopolymer modification”, and “Protein modification process” to be enriched in conditioned media of myxothiazol treated muscle fibers. In conditioned media of control fibers, there were no GO terms or KEGG pathways found to be significantly enriched.

336 proteins were predicted to be secreted by either analysis with SecretomeP or SignalP or were also contained in the putative human secretome published by Eichelbaum and colleagues [175] (Fig. 11b). In total, 412 proteins were significantly induced by 16 h myxothiazol treatment, of which 198 proteins were predicted or published to be secreted (48%). 82 (61 secretory, 74%) proteins were significantly decreased by myxothiazol treatment, whereas 152 (77 secretory, 51%) proteins were not significantly altered (Fig. 11c).

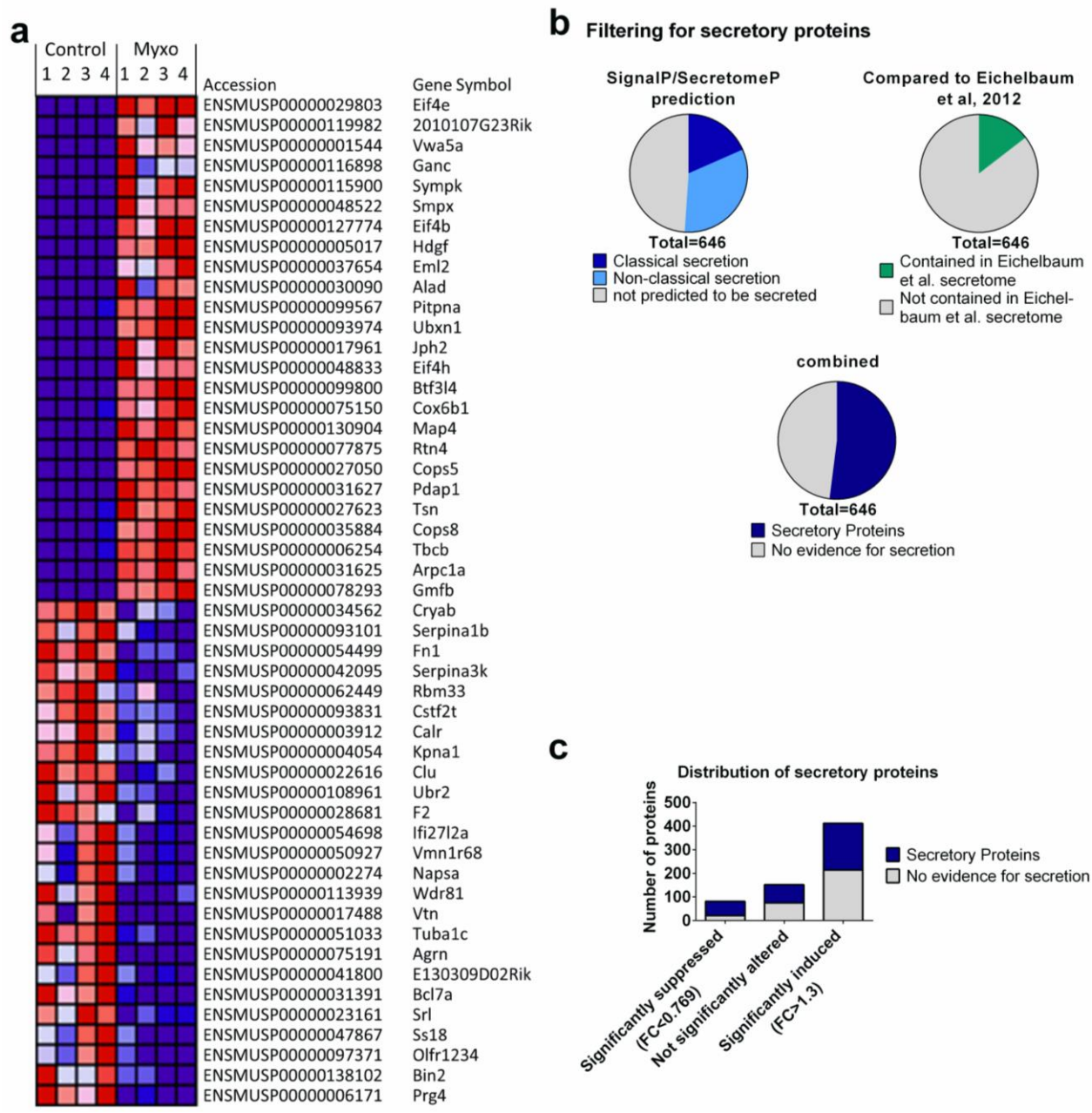

Figure 11: Myxothiazol treatment induces the secretion of 336 potential myokines from primary muscle fibers directly to the culture medium. Conditioned media of control vs. myxothiazol treated fibers were collected after 16 h of incubation. Vesicles were separated from the medium by centrifugation and the supernatant ("medium fraction") was subjected to unbiased proteomic analysis (n=4). In total, 646 proteins were detected. The top 25 proteins induced and suppressed by 8 h of myxothiazol treatment are shown in the heatmap sorted by fold change (a). b) SignalP and SecretomeP were used to predict classical and non-classical secretion of all proteins identified (upper left panel). Furthermore, they were compared to a published putative human secretome [175] (upper right panel). In total, 336 proteins were classified as secretory proteins with both approaches combined (lower panel). The majority of secretory and non-secretory proteins was induced by myxothiazol treatment (c).

3.5.2 The myxothiazol-induced secretome of primary muscle fibers II: vesicle-enriched fraction

In the vesicle-enriched fraction, 704 proteins were identified by LC-MS/MS, of which the top 25 up- and downregulated are shown in the heatmap (Fig. 12a) sorted by fold induction through myxothiazol treatment. Gene Set Enrichment Analysis found no GO terms and only one KEGG pathway ("Small cell lung cancer") to be enriched in control fiber vesicles. In vesicles of myxothiazol treated fibers, the GO terms for "DNA Metabolic Process", "Nucleobase, nucleoside, nucleotide, and nucleic acid metabolic process", "Signal transduction", "Intracellular signaling cascade", "Regulation of metabolic process", "Biopolymer metabolic process", "Proteasome complex", "Regulation of cellular metabolic process", and "Transcription" as well as the KEGG pathway "Proteasome" were enriched.

339 of the proteins identified in the vesicles were predicted or published to be secreted (Fig. 12b), of which the majority was induced by myxothiazol treatment (Fig. 12c). In addition to the prediction of secretory proteins, enrichment analysis of all proteins found in the vesicles revealed the strongest enriched GO term for cellular compartment to be "Extracellular vesicular exosome" (Enrichr combined score=373.7, p=0). 345 of 704 proteins found in the vesicles are assigned to this GO-term (49%). There also were 71 proteins assigned to one of the GO terms that are connected to apoptosis or regulation of apoptosis in the vesicle-secretome. However, 24 of them are involved in negative regulation of apoptosis and no GO term for apoptotic bodies is enriched. Furthermore, skeletal muscle has previously been published to secrete proteins via vesicle budding and there are 239 proteins in the vesicle-enriched fraction that were also found in vesicles by Le Bihan *et al.* [27]. Therefore, the vesicles were assumed not to represent apoptotic bodies but to rather contribute to targeted protein secretion. Consequently, the medium-fraction and vesicle-enriched fraction of the primary muscle fibers were combined to represent the full primary muscle fiber secretome for all further analyses. In total, 1009 proteins were contained in this secretome, of which 506 were predicted or published to be secreted. 339 proteins were both identified in primary muscle fiber medium and vesicles (Fig. 13a), of which 167 were predicted or published to be secreted (Fig. 13b). 206 of those proteins were significantly altered by myxothiazol treatment for 16 h (Fig. 13c), of which 99 were secretory (Fig. 13d) and the majority of proteins was induced in both datasets (Fig 13e-f).

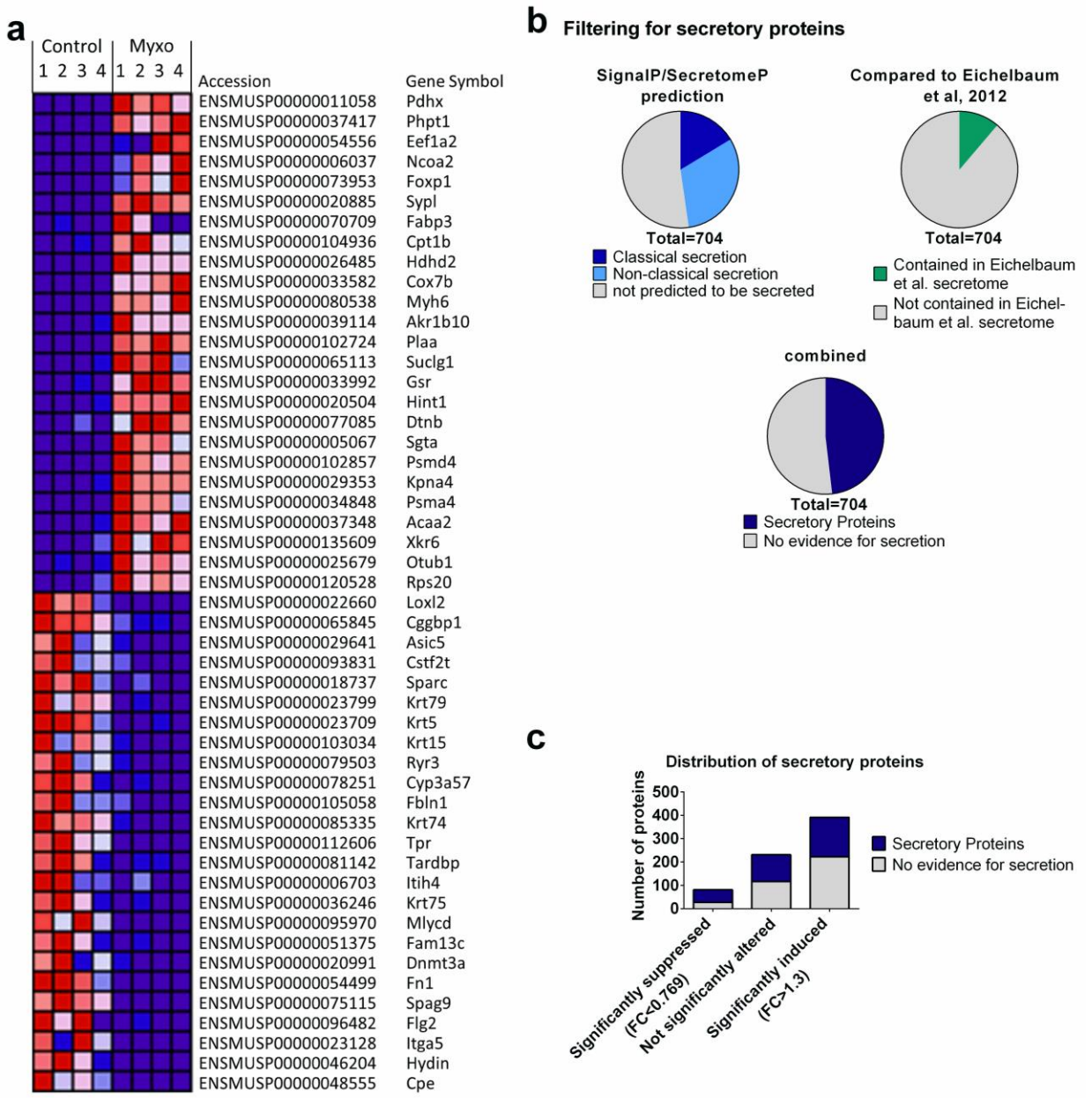

Figure 12: Myxothiazol treatment induces the secretion of 339 potential myokines from primary muscle fibers via vesicle budding. Conditioned media of control vs. myxothiazol treated fibers were collected after 16 h of incubation. Vesicles were enriched by centrifugation and subjected to unbiased proteomic analysis separately from the supernatant (n=4). In total, 704 proteins were detected. The top 25 proteins induced and suppressed by 8 h of myxothiazol treatment are shown in the heatmap sorted by fold change (a). b) SignalP and SecretomeP were used to predict classical and non-classical secretion of all proteins identified (upper left panel). Furthermore, they were compared to a published putative human secretome (Eichelbaum *et al*., 2012) (upper right panel). In total, 339 proteins were classified as secretory proteins with both approaches combined (lower panel). The majority of secretory and non-secretory proteins were induced by myxothiazol treatment (c).

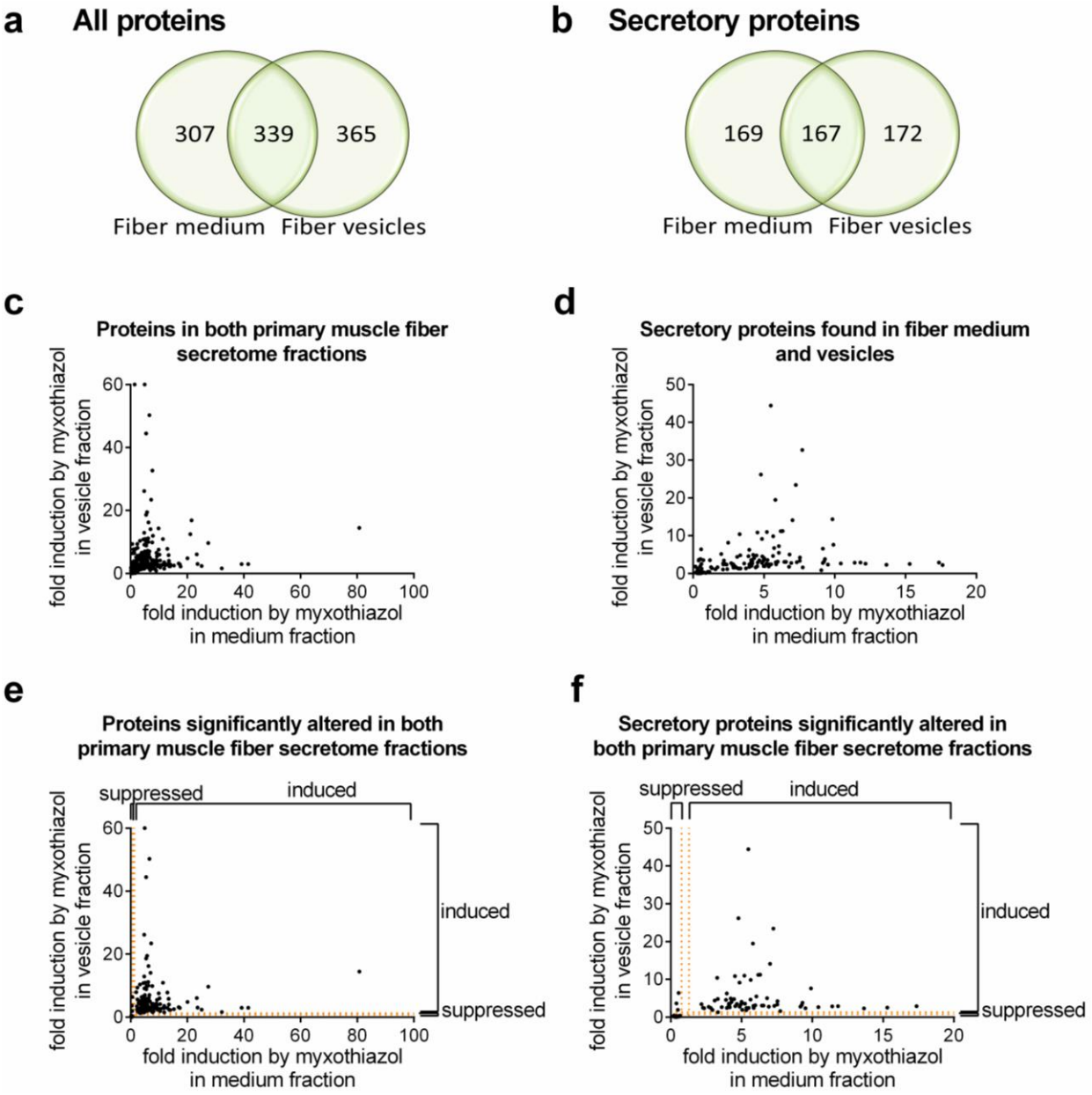

Figure 13: Primary muscle fibers secrete a total of 508 proteins via vesicle budding and other secretory mechanisms. In the medium-fraction and the vesicle-enriched fraction of the primary muscle fibers, a total of 1011 (a) proteins were detected, of which 508 (b) were predicted or published to be secreted. a-b) The Venn diagrams indicate the total numbers of all proteins (a) and proteins that are predicted or published to be secreted (b) that are common and specific for the medium fraction and vesicle-enriched fraction of the primary muscle fiber secretome. c-d) The 339 proteins (c) common to both sets of protein are shown with their respective fold changes. The same is shown only for the 167 proteins predicted or published to be secreted in (d). e) only the 206 proteins that are significantly altered ($p<0.05$) by 16 h of myxothiazol treatment are indicated with their respective fold changes (f) shows the respective fold changes of the 99 proteins that are significantly altered by myxothiazol treatment and predicted or published to be secreted.

3.6 Comparison of the secretomes of nutrient deprived C2C12 myotubes and myxothiazol treated primary muscle fibers

3.6.1 Comparison of the secretomes of C2C12 cells and primary muscle fibers

In order to find potential myokines among the proteins identified in conditioned media of C2C12 myocytes and/or primary murine muscle fibers, the two sets of proteins were compared. In total, 1960 proteins encoded by 1732 genes were identified by the two approaches. 548 proteins were common to both secretomes (Fig. 14a, c, Supplemental Table 1), of which 274 were predicted or published to be secreted (Fig. 14b, d). Only 13 were significantly induced by both respective treatments, namely AHNAK nucleoprotein (desmoyokin) (Ahnak), basic transcription factor 3 (Btf3), basic transcription factor 3-like 4 (Btf3l4), Cox6b1, DnaJ (Hsp40) homolog, subfamily A, member 2 (Dnaja2), glutamyl-prolyl-tRNA synthetase (Eprs), Heterogeneous nuclear ribonucleoprotein A3 (HnRNP A3 / Gm8991), HECT, UBA and WWE domain containing 1 (Huwe1), ribosomal protein S2 (Rps2), ribosomal protein S3A1 (Rps3a1), ribosomal protein S9 (Rps9), and ribosomal protein S15 (Rps15) (Fig. 14e). Of those proteins, only Cox6b1, HnRNP A3, Rps2, and Rps15 were predicted to be secreted by SecretomeP, i.e. via non-classical secretion, and Rps3a1 was predicted to be secreted by SignalP, i.e. via classical secretion (Fig. 14f, Supplemental Table 1). Rps2, Rps3a1, and Rps15 are the 40S ribosomal proteins 2, 3a1, and 15, i.e. components of the small ribosomal unit. HnRNP A3/Gm8991, a member of the family of heterogeneous nuclear ribonucleoproteins which is involved in pre-mRNA processing, transcriptional regulation, recombination, and telomere maintenance, was previously published to protect mammalian telomeric repeats *in vitro* [180]. Cox6b1 as a secretory protein is particularly interesting, as it is a mitochondrial protein and only few mitochondrial proteins have been described to be secreted so far [e.g. 181, 182]. Cox6b1 is an accessory subunit of cytochrome c oxidase (Cox), which is complex IV of the respiratory electron transport chain. It is believed to connect the two Cox-subunits to form a dimer and is therefore located in the intermembrane space [183]. It was previously reported to be shuttled out of the mitochondria [184], but to the best of my knowledge it has not been reported to be secreted from cells to date.

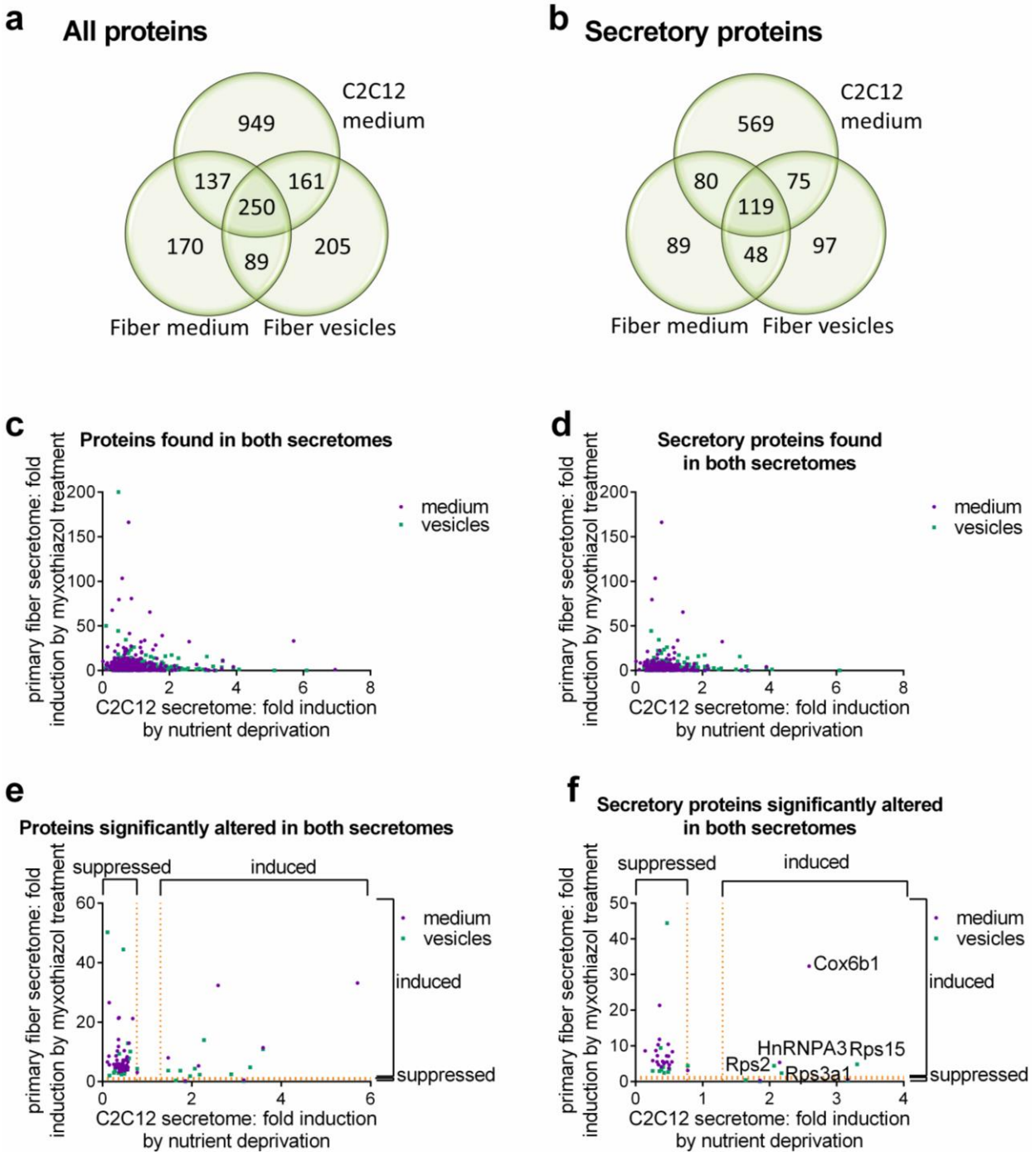

Figure 14 Comparison of both secretomes confirms secretion of 274 proteins from skeletal muscle. The secretomes of C2C12 myotubes and primary muscle fibers were compared. In total, 1960 proteins were identified in all three datasets, of which 548 were common to both secretomes (a). 1077 were secretory proteins of which 274 were common to both secretomes (b). The total number of proteins (c) or only the secretory proteins (d) common to both secretomes is plotted with their fold changes induced by nutrient deprivation of C2C12 myotubes or myxothiazol treatment of primary muscle fibers, respectively. Proteins identified in the medium fraction of primary muscle fibers are shown in purple, those from the vesicle-enriched fraction are shown in turquoise. All proteins (e) and only secretory proteins (f) significantly ($p<0.05$) altered by the respective treatments are shown. Only five secretory proteins were significantly induced by both treatments, namely Cox6b1, HnRNPA3, Rps2, Rps3a1, and Rps15.

3.6.2 Filtering the secretomes with the MitoCarta 2.0

In order to find out whether there are more proteins than Cox6b1 contained in the secretome datasets that are normally located within mitochondria, the secretomes were compared to the MitoCarta 2.0, which is a compendium of proteins located inside mitochondria [176]. 195 proteins in total were found to be of mitochondrial origin, of which 120 were predicted or published to be secreted. 45 secretory proteins (74 proteins in total) were identified in both secretomes, 32 secretory proteins (49 proteins in total) were specifically identified in the C2C12 secretome, and 43 secretory proteins (72 proteins in total) were found only in the secretome of primary muscle fibers (Fig. 15a-b). The Mouse MitoCarta 2.0 contains 1158 genes encoding proteins located in the mitochondria, of which only 195 were contained in the three secretome datasets. 16 of them were also contained in the putative human secretome published by Eichelbaum *et al.* [175]. Further, only distinct mitochondrial proteins were contained in the three secretomic datasets as can be seen at the example of the complexes of the electron transport chain. For example, there were only four of 44 subunits of complex I, namely Ndufa8, Ndufa10, Ndufa13, and Ndufab1, which were all only found in the secretome of primary muscle fibers. Further, only one of four complex II subunits, namely Sdha, was identified in the vesicle fraction of the primary muscle fiber secretome. Four of ten subunits of complex III (Cyc1, Uqcrc1, Uqcrc2, and Uqcrfs1) were identified in both the C2C12 and the primary fiber secretome, but only in the secretome of primary muscle fibers they were significantly induced. Five of 13 subunits of complex IV, namely Cox4i1, Cox6b1, Cox7a1, Cox7b, and Cox17 were identified in the secretomes, but only Cox6b1 was found in both the C2C12 secretome and the primary muscle fiber secretome. This indicates that at least the mitochondrial proteins that are contained in the secretomes of both C2C12 myotubes and primary muscle fibers and are predicted or published to be secreted are secreted from skeletal muscle in a controlled fashion and not shed into the medium due to disrupted membranes. This applied to 45 proteins (Fig. 15b), of which Cox6b1 was the only one that was significantly induced by nutrient deprivation in C2C12 myotubes and myxothiazol treatment in primary muscle fibers (Fig. 14f). Thus, it was concluded that Cox6b1 is specifically shuttled from mitochondria to the cytoplasm and secreted from skeletal muscle upon energy deprivation.

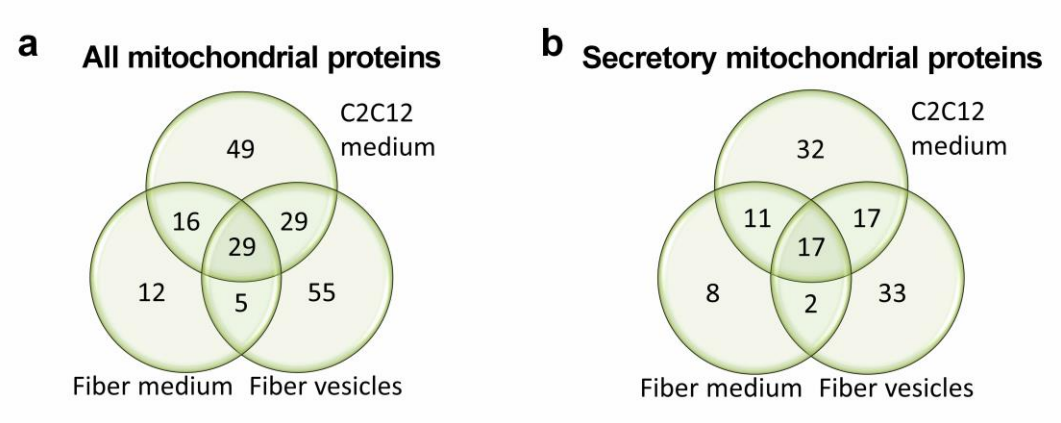

Figure 15: The secretomes of C2C12 myotubes and primary muscle fibers contain 120 secretory mitochondrial proteins. The secretomes of nutrient deprived C2C12 myotubes and myxothiazol treated primary muscle fibers were compared to the MitoCarta 2.0, a compendium of proteins located in mitochondria [176]. A total of 195 mitochondrial proteins were identified in the three secretome datasets (a), of which 120 were secretory (b). 45 mitochondrial secretory proteins were common to both secretomes.

3.7 *In vitro* assessment of selected candidate myokines from the experimental skeletal muscle secretome

In order to examine their effects on different target cells, a set of putative myokines was chosen, of which each was predicted to be secreted and fulfilled at least one of the following requirements: They belonged to the proteins with the highest significant induction in either nutrient deprived C2C12 myotubes or myxothiazol treated muscle fibers and were quantified with more than one peptide; They were induced in both nutrient deprived C2C12 myotubes and myxothiazol treated muscle fibers but not necessarily significantly in both datasets; Their protein abundance correlated significantly with the Fgf21 protein abundance and they were significantly induced by nutrient deprivation. The resulting list of candidates was strongly limited by the availability of recombinant proteins that were preferentially produced in mammalian cells to ensure correct glycosylation, where necessary. The 10 candidate proteins that were chosen for *in vitro* tests are listed in Table 7.

Table 7: Candidate proteins that were selected to examine their effects on different target cells *in vitro*. For each candidate myokine the fulfillment of the different requirements stated in column 1 is reported. If yes is put in brackets for "Top induced proteins in C2C12/primary muscle fiber secretome", this indicates that the respective protein was quantified with only one peptide in this dataset.

Protein	Angpt1	Casq	Cox6b1	Fn1	Il5ra	Npnt	Pdlim1	Plau	Rps5	Rsu1
Induced in both secretomes	no	yes	yes	no	no	no	yes	no	yes	yes
Significantly induced in both secretomes	no	no	yes	no	no	no	no	no	yes	no
Top Induced Proteins in C2C12 secretome	(yes)	yes	(yes)	yes	(yes)	yes	no	yes	yes	no
Top Induced Proteins in primary muscle fiber secretome	no	no	yes	no	no	no	yes	no	yes	yes
Correlation with Fgf21	yes	no	yes	yes	yes	no	no	yes	no	no

3.7.1 Effects of candidate proteins on *Ucp1* mRNA expression in primary murine adipocytes

As one rationale of this study was finding a novel myokine that can induce browning of white adipose tissue, primary murine white and brown adipocytes were treated with the candidate proteins and *Ucp1* mRNA expression was measured as a hallmark for browning. The adipocytes were first treated with 100 ng/ml of each candidate in a pilot experiment. The treatment was only repeated for those candidates that seemed to influence *Ucp1* expression (Fig. 16a). However, none of the candidates significantly altered *Ucp1* expression in white or brown primary adipocytes at a concentration of 100 ng/ml or lower (Fig. 16b). Therefore, the concentration was increased to 25 nM, but still no significant effects on *Ucp1* mRNA expression were observed (Fig. 16c).

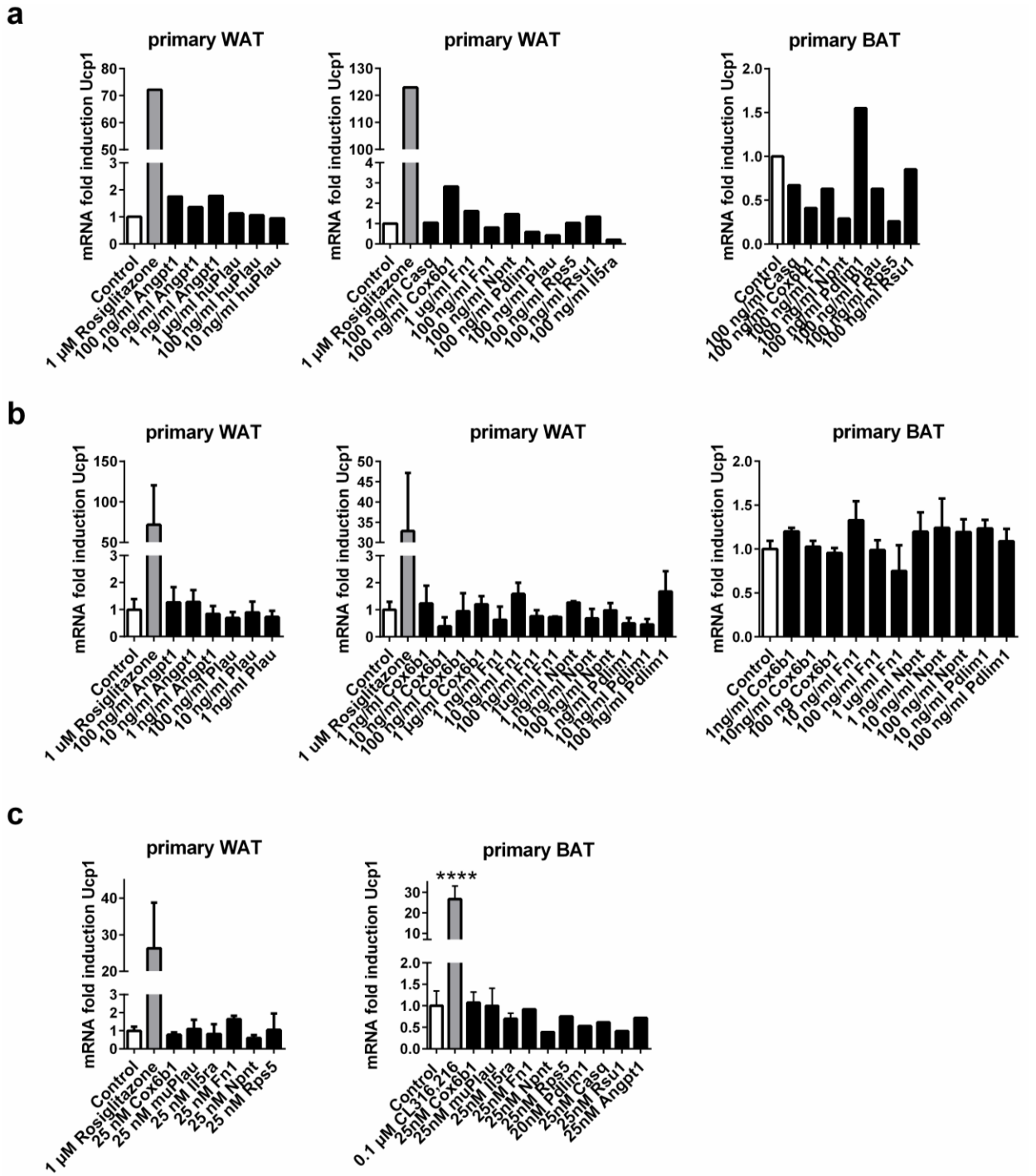

Figure 16: None of the candidate myokines induces *Ucp1* expression in white or brown primary murine adipocytes. Primary white (WAT) and brown adipocytes (BAT) were isolated from C57BL/6J and differentiated *in vitro*. a) In a pilot experiment primary WAT was treated with 100 ng/ml of all candidate myokines separately for 48 h, primary BAT was treated for 24 h, and *Ucp1* mRNA expression was determined by qPCR and normalized to *Hprt* expression (left panel) or *CypA* expression (center and right panel). Data represent n=1 experiment. b) based on the previous experiments (a), a subset of the candidate myokines was chosen to repeat the previous experiments. *Ucp1* expression was measured by qPCR and normalized to *Fabp4* expression. Data are shown as mean ± standard error of mean and represent n=4 independent experiments. c) As no induction of *Ucp1* expression was observed, the concentration was increased to 25 nM. mRNA expression of *Ucp1* was measured by qPCR and normalized to *Fabp4* expression Data are shown as mean ± standard error of mean and represent n=1-3 independent experiments.****p<0.0001 compared to control by Kruskal-Wallis test and Dunn's multiple comparisons test. White: medium control; grey: positive control; black: treated with candidate proteins.

3.7.1 Effects of candidate proteins on the mRNA expression of hunger-signal *Agrp* in murine hypothalamic cells

As the muscle cells/fibers were deprived of energy, one would suspect some of the myokines to communicate the muscular lack of energy to other organs. Therefore, murine hypothalamic cells (N41 cell line) were treated with 25 nM of the candidate proteins for 24 h and the mRNA expression of the hunger signal *agouti related neuropeptide* (*Agrp*) [185] was measured. In this first experiment, Cox6b1 seemed to induce *Agrp* expression (Fig. 17a), but when the experiment was repeated with a different batch of the purchased recombinant protein and a chemically synthesized form of Cox6b1 (FZ-8-416) there was no induction of *Agrp*.

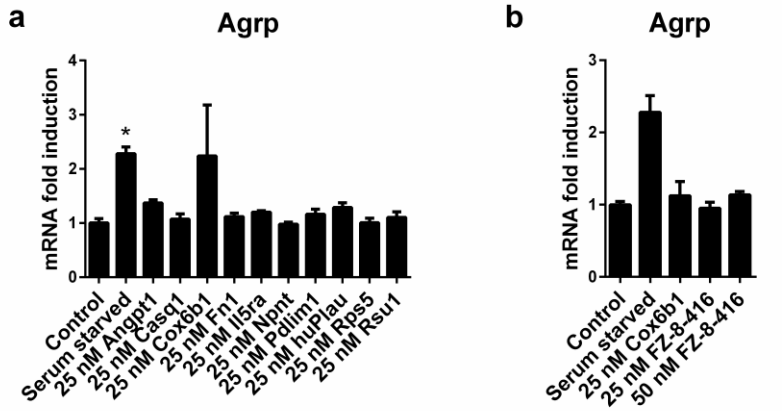

Figure 17: *Agrp* expression is not induced by any of the candidates in N41 hypothalamic cells. a) Murine hypothalamic N41 cells were treated with 25 nM of the chosen candidate myokines for 24 h and *Agrp* mRNA expression was determined by qPCR and normalized to *Hprt* expression. b) As Cox6b1 seemed to induce *Agrp* expression, the experiment was repeated with the purchased recombinant protein and a synthesized Cox6b1 (FZ-8-416). The induction of *Agrp* was not reproducible. Data are shown as mean ± standard error of mean and represent n=4 independent experiments.*$p<0.05$ compared to control as determined by Kruskal-Wallis test and Dunn's multiple comparisons test.

3.7.3 Candidate myokine Npnt induces inflammation in human hepatoma cells

Human hepatoma (HepG2) cells were cultured in either low glucose (LG) DMEM as control cells or in high glucose (HG) DMEM to induce insulin resistance as previously published [186]. Both LG and HG HepG2 cells were treated with the 10 candidate proteins for 24 h. mRNA expression of different genes involved in fatty acid oxidation, lipogenesis, cholesterol metabolism, glycolysis, gluconeogenesis, and Fgf21-signaling was measured. No significant effects of any of the candidates were observed when compared to the respective low/high glucose control cells (Fig. 18-19). However, treatment with 25 nM of Nephronectin (Npnt) altered the morphology of the cells both grown in LG and HG DMEM. HepG2 cells normally grow in clusters of spherical cells, but upon treatment with Npnt they changed to a confluent monolayer of cells (Fig. 20a). Therefore, *interleukin 8 (Il8)* mRNA expression was measured as a marker for inflammation, which tended to be induced in both low and high glucose cells treated with Npnt, although n=3 experiments were not sufficient to reach significance (Fig. 20b).

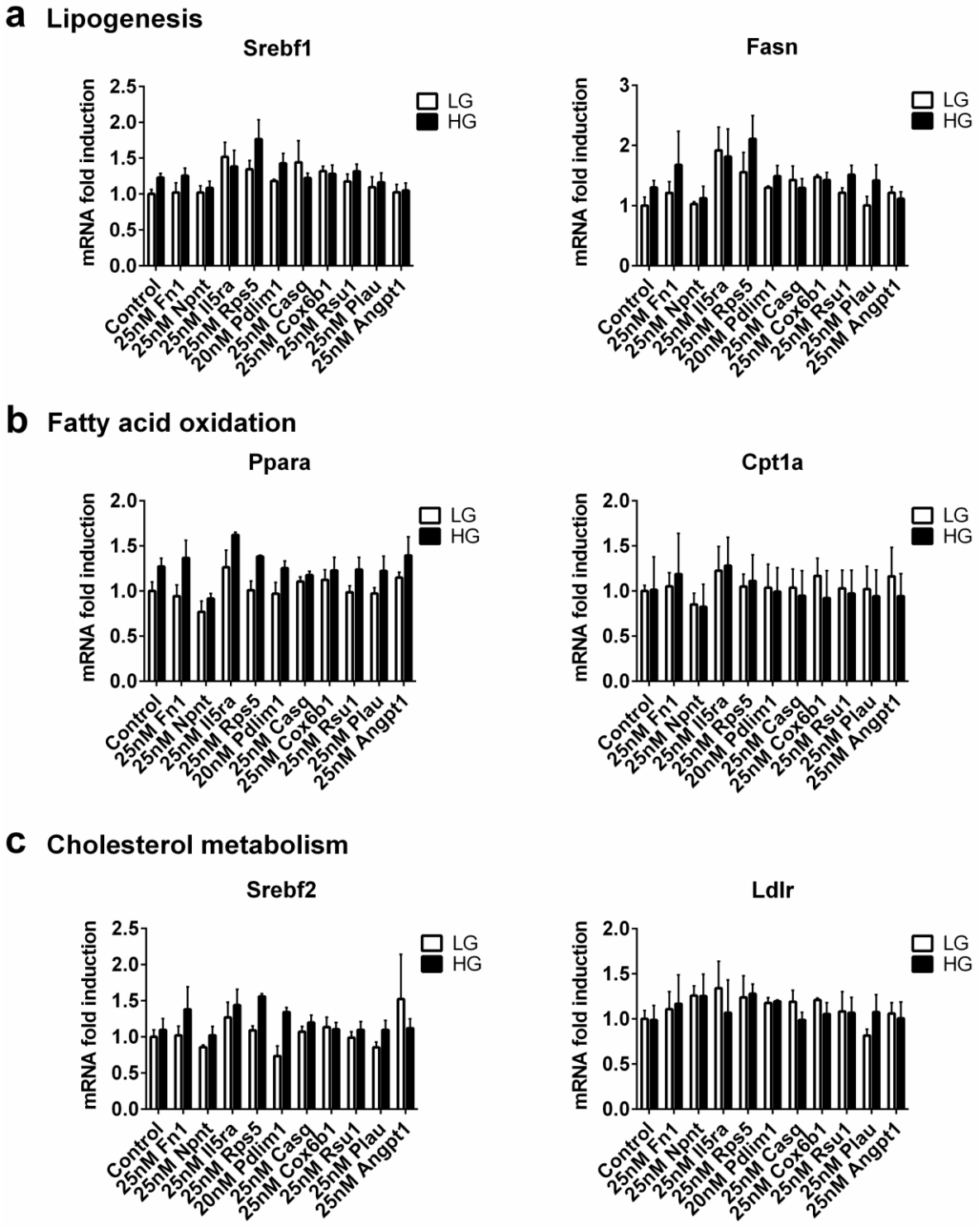

Figure 18: The candidate myokines do not influence expression of genes involved in fatty acid or cholesterol metabolism in human hepatoma cells. HepG2 cells were grown in low glucose DMEM (LG) or high glucose DMEM (HG) to induce insulin resistance as previously published [186]. They were treated with the candidate myokines for 24 h and the mRNA expression of genes involved in lipogenesis (a), fatty acid oxidation (b), and cholesterol metabolism (c) was determined by qPCR and normalized to Hprt expression. None of the candidate myokines altered the expression of any of the genes. Srebf1/2: Sterol regulatory element binding transcription factor 1/2; Fasn: Fatty acid synthase; Ppara: peroxisome proliferator activated receptor alpha; Cpt1a: carnitine palmitoyltransferase 1A; Ldlr: low density lipoprotein receptor. Data are shown as mean ± standard error of mean and represent n=3 independent experiments.

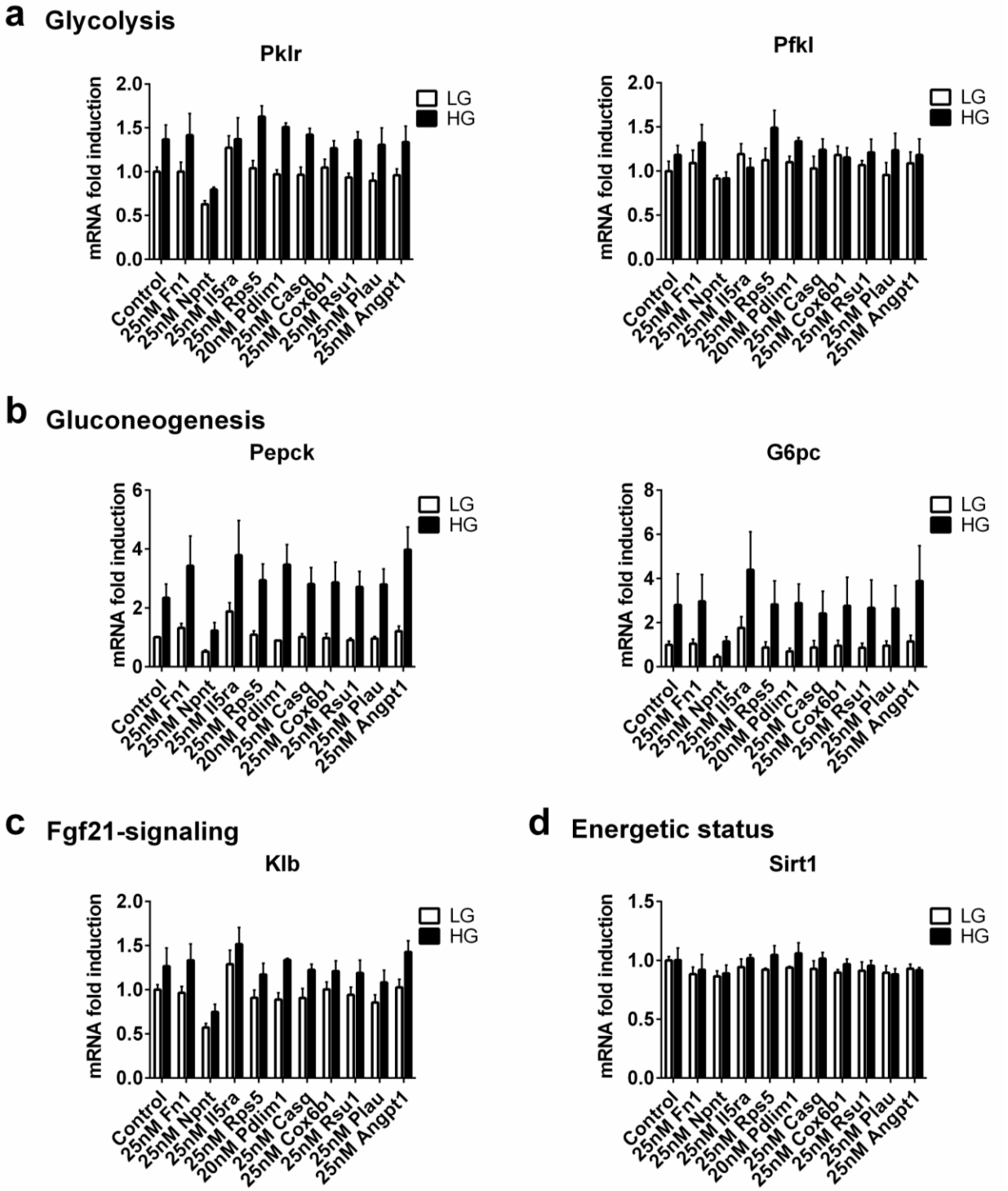

Figure 19: The candidate myokines do not influence expression of genes involved in glucose metabolism in human hepatoma cells. HepG2 cells were grown in low glucose DMEM (LG) or high glucose DMEM (HG) to induce insulin resistance as previously published [186]. They were treated with the candidate myokines for 24 h and the mRNA expression of genes involved in glycolysis (a), gluconeogenesis (b), Fgf21 signaling (c), and energetic status (d) was determined by qPCR. None of the candidate myokines altered the expression of any of the genes involved in glucose metabolism or *Sirt1* expression which is regarded an indicator of energetic status. Pklr: pyruvate kinase, liver and red blood cells; Pfkl: phosphofructokinase, liver, B-type; Pepck: phosphoenolpyruvate carboxykinase 1, cytosolic; glucose-6-phosphatase, catalytic; Klb: klotho beta; Sirt1: Sirtuin 1. Data are shown as mean ± standard error of mean and represent n=3 independent experiments.

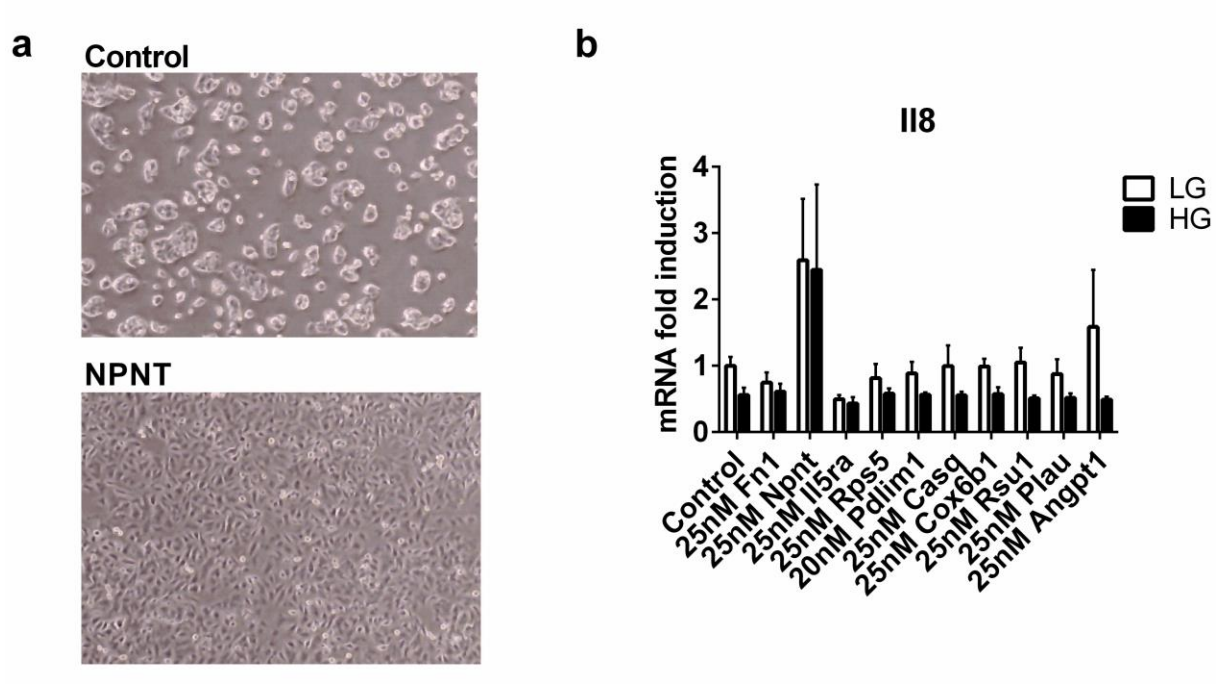

Figure 20: Npnt induces inflammation in human hepatoma cells. HepG2 cells were grown in low glucose DMEM (LG) or high glucose DMEM (HG) to induce insulin resistance as previously published [186]. They were treated with the candidate myokines for 24 h. Npnt changed the morphology of the cells irrespective of the glucose content of the culture media (a) and induced inflammation as represented by Interleukin (Il)-8 mRNA induction (b). Representative pictures were chosen for each condition. Data are shown as mean ± standard error of mean and represent n=3 independent experiments.

4. Discussion

4.1 Irisin does not induce browning in human SGBS adipocytes

Irisin was published to be a myokine secreted upon Pgc1α overexpression or exercise by Boström and colleagues [70]. It was further reported to induce browning of white adipose tissue, thereby inducing thermogenesis and elevated energy expenditure [70]. Therefore, human Simpson-Golabi-Behmel-Syndrome (SGBS) adipocytes were treated with native (i.e. glycosylated) and synthesized irisin for up to two days using the same concentration (20 nM) for which Boström and colleagues reported increased *Ucp1* expression and increased oxygen consumption. However, there was neither a significant induction of *Ucp1* mRNA expression nor an increase in basal, ATP-production linked or maximal oxygen consumption rates. Further, there was no change in proton-leak-linked respiration or coupling efficiency. Erickson *et al.* found full length FNDC5 to induce *Ucp1* in white adipocytes only at a 5-fold concentration compared to the initial study by Boström *et al.* [187]. However, even with 100 nM of irisin, there were no significant changes in oxygen consumption rates. This implies that irisin may not have an effect on browning of human SGBS adipocytes, which originate from subcutaneous WAT. This observation is in accordance with studies showing irisin to have no browning effect on primary human adipocytes isolated from subcutaneous or visceral depots but only on primary adipocytes isolated from deep neck adipose tissue depots [109, 188]. Thus, browning effects of irisin were assumed to be strictly limited to a small subpopulation of beige/brite adipocytes not including the major human adipose depots, i.e. subcutaneous and visceral adipose depots. Therefore, irisin was suggested to be of limited translational relevance to combat obesity [51, 109, 188, 189]. More recently, however, irisin was reported to induce browning in mature primary human subcutaneous adipocytes within two days of treatment. If irisin was added during adipogenic differentiation, on the other hand, adipocyte differentiation as well as the expression of browning markers was decreased. Zhang and colleagues therefore concluded that irisin affects adipocytes dependent on their maturity [190]. Moreover, the irisin used by Zhang and colleagues was produced in yeast [190], whereas in this study non-glycosylated chemically synthesized irisin as well as glycosylated irisin produced in CHO cells were used. Glycosylation is crucial for biological activity and function and differs considerably in yeast and mammalian cells like CHO cells [191]. Thus, it is not very likely that both proteins express the same biological activity. To

date, it is not clear whether the conflicting results observed in irisin treated subcutaneous adipocytes are due to the differences in glycosylation, a difference in the stage of differentiation, or whether other factors might also play a role. The present study, however, proceeded with the attempt to identify other, new myokines, as the results obtained within this study indicated that neither chemically synthesized nor glycosylated irisin induces browning in human SGBS adipocytes.

4.2 Analysis of the skeletal muscle secretome in states of energy deprivation

The role of myokines in regulation of whole body metabolism has become increasingly recognized in the recent years. One very prominent example is Fgf21, which was first identified to be secreted from the liver upon fasting [146]. Later, its release from skeletal muscle was shown in states of energy deprivation, either induced by uncoupling or inhibition of the respiratory electron transport chain or autophagy deficiency-induced mitochondrial dysfunction [23, 24]. Hypothesizing that states of energy deprivation induce not only one myokine but a complex signaling program, the secretomes of nutrient deprived C2C12 myotubes and myxothiazol-treated primary muscle fibers were analyzed by unbiased LC-MS/MS. In total, 1960 proteins were identified in the two experimental settings, of which 548 proteins were common to the secretomes of energy-deprived C2C12 myotubes and primary muscle fibers. In order to exclude proteins that may have been released by disrupted cells, the secretomes were filtered for classical or non-classical secretion by bioinformatics prediction and compared with a published putative secretome [175]. This combined approach revealed 274 proteins to be secreted from skeletal muscle upon energy deprivation with high confidence. Only 5 of those proteins were significantly induced in both experimental settings, namely Cox6b1, HnRNP A3 (Gm8991), Rps2, Rps3a1, and Rps15. Of those proteins, only Cox6b1 levels correlated significantly with Fgf21 levels in the C2C12 secretome, which might represent a functional connection. Interestingly, Cox6b1 is a mitochondrial protein, namely the ubiquitously expressed subunit VIb of Cox, complex IV of the respiratory electron transport chain. It is a hydrophilic extramembrane protein that faces the intermembrane space when built in the cox complex and is believed to connect the two monomers of the cox dimer [183]. Further, it is supposed to be involved in the formation of supercomplexes consisting of complexes I, III, and IV [192]. In the liver, it was reported to be increased by caloric restriction and has been suspected to contribute to the beneficial effects of caloric restriction [192]. Cox6b1 has previously been shown to be

shuttled out of human mitochondria, which was hypothesized to be a mechanism that transports misfolded mitochondrial proteins from the intermembrane space to the cytosol [184]. However, to the best of my knowledge, it has not yet been shown to be released from cells.

While myokines and their systemic activities are well recognized [e.g. reviewed in 30, 193], so-called "mitokines" are a rather new class of hormone-like factors. Mitochondrial stress and dysfunction have long been suggested to affect systemic metabolism [194-196]. Evidence for secretion and systemic action of mitochondrial factors or "mitokines" was published by Durieux and colleagues in 2011. They described activation of mitochondrial unfolded protein response in the intestine and increased life-span of the whole organism after neuronal knock-down of a component of the electron transport chain in *C. elegans*. However, it was not clear whether this factor was a protein, nucleic acid or a small molecule [197]. Secretion of mitochondrial peptides and proteins to the extracellular space and circulation has previously been observed in few cases. Zhang and colleagues have reported cellular injury to lead to the release of so called "mitochondrial damage-associated molecular patterns" activating innate immunity. In their study, they reported the release of formyl peptides and mitochondrial DNA suspecting that they represent only a subset of mitochondrial damage-associated molecular patterns [198]. More recently, two mitochondrial encoded peptides have been described to be secreted and act as "mitochondrial hormones" or mitokines, namely humanin and MOTS-c (mitochondrial open reading frame (ORF) of the twelfe S c) [181, 182]. Humanin is a 24-amino-acid peptide encoded by an ORF of the mitochondrial 16S rRNA that contains a "pseudo-signal peptide" and appears to be secreted via classical secretion. It was shown to have anti-apoptotic, cytoprotective, anti-inflammatory, and neuroprotective effects. Furthermore, it restored ATP levels in patients suffering from a mitochondrial disorder that leads to defective ATP synthesis, and intravenous and central intra-cerebro-ventricular infusion of humanin improved insulin sensitivity via STAT3 activation [182]. MOTS-c is a 16-amino-acid peptide that appears to target primarily skeletal muscle and to regulate insulin sensitivity and metabolic homeostasis. In mice, it prevented diet-induced obesity as well as age-dependent and high-fat-diet-induced insulin resistance [181]. In contrast to humanin and MOTS-c, Cox6b1 with its 86 amino acids and its mass of 10.1 kDa is not a peptide but a protein and encoded not by mitochondrial but nuclear DNA. However, as a component of the mitochondrial electron transport chain it is undoubtedly located within mitochondria. The possibility that Cox6b1 is not secreted but shed through disrupted cells can be

excluded with high confidence, as membrane disruption would lead to a release of most if not all complexes of the electron transport chain and their respective subunits. However, only a limited number of complex subunits was contained within the secretomic datasets and the majority of them was contained in only a single one of them. Cox6b1 was the only one that was induced in both the C2C12 secretome and the primary muscle fiber secretome. Thus, it was concluded that it is secreted from skeletal muscle upon energy deprivation in a controlled fashion. However, it is not clear whether Cox6b1 is transported from the mitochondrial intermembrane space to the cytoplasm due to increased misfolding induced by energy deprivation via the mechanism proposed by Bragoszewski *et al.* [184] or whether it is shuttled out as a signaling molecule communicating the lack of energy to other cells or organs. Furthermore, it is not clear how it is secreted from the muscle cells once it reached the cytoplasm. Sequence based prediction models of SecretomeP predict it to be secreted via non-classical secretion, i.e. it may be secreted via transporters, fusion of lysosomes with the plasma membrane, vesicle shedding, or as exosomes [199]. When primary muscle fibers were treated with myxothiazol for 16 h, they appeared to shed vesicles which were enriched by differential centrifugation and analyzed separately from the medium fraction by LC-MS/MS. Cox6b1 was contained in the medium but not in the vesicle-enriched fraction. This implies a secretion mechanism other than vesicle budding or exosomes although the possibility cannot be excluded completely, as there may have been additional vesicles that were too small to be enriched by the centrifugation method applied.

4.3 Effects of chosen candidates on different target cells

A set of proteins including Cox6b1 was chosen from the potential novel myokines contained in both secretomes for pilot experiments to explore their effects on different target cells. This set of proteins was chosen based on the fold induction of secretion from C2C12 myotubes by nutrient deprivation for 8h or from primary muscle fibers upon 16 h of myxothiazol treatment. Proteins were considered as promising candidates if they belonged to the group with highest fold induction in one of the secretomes, were induced in both secretomes, and/or their abundance correlated with Fgf21 protein abundance in the C2C12 secretome. From those proteins, 10 were chosen which were commercially available as recombinant proteins, preferentially produced in mammalian cells to ensure correct glycosylation, where necessary. As the original aim of the study was the identification of novel myokines that can induce browning of WAT, the effect of each of the candidates on *Ucp1* mRNA expression in primary white and brown adipocytes was

examined first. However, none of the candidates significantly altered *Ucp1* expression on mRNA level at the concentrations tested.

As the muscle cells were deprived of energy by nutrient deprivation or inhibition of the electron transport chain, one could expect myokines to be secreted that can communicate hunger / need for nutrients to the brain. Therefore, the candidates were tested for their effect on the mRNA expression of *Agrp*, which is activated by fasting [185], in hypothalamic N41 cells. However, there was no reproducible significant effect of any of the candidates.

Another possible way for myokines to influence substrate availability goes via liver metabolism [9, 34-36, 160]. Therefore, the effects of each candidate on the expression of genes involved in glucose, lipid, and cholesterol metabolism, as well as in energy sensing and Fgf21-signaling was examined in the hepatoma cell line HepG2 which was grown in low glucose medium or high glucose medium to induce insulin resistance as previously published [186]. Again there were no significant effects. However, Npnt treatment changed the morphology of the cells from clusters of spherical cells to a confluent monolayer of cells. Suspecting this to be a stress response, *Il8* mRNA expression as an inflammatory marker was examined. Indeed, *Il8* expression tended to be increased in Npnt treated cells irrespective of the glucose concentrations in the culture media. This is in accordance with previous reports of Npnt being upregulated in hepatitis and aggravating liver injury [200]. Although this effect of Npnt is not desirable in a translational setting, it shows that the conditions applied for testing the effects of the candidate proteins are sufficient to cause biological effects. However, it is still not clear whether the chosen candidates act on target cells in an endocrine fashion and – if they do – how they affect systemic metabolism. This may be due to the only limited number of readouts used in this study as well as the protein concentrations or time points chosen. For a comprehensive understanding of muscle-derived stress signaling upon energy deprivation, a screening approach covering a higher number of proteins, a wider range of protein concentrations in time-course experiments may be needed in concert with current "omics" technology. Cox6b1 is especially suggested to be a promising candidate for further *in vitro* and *in vivo* testing which may require the use of proteomic analysis to uncover its effects and molecular mechanism.

4.4 Conclusion and outlook

Taken together, energy deprivation – either induced by nutrient deprivation or inhibition of the electron transport chain – induces a specific secretome in skeletal muscle. This secretome from either C2C12 or murine primary muscle fibers was analyzed to identify physiologically relevant proteins that may affect other organs, e.g. induce browning of WAT in the best case scenario. Interestingly, this secretome included mitochondrial proteins. Here, a promising candidate, Cox6b1, was investigated as a potential new mitokine. In contrast to the mitochondrial derived peptides humanin and MOCS-c, Cox6b1 is not encoded by mitochondrial but by genomic DNA and is a protein, not a peptide. Its secretion mechanism and physiological role as a mitokine still remain to be elucidated and further experiments are required to unravel its effects on different target organs. For example, it would be interesting to investigate whether Cox6b1 is released directly after protein translation or whether it is first incorporated into the electron transport chain and then released from mitochondria upon energy deprivation. Furthermore, blood plasma levels may be examined under different conditions. Finally, pharmacological studies administering Cox6b1 may assist to identify its physiological effects.

5. References

[1] G. L. Close, A. Kayani, A. Vasilaki, and A. McArdle, "Skeletal Muscle Damage with Exercise and Aging," *Sports Medicine,* vol. 35, pp. 413-427, 2005// 2005.

[2] F. Zurlo, K. Larson, C. Bogardus, and E. Ravussin, "Skeletal muscle metabolism is a major determinant of resting energy expenditure," *Journal of Clinical Investigation,* vol. 86, pp. 1423-1427, 1990.

[3] H. Westerblad, J. D. Bruton, and A. Katz, "Skeletal muscle: Energy metabolism, fiber types, fatigue and adaptability," *Experimental Cell Research,* vol. 316, pp. 3093-3099, 11/1/ 2010.

[4] R. R. Wolfe, "The underappreciated role of muscle in health and disease," *The American Journal of Clinical Nutrition,* vol. 84, pp. 475-482, September 1, 2006 2006.

[5] G. F. Cahill, "Fuel Metabolism in Starvation," *Annual Review of Nutrition,* vol. 26, pp. 1-22, 2006/08/01 2006.

[6] P. Felig, "The glucose-alanine cycle," *Metabolism,* vol. 22, pp. 179-207, 1973/02/01 1973.

[7] R. A. DeFronzo and D. Tripathy, "Skeletal Muscle Insulin Resistance Is the Primary Defect in Type 2 Diabetes," *Diabetes Care,* vol. 32, pp. S157-S163, 2009.

[8] B. K. Pedersen, "The diseasome of physical inactivity--and the role of myokines in muscle--fat cross talk," *J Physiol,* vol. 587, pp. 5559-68, Dec 1 2009.

[9] C. Fiuza-Luces, N. Garatachea, N. A. Berger, and A. Lucia, "Exercise is the real polypill," *Physiology (Bethesda),* vol. 28, pp. 330-58, Sep 2013.

[10] S. E. Wohlgemuth, A. Y. Seo, E. Marzetti, H. A. Lees, and C. Leeuwenburgh, "Skeletal muscle autophagy and apoptosis during aging: Effects of calorie restriction and life-long exercise," *Experimental Gerontology,* vol. 45, pp. 138-148, 2// 2010.

[11] R. J. Colman, R. M. Anderson, S. C. Johnson, E. K. Kastman, K. J. Kosmatka, T. M. Beasley, *et al.*, "Caloric Restriction Delays Disease Onset and Mortality in Rhesus Monkeys," *Science,* vol. 325, pp. 201-204, 2009.

[12] R. S. Sohal and R. Weindruch, "Oxidative Stress, Caloric Restriction, and Aging," *Science (New York, N.Y.),* vol. 273, pp. 59-63, 1996.

[13] D. K. Ingram, R. Weindruch, E. L. Spangler, J. R. Freeman, and R. L. Walford, "Dietary Restriction Benefits Learning and Motor Performance of Aged Mice," *Journal of Gerontology,* vol. 42, pp. 78-81, January 1, 1987 1987.

[14] A. E. Civitarese, S. Carling, L. K. Heilbronn, M. H. Hulver, B. Ukropcova, W. A. Deutsch, *et al.*, "Calorie Restriction Increases Muscle Mitochondrial Biogenesis in Healthy Humans," *PLoS Med,* vol. 4, p. e76, 2007.

[15] A. Lass, B. H. Sohal, R. Weindruch, M. J. Forster, and R. S. Sohal, "Caloric restriction prevents age-associated accrual of oxidative damage to mouse skeletal muscle mitochondria," *Free Radical Biology and Medicine,* vol. 25, pp. 1089-1097, 12// 1998.

[16] T. A. Zainal, T. D. Oberley, D. B. Allison, L. I. Szweda, and R. Weindruch, "Caloric restriction of rhesus monkeys lowers oxidative damage in skeletal muscle," *The FASEB Journal,* vol. 14, pp. 1825-1836, September 1, 2000 2000.

[17] B. K. Pedersen, "Exercise-induced myokines and their role in chronic diseases," *Brain Behav Immun,* vol. 25, pp. 811-6, Jul 2011.

[18] B. K. Pedersen, T. C. Akerstrom, A. R. Nielsen, and C. P. Fischer, "Role of myokines in exercise and metabolism," *J Appl Physiol (1985),* vol. 103, pp. 1093-8, Sep 2007.

[19] N. Sharma, C. M. Castorena, and G. D. Cartee, "Greater insulin sensitivity in calorie restricted rats occurs with unaltered circulating levels of several important myokines and cytokines," *Nutr Metab (Lond),* vol. 9, p. 90, 2012.

[20] S. Kersten, L. Lichtenstein, E. Steenbergen, K. Mudde, H. F. J. Hendriks, M. K. Hesselink, *et al.*, "Caloric Restriction and Exercise Increase Plasma ANGPTL4 Levels in Humans via Elevated Free Fatty Acids," *Arteriosclerosis, Thrombosis, and Vascular Biology,* vol. 29, pp. 969-974, 2009.

[21] B. K. Pedersen and M. A. Febbraio, "Muscle as an endocrine organ: focus on muscle-derived interleukin-6," *Physiol Rev,* vol. 88, pp. 1379-406, Oct 2008.

[22] B. K. Pedersen and C. P. Fischer, "Beneficial health effects of exercise--the role of IL-6 as a myokine," *Trends Pharmacol Sci,* vol. 28, pp. 152-6, Apr 2007.

[23] K. H. Kim, Y. T. Jeong, H. Oh, S. H. Kim, J. M. Cho, Y. N. Kim, *et al.*, "Autophagy deficiency leads to protection from obesity and insulin resistance by inducing Fgf21 as a mitokine," *Nat Med,* vol. 19, pp. 83-92, Jan 2013.

[24] S. Keipert, M. Ost, K. Johann, F. Imber, M. Jastroch, E. M. van Schothorst, *et al.*, "Skeletal muscle mitochondrial uncoupling drives endocrine cross-talk through the induction of FGF21 as a myokine," *Am J Physiol Endocrinol Metab,* vol. 306, pp. E469-82, Mar 1 2014.

[25] B. K. Pedersen and B. Saltin, "Exercise as medicine - evidence for prescribing exercise as therapy in 26 different chronic diseases," *Scand J Med Sci Sports,* vol. 25 Suppl 3, pp. 1-72, Dec 2015.

[26] M. Gleeson, N. C. Bishop, D. J. Stensel, M. R. Lindley, S. S. Mastana, and M. A. Nimmo, "The anti-inflammatory effects of exercise: mechanisms and implications for the prevention and treatment of disease," *Nat Rev Immunol,* vol. 11, pp. 607-615, 09//print 2011.

[27] M. C. Le Bihan, A. Bigot, S. S. Jensen, J. L. Dennis, A. Rogowska-Wrzesinska, J. Laine, *et al.*, "In-depth analysis of the secretome identifies three major independent secretory pathways in differentiating human myoblasts," *J Proteomics,* vol. 77, pp. 344-56, Dec 21 2012.

[28] S. Raschke, K. Eckardt, K. Bjorklund Holven, J. Jensen, and J. Eckel, "Identification and validation of novel contraction-regulated myokines released from primary human skeletal muscle cells," *PLoS One,* vol. 8, p. e62008, 2013.

[29] S. Hartwig, S. Raschke, B. Knebel, M. Scheler, M. Irmler, W. Passlack, *et al.*, "Secretome profiling of primary human skeletal muscle cells," *Biochim Biophys Acta,* vol. 1844, pp. 1011-7, May 2014.

[30] K. Eckardt, S. W. Gorgens, S. Raschke, and J. Eckel, "Myokines in insulin resistance and type 2 diabetes," *Diabetologia,* vol. 57, pp. 1087-99, Jun 2014.

[31] E. Louis, U. Raue, Y. Yang, B. Jemiolo, and S. Trappe, "Time course of proteolytic, cytokine, and myostatin gene expression after acute exercise in human skeletal muscle," *Journal of Applied Physiology,* vol. 103, pp. 1744-1751, 2007.

[32] J. B. Kurek, J. J. Bower, M. Romanella, F. Koentgen, M. Murphy, and L. Austin, "The role of leukemia inhibitory factor in skeletal muscle regeneration," *Muscle & Nerve,* vol. 20, pp. 815-822, 1997.

[33] A. Steensberg, C. Keller, R. L. Starkie, T. Osada, M. A. Febbraio, and B. K. Pedersen, "IL-6 and TNF-α expression in, and release from, contracting human skeletal muscle," *American Journal of Physiology - Endocrinology And Metabolism*, vol. 283, pp. E1272-E1278, 2002.

[34] B. K. Pedersen, "Muscular interleukin-6 and its role as an energy sensor," *Med Sci Sports Exerc*, vol. 44, pp. 392-6, Mar 2012.

[35] L. Pedersen and P. Hojman, "Muscle-to-organ cross talk mediated by myokines," *Adipocyte*, vol. 1, pp. 164-167, Jul 1 2012.

[36] A. R. Nielsen and B. K. Pedersen, "The biological roles of exercise-induced cytokines: IL-6, IL-8, and IL-15," *Appl Physiol Nutr Metab*, vol. 32, pp. 833-9, Oct 2007.

[37] P. Munoz-Canoves, C. Scheele, B. K. Pedersen, and A. L. Serrano, "Interleukin-6 myokine signaling in skeletal muscle: a double-edged sword?," *FEBS J*, vol. 280, pp. 4131-48, Sep 2013.

[38] R. Shirazi, V. Palsdottir, J. Collander, F. Anesten, H. Vogel, F. Langlet, *et al.*, "Glucagon-like peptide 1 receptor induced suppression of food intake, and body weight is mediated by central IL-1 and IL-6," *Proceedings of the National Academy of Sciences of the United States of America*, vol. 110, pp. 16199-16204, 09/18 2013.

[39] D. A. Sarruf, J. P. Thaler, G. J. Morton, J. German, J. D. Fischer, K. Ogimoto, *et al.*, "Fibroblast growth factor 21 action in the brain increases energy expenditure and insulin sensitivity in obese rats," *Diabetes*, vol. 59, pp. 1817-24, Jul 2010.

[40] B. M. Owen, X. Ding, D. A. Morgan, K. C. Coate, A. L. Bookout, K. Rahmouni, *et al.*, "FGF21 Acts Centrally to Induce Sympathetic Nerve Activity, Energy Expenditure, and Weight Loss," *Cell Metab*, vol. 20, pp. 670-7, Oct 7 2014.

[41] C. D. Wrann, J. P. White, J. Salogiannnis, D. Laznik-Bogoslavski, J. Wu, D. Ma, *et al.*, "Exercise induces hippocampal BDNF through a PGC-1alpha/FNDC5 pathway," *Cell Metab*, vol. 18, pp. 649-59, Nov 5 2013.

[42] M. J. Betz and S. Enerbäck, "Human Brown Adipose Tissue: What We Have Learned So Far," *Diabetes*, vol. 64, pp. 2352-2360, 2015-07-01 00:00:00 2015.

[43] B. Cannon and J. Nedergaard, "Brown Adipose Tissue: Function and Physiological Significance," *Physiol Rev*, vol. 84, pp. 277-359, 2004.

[44] M. L. Bonet, P. Oliver, and A. Palou, "Pharmacological and nutritional agents promoting browning of white adipose tissue," *Biochim Biophys Acta*, vol. 1831, pp. 969-85, May 2013.

[45] A. Hamann, J. S. Flier, and B. B. Lowell, "Decreased brown fat markedly enhances susceptibility to diet-induced obesity, diabetes, and hyperlipidemia," *Endocrinology*, vol. 137, pp. 21-29, 1996.

[46] J. Kopecky, G. Clarke, S. Enerback, B. Spiegelman, and L. P. Kozak, "Expression of the mitochondrial uncoupling protein gene from the aP2 gene promoter prevents genetic obesity," *The Journal of Clinical Investigation*, vol. 96, pp. 2914-2923, 1995/12/01 1995.

[47] S. Collins, K. W. Daniel, A. E. Petro, and R. S. Surwit, "Strain-Specific Response to β 3-Adrenergic Receptor Agonist Treatment of Diet-Induced Obesity in Mice," *Endocrinology*, vol. 138, pp. 405-413, 1997.

[48] A. Vegiopoulos, K. Müller-Decker, D. Strzoda, I. Schmitt, E. Chichelnitskiy, A. Ostertag, *et al.*, "Cyclooxygenase-2 Controls Energy Homeostasis in Mice by de Novo Recruitment of Brown Adipocytes," *Science,* vol. 328, pp. 1158-1161, 2010-05-28 00:00:00 2010.

[49] P. Lee, C. D. Werner, E. Kebebew, and F. S. Celi, "Functional thermogenic beige adipogenesis is inducible in human neck fat," *Int J Obes (Lond),* vol. 38, pp. 170-6, Feb 2014.

[50] T. B. Walden, I. R. Hansen, J. A. Timmons, B. Cannon, and J. Nedergaard, "Recruited vs. nonrecruited molecular signatures of brown, "brite," and white adipose tissues," *Am J Physiol Endocrinol Metab,* vol. 302, pp. E19-31, Jan 1 2012.

[51] J. Wu, P. Boström, Lauren M. Sparks, L. Ye, Jang H. Choi, A.-H. Giang, *et al.*, "Beige Adipocytes Are a Distinct Type of Thermogenic Fat Cell in Mouse and Human," *Cell,* vol. 150, pp. 366-376, 7/20/ 2012.

[52] N. Petrovic, T. B. Walden, I. G. Shabalina, J. A. Timmons, B. Cannon, and J. Nedergaard, "Chronic peroxisome proliferator-activated receptor gamma (PPARgamma) activation of epididymally derived white adipocyte cultures reveals a population of thermogenically competent, UCP1-containing adipocytes molecularly distinct from classic brown adipocytes," *J Biol Chem,* vol. 285, pp. 7153-64, Mar 5 2010.

[53] T. B. Walden, J. A. Timmons, P. Keller, J. Nedergaard, and B. Cannon, "Distinct expression of muscle-specific MicroRNAs (myomirs) in brown adipocytes," *Journal of Cellular Physiology,* vol. 218, pp. 444-449, 2009.

[54] M. W. Rajala and P. E. Scherer, "Minireview: The Adipocyte—At the Crossroads of Energy Homeostasis, Inflammation, and Atherosclerosis," *Endocrinology,* vol. 144, pp. 3765-3773, 2003.

[55] J. M. Friedman, "The Function of Leptin in Nutrition, Weight, and Physiology," *Nutrition Reviews,* vol. 60, pp. S1-S14, 2002-10-01 00:00:00 2002.

[56] J. Himms-Hagen, A. Melnyk, M. C. Zingaretti, E. Ceresi, G. Barbatelli, and S. Cinti, "Multilocular fat cells in WAT of CL-316243-treated rats derive directly from white adipocytes," *American Journal of Physiology - Cell Physiology,* vol. 279, pp. C670-C681, 2000-09-01 00:00:00 2000.

[57] M. S. Rodeheffer, K. Birsoy, and J. M. Friedman, "Identification of White Adipocyte Progenitor Cells In Vivo," *Cell,* vol. 135, pp. 240-249.

[58] M. J. R. Dawkins and D. Hull, "Brown adipose tissue and the response of new-born rabbits to cold," *The Journal of Physiology,* vol. 172, pp. 216-238, 1964.

[59] M. J. R. Dawkins and J. W. Scopes, "Non-shivering Thermogenesis and Brown Adipose Tissue in the Human New-born Infant," *Nature,* vol. 206, pp. 201-202, 04/10/print 1965.

[60] W. Aherne and D. Hull, "Brown adipose tissue and heat production in the newborn infant," *The Journal of Pathology and Bacteriology,* vol. 91, pp. 223-234, 1966.

[61] H. Aquila, T. A. Link, and M. Klingenberg, "The uncoupling protein from brown fat mitochondria is related to the mitochondrial ADP/ATP carrier. Analysis of sequence homologies and of folding of the protein in the membrane," *The EMBO Journal,* vol. 4, pp. 2369-2376, 1985.

[62] G. M. Heaton, R. J. Wagenvoord, A. Kemp, and D. G. Nicholls, "Brown-Adipose-Tissue Mitochondria: Photoaffinity Labelling of the Regulatory Site of Energy Dissipation," *European Journal of Biochemistry,* vol. 82, pp. 515-521, 1978.

[63] I. L. Cameron and R. E. Smith, "CYTOLOGICAL RESPONSES OF BROWN FAT TISSUE IN COLD-EXPOSED RATS," *The Journal of Cell Biology,* vol. 23, pp. 89-100, 1964.

[64] S. Klaus, L. Casteilla, F. Bouillaud, and D. Ricquier, "The uncoupling protein ucp: A membraneous mitochondrial ion carrier exclusively expressed in brown adipose tissue," *International Journal of Biochemistry*, vol. 23, pp. 791-801, 1991/01/01 1991.

[65] S. Cinti, C. Zancanaro, A. Sbarbati, M. Cicolini, P. Vogel, D. Ricquier, *et al.*, "Immunoelectron microscopical identification of the uncoupling protein in brown adipose tissue mitochondria," *Biology of the Cell*, vol. 67, pp. 359-362, 1989.

[66] B. Cannon, A. Hedin, and J. Nedergaard, "Exclusive occurrence of thermogenin antigen in brown adipose tissue," *FEBS Letters*, vol. 150, pp. 129-132, 1982.

[67] R. B. Vega, J. M. Huss, and D. P. Kelly, "The Coactivator PGC-1 Cooperates with Peroxisome Proliferator-Activated Receptor α in Transcriptional Control of Nuclear Genes Encoding Mitochondrial Fatty Acid Oxidation Enzymes," *Molecular and Cellular Biology*, vol. 20, pp. 1868-1876, March 1, 2000 2000.

[68] A. Fedorenko, Polina V. Lishko, and Y. Kirichok, "Mechanism of Fatty-Acid-Dependent UCP1 Uncoupling in Brown Fat Mitochondria," *Cell*, vol. 151, pp. 400-413, 10/12/ 2012.

[69] M. Klingenberg and S.-G. Huang, "Structure and function of the uncoupling protein from brown adipose tissue," *Biochimica et Biophysica Acta (BBA) - Biomembranes*, vol. 1415, pp. 271-296, 1/8/ 1999.

[70] P. Bostrom, J. Wu, M. P. Jedrychowski, A. Korde, L. Ye, J. C. Lo, *et al.*, "A PGC1-alpha-dependent myokine that drives brown-fat-like development of white fat and thermogenesis," *Nature*, vol. 481, pp. 463-8, Jan 26 2012.

[71] P. Seale, H. M. Conroe, J. Estall, S. Kajimura, A. Frontini, J. Ishibashi, *et al.*, "Prdm16 determines the thermogenic program of subcutaneous white adipose tissue in mice," *The Journal of Clinical Investigation*, vol. 121, pp. 96-105, 2011/01/04 2011.

[72] M. Petruzzelli, M. Schweiger, R. Schreiber, R. Campos-Olivas, M. Tsoli, J. Allen, *et al.*, "A Switch from White to Brown Fat Increases Energy Expenditure in Cancer-Associated Cachexia," *Cell Metabolism*, vol. 20, pp. 433-447, 9/2/ 2014.

[73] Labros S. Sidossis, C. Porter, Manish K. Saraf, E. Børsheim, Ravi S. Radhakrishnan, T. Chao, *et al.*, "Browning of Subcutaneous White Adipose Tissue in Humans after Severe Adrenergic Stress," *Cell Metabolism*, vol. 22, pp. 219-227, 8/4/ 2015.

[74] M. Harms and P. Seale, "Brown and beige fat: development, function and therapeutic potential," *Nat Med*, vol. 19, pp. 1252-1263, 10//print 2013.

[75] K. I. Stanford, R. J. W. Middelbeek, K. L. Townsend, M.-Y. Lee, H. Takahashi, K. So, *et al.*, "A Novel Role for Subcutaneous Adipose Tissue in Exercise-Induced Improvements in Glucose Homeostasis," *Diabetes*, vol. 64, pp. 2002-2014, 2015.

[76] M. A. Bredella, C. M. Gill, C. J. Rosen, A. Klibanski, and M. Torriani, "Positive effects of brown adipose tissue on femoral bone structure," *Bone*, vol. 58, pp. 55-58, 1// 2014.

[77] P. Cohen, Julia D. Levy, Y. Zhang, A. Frontini, Dmitriy P. Kolodin, Katrin J. Svensson, *et al.*, "Ablation of PRDM16 and Beige Adipose Causes Metabolic Dysfunction and a Subcutaneous to Visceral Fat Switch," *Cell*, vol. 156, pp. 304-316, 1/16/ 2014.

[78] S. Ponrartana, H. H. Hu, and V. Gilsanz, "On the relevance of brown adipose tissue in children," *Annals of the New York Academy of Sciences*, vol. 1302, pp. 24-29, 2013.

[79] É. Szentirmai and L. Kapás, "Intact brown adipose tissue thermogenesis is required for restorative sleep responses after sleep loss," *European Journal of Neuroscience,* vol. 39, pp. 984-998, 2014.

[80] Aaron M. Cypess, Carol R. Haft, Maren R. Laughlin, and Houchun H. Hu, "Brown Fat in Humans: Consensus Points and Experimental Guidelines," *Cell Metabolism,* vol. 20, pp. 408-415, 9/2/ 2014.

[81] A. Bartelt, O. T. Bruns, R. Reimer, H. Hohenberg, H. Ittrich, K. Peldschus, *et al.*, "Brown adipose tissue activity controls triglyceride clearance," *Nat Med,* vol. 17, pp. 200-205, 02//print 2011.

[82] P. Young, J. R. S. Arch, and M. Ashwell, "Brown adipose tissue in the parametrial fat pad of the mouse," *FEBS Letters,* vol. 167, pp. 10-14, 1984.

[83] D. Lončar, "Convertible adipose tissue in mice," *Cell and Tissue Research,* vol. 266, pp. 149-161, 1991.

[84] C. Guerra, R. A. Koza, H. Yamashita, K. Walsh, and L. P. Kozak, "Emergence of brown adipocytes in white fat in mice is under genetic control. Effects on body weight and adiposity," *The Journal of Clinical Investigation,* vol. 102, pp. 412-420, 1998/07/15 1998.

[85] C. Picó, L. M. Bonet, and A. Palou, "Stimulation of uncoupling protein synthesis in white adipose tissue of mice treated with the β3-adrenergic agonist CGP-12177," *Cellular and Molecular Life Sciences CMLS,* vol. 54, pp. 191-195, 1998.

[86] J. G. Granneman, P. Li, Z. Zhu, and Y. Lu, "Metabolic and cellular plasticity in white adipose tissue I: effects of β3-adrenergic receptor activation," *American Journal of Physiology - Endocrinology and Metabolism,* vol. 289, pp. E608-E616, 2005-10-01 00:00:00 2005.

[87] B. Cousin, S. Cinti, M. Morroni, S. Raimbault, D. Ricquier, L. Penicaud, *et al.*, "Occurrence of brown adipocytes in rat white adipose tissue: molecular and morphological characterization," *Journal of Cell Science,* vol. 103, pp. 931-942, 1992-12-01 00:00:00 1992.

[88] M. J. Barberá, A. Schlüter, N. Pedraza, R. Iglesias, F. Villarroya, and M. Giralt, "Peroxisome Proliferator-activated Receptor α Activates Transcription of the Brown Fat Uncoupling Protein-1 Gene: A LINK BETWEEN REGULATION OF THE THERMOGENIC AND LIPID OXIDATION PATHWAYS IN THE BROWN FAT CELL," *Journal of Biological Chemistry,* vol. 276, pp. 1486-1493, January 12, 2001 2001.

[89] P. Li, Z. Zhu, Y. Lu, and J. G. Granneman, "Metabolic and cellular plasticity in white adipose tissue II: role of peroxisome proliferator-activated receptor-α," *American Journal of Physiology - Endocrinology and Metabolism,* vol. 289, pp. E617-E626, 2005-10-01 00:00:00 2005.

[90] I. B. Sears, M. A. MacGinnitie, L. G. Kovacs, and R. A. Graves, "Differentiation-dependent expression of the brown adipocyte uncoupling protein gene: regulation by peroxisome proliferator-activated receptor gamma," *Molecular and Cellular Biology,* vol. 16, pp. 3410-9, July 1, 1996 1996.

[91] N. Petrovic, I. G. Shabalina, J. A. Timmons, B. Cannon, and J. Nedergaard, "Thermogenically competent nonadrenergic recruitment in brown preadipocytes by a PPARγ agonist," *American Journal of Physiology - Endocrinology and Metabolism,* vol. 295, pp. E287-E296, 2008-08-01 00:00:00 2008.

[92] Y. Fukui, S. Masui, S. Osada, K. Umesono, and K. Motojima, "A new thiazolidinedione, NC-2100, which is a weak PPAR-gamma activator, exhibits potent antidiabetic effects and induces uncoupling protein 1 in white adipose tissue of KKAy obese mice," *Diabetes,* vol. 49, pp. 759-767, 2000-05-01 00:00:00 2000.

[93] H. Sell, J. P. Berger, P. Samson, G. Castriota, J. Lalonde, Y. Deshaies, *et al.*, "Peroxisome Proliferator-Activated Receptor γ Agonism Increases the Capacity for Sympathetically Mediated Thermogenesis in Lean and ob/ob Mice," *Endocrinology,* vol. 145, pp. 3925-3934, 2004.

[94] L. Wilson-Fritch, S. Nicoloro, M. Chouinard, M. A. Lazar, P. C. Chui, J. Leszyk, *et al.*, "Mitochondrial remodeling in adipose tissue associated with obesity and treatment with rosiglitazone," *The Journal of Clinical Investigation*, vol. 114, pp. 1281-1289, 2004/11/01.

[95] Y. J. Koh, B.-H. Park, J.-H. Park, J. Han, I.-K. Lee, J. W. Park, *et al.*, "Activation of PPAR[gamma] induces profound multilocularization of adipocytes in adult mouse white adipose tissues," *Exp Mol Med*, vol. 41, pp. 880-895, 12/31/online 2009.

[96] R. Alvarez, J. de Andrés, P. Yubero, O. Viñas, T. Mampel, R. Iglesias, *et al.*, "A Novel Regulatory Pathway of Brown Fat Thermogenesis: RETINOIC ACID IS A TRANSCRIPTIONAL ACTIVATOR OF THE MITOCHONDRIAL UNCOUPLING PROTEIN GENE," *Journal of Biological Chemistry*, vol. 270, pp. 5666-5673, March 10, 1995 1995.

[97] P. Puigserver, F. Vázquez, M. L. Bonet, C. Picó, and A. Palou, "In vitro and in vivo induction of brown adipocyte uncoupling protein (thermogenin) by retinoic acid," *Biochemical Journal*, vol. 317, pp. 827-833, 1996-08-01 00:00:00 1996.

[98] M. Kumar and P. Scarpace, "Differential effects of retinoic acid on uncoupling protein-1 and leptin gene expression," *Journal of Endocrinology*, vol. 157, pp. 237-243, May 1, 1998 1998.

[99] J. Mercader, J. Ribot, I. Murano, F. Felipe, S. Cinti, M. L. Bonet, *et al.*, "Remodeling of White Adipose Tissue after Retinoic Acid Administration in Mice," *Endocrinology*, vol. 147, pp. 5325-5332, 2006.

[100] A. M. Cassard-Doulcier, M. Larose, J. C. Matamala, O. Champigny, F. Bouillaud, and D. Ricquier, "In vitro interactions between nuclear proteins and uncoupling protein gene promoter reveal several putative transactivating factors including Ets1, retinoid X receptor, thyroid hormone receptor, and a CACCC box-binding protein," *Journal of Biological Chemistry*, vol. 269, pp. 24335-24342, September 30, 1994 1994.

[101] C. Guerra, C. Roncero, A. Porras, M. Fernández, and M. Benito, "Triiodothyronine Induces the Transcription of the Uncoupling Protein Gene and Stabilizes Its mRNA in Fetal Rat Brown Adipocyte Primary Cultures," *Journal of Biological Chemistry*, vol. 271, pp. 2076-2081, January 26, 1996 1996.

[102] R. Rabelo, C. Reyes, A. Schifman, and J. E. Silva, "Interactions among receptors, thyroid hormone response elements, and ligands in the regulation of the rat uncoupling protein gene expression by thyroid hormone," *Endocrinology*, vol. 137, pp. 3478-3487, 1996.

[103] J.-Y. Lee, N. Takahashi, M. Yasubuchi, Y.-I. Kim, H. Hashizaki, M.-J. Kim, *et al.*, "Triiodothyronine induces UCP-1 expression and mitochondrial biogenesis in human adipocytes," *American Journal of Physiology - Cell Physiology*, vol. 302, pp. C463-C472, 2012-01-15 00:00:00 2012.

[104] M. C. Skarulis, F. S. Celi, E. Mueller, M. Zemskova, R. Malek, L. Hugendubler, *et al.*, "Thyroid Hormone Induced Brown Adipose Tissue and Amelioration of Diabetes in a Patient with Extreme Insulin Resistance," *The Journal of Clinical Endocrinology & Metabolism*, vol. 95, pp. 256-262, 2010.

[105] A. Rubio, A. Raasmaja, A. L. Maia, K. R. Kim, and J. E. Silva, "Effects of thyroid hormone on norepinephrine signaling in brown adipose tissue. I. Beta 1- and beta 2-adrenergic receptors and cyclic adenosine 3',5'-monophosphate generation," *Endocrinology*, vol. 136, pp. 3267-3276, 1995.

[106] A. Rubio, A. Raasmaja, and J. E. Silva, "Thyroid hormone and norepinephrine signaling in brown adipose tissue. II: Differential effects of thyroid hormone on beta 3-adrenergic receptors in brown and white adipose tissue," *Endocrinology*, vol. 136, pp. 3277-3284, 1995.

[107] J. I. Joo, D. H. Kim, J.-W. Choi, and J. W. Yun, "Proteomic Analysis for Antiobesity Potential of Capsaicin on White Adipose Tissue in Rats Fed with a High Fat Diet," *Journal of Proteome Research*, vol. 9, pp. 2977-2987, 2010/06/04 2010.

[108] F. M. Fisher, S. Kleiner, N. Douris, E. C. Fox, R. J. Mepani, F. Verdeguer, *et al.*, "FGF21 regulates PGC-1alpha and browning of white adipose tissues in adaptive thermogenesis," *Genes Dev,* vol. 26, pp. 271-81, Feb 1 2012.

[109] S. Raschke, M. Elsen, H. Gassenhuber, M. Sommerfeld, U. Schwahn, B. Brockmann, *et al.*, "Evidence against a beneficial effect of irisin in humans," *PLoS One,* vol. 8, p. e73680, 2013.

[110] M. S. Wen, C. Y. Wang, S. L. Lin, and K. C. Hung, "Decrease in irisin in patients with chronic kidney disease," *PLoS One,* vol. 8, p. e64025, 2013.

[111] J. Y. Huh, G. Panagiotou, V. Mougios, M. Brinkoetter, M. T. Vamvini, B. E. Schneider, *et al.*, "FNDC5 and irisin in humans: I. Predictors of circulating concentrations in serum and plasma and II. mRNA expression and circulating concentrations in response to weight loss and exercise," *Metabolism,* vol. 61, pp. 1725-38, Dec 2012.

[112] J. J. Liu, M. D. Wong, W. C. Toy, C. S. Tan, S. Liu, X. W. Ng, *et al.*, "Lower circulating irisin is associated with type 2 diabetes mellitus," *J Diabetes Complications,* vol. 27, pp. 365-9, Jul-Aug 2013.

[113] A. Stengel, T. Hofmann, M. Goebel-Stengel, U. Elbelt, P. Kobelt, and B. F. Klapp, "Circulating levels of irisin in patients with anorexia nervosa and different stages of obesity--correlation with body mass index," *Peptides,* vol. 39, pp. 125-30, Jan 2013.

[114] A. G. Swick, S. Orena, and A. O'Connor, "Irisin levels correlate with energy expenditure in a subgroup of humans with energy expenditure greater than predicted by fat free mass," *Metabolism,* vol. 62, pp. 1070-3, Aug 2013.

[115] H. J. Zhang, X. F. Zhang, Z. M. Ma, L. L. Pan, Z. Chen, H. W. Han, *et al.*, "Irisin is inversely associated with intrahepatic triglyceride contents in obese adults," *J Hepatol,* vol. 59, pp. 557-62, Sep 2013.

[116] F. Norheim, T. M. Langleite, M. Hjorth, T. Holen, A. Kielland, H. K. Stadheim, *et al.*, "The effects of acute and chronic exercise on PGC-1alpha, irisin and browning of subcutaneous adipose tissue in humans," *FEBS J,* vol. 281, pp. 739-49, Feb 2014.

[117] A. Hecksteden, M. Wegmann, A. Steffen, J. Kraushaar, A. Morsch, S. Ruppenthal, *et al.*, "Irisin and exercise training in humans - results from a randomized controlled training trial," *BMC Med,* vol. 11, p. 235, 2013.

[118] M. Alvehus, N. Boman, K. Soderlund, M. B. Svensson, and J. Buren, "Metabolic adaptations in skeletal muscle, adipose tissue, and whole-body oxidative capacity in response to resistance training," *Eur J Appl Physiol,* vol. 114, pp. 1463-71, Jul 2014.

[119] S. H. Lecker, A. Zavin, P. Cao, R. Arena, K. Allsup, K. M. Daniels, *et al.*, "Expression of the irisin precursor FNDC5 in skeletal muscle correlates with aerobic exercise performance in patients with heart failure," *Circ Heart Fail,* vol. 5, pp. 812-8, Nov 2012.

[120] S. Pekkala, P. K. Wiklund, J. J. Hulmi, J. P. Ahtiainen, M. Horttanainen, E. Pollanen, *et al.*, "Are skeletal muscle FNDC5 gene expression and irisin release regulated by exercise and related to health?," *J Physiol,* vol. 591, pp. 5393-400, Nov 1 2013.

[121] J. A. Timmons, K. Baar, P. K. Davidsen, and P. J. Atherton, "Is irisin a human exercise gene?," *Nature,* vol. 488, pp. E9-10; discussion E10-1, Aug 30 2012.

[122] T. Kurdiova, M. Balaz, M. Vician, D. Maderova, M. Vlcek, L. Valkovic, *et al.*, "Effects of obesity, diabetes and exercise on Fndc5 gene expression and irisin release in human skeletal muscle and adipose tissue: in vivo and in vitro studies," *J Physiol,* vol. 592, pp. 1091-107, Mar 1 2014.

[123] F. Scharhag-Rosenberger, T. Meyer, M. Wegmann, S. Ruppenthal, L. Kaestner, A. Morsch, *et al.*, "Irisin does not mediate resistance training-induced alterations in resting metabolic rate," *Med Sci Sports Exerc,* vol. 46, pp. 1736-43, Sep 2014.

[124] D. Loffler, U. Muller, K. Scheuermann, D. Friebe, J. Gesing, J. Bielitz, *et al.*, "Serum irisin levels are regulated by acute strenuous exercise," *J Clin Endocrinol Metab,* vol. 100, pp. 1289-99, Apr 2015.

[125] T. Hew-Butler, K. Landis-Piwowar, G. Byrd, M. Seimer, N. Seigneurie, B. Byrd, *et al.*, "Plasma irisin in runners and nonrunners: no favorable metabolic associations in humans," *Physiol Rep,* vol. 3, Jan 1 2015.

[126] A. Besse-Patin, E. Montastier, C. Vinel, I. Castan-Laurell, K. Louche, C. Dray, *et al.*, "Effect of endurance training on skeletal muscle myokine expression in obese men: identification of apelin as a novel myokine," *Int J Obes (Lond),* vol. 38, pp. 707-13, May 2014.

[127] M. V. Wu, G. Bikopoulos, S. Hung, and R. B. Ceddia, "Thermogenic capacity is antagonistically regulated in classical brown and white subcutaneous fat depots by high-fat diet and endurance training in rats: Impact on whole-body energy expenditure," *J Biol Chem,* Oct 25 2014.

[128] J. M. Moreno-Navarrete, F. Ortega, M. Serrano, E. Guerra, G. Pardo, F. Tinahones, *et al.*, "Irisin is expressed and produced by human muscle and adipose tissue in association with obesity and insulin resistance," *J Clin Endocrinol Metab,* vol. 98, pp. E769-78, Apr 2013.

[129] A. Roca-Rivada, C. Castelao, L. L. Senin, M. O. Landrove, J. Baltar, A. Belen Crujeiras, *et al.*, "FNDC5/irisin is not only a myokine but also an adipokine," *PLoS One,* vol. 8, p. e60563, 2013.

[130] A. Crujeiras, M. Pardo, and F. Casanueva, "Irisin: "Fat" Or Artifact," *Clin Endocrinol (Oxf),* Oct 7 2014.

[131] A. B. Crujeiras, M. Pardo, R. R. Arturo, S. Navas-Carretero, M. A. Zulet, J. A. Martinez, *et al.*, "Longitudinal variation of circulating irisin after an energy restriction-induced weight loss and following weight regain in obese men and women," *Am J Hum Biol,* vol. 26, pp. 198-207, Mar-Apr 2014.

[132] K. H. Park, L. Zaichenko, M. Brinkoetter, B. Thakkar, A. Sahin-Efe, K. E. Joung, *et al.*, "Circulating irisin in relation to insulin resistance and the metabolic syndrome," *J Clin Endocrinol Metab,* vol. 98, pp. 4899-907, Dec 2013.

[133] J. J. Liu, S. Liu, M. D. Wong, C. S. Tan, S. Tavintharan, C. F. Sum, *et al.*, "Relationship between circulating irisin, renal function and body composition in type 2 diabetes," *J Diabetes Complications,* vol. 28, pp. 208-13, Mar-Apr 2014.

[134] S. Aydin, S. Aydin, T. Kuloglu, M. Yilmaz, M. Kalayci, I. Sahin, *et al.*, "Alterations of irisin concentrations in saliva and serum of obese and normal-weight subjects, before and after 45 min of a Turkish bath or running," *Peptides,* vol. 50, pp. 13-8, Dec 2013.

[135] Y. K. Choi, M. K. Kim, K. H. Bae, H. A. Seo, J. Y. Jeong, W. K. Lee, *et al.*, "Serum irisin levels in new-onset type 2 diabetes," *Diabetes Res Clin Pract,* vol. 100, pp. 96-101, Apr 2013.

[136] S. A. Polyzos, J. Kountouras, A. D. Anastasilakis, E. V. Geladari, and C. S. Mantzoros, "Irisin in patients with nonalcoholic fatty liver disease," *Metabolism,* vol. 63, pp. 207-17, Feb 2014.

[137] T. Ebert, D. Focke, D. Petroff, U. Wurst, J. Richter, A. Bachmann, *et al.*, "Serum levels of the myokine irisin in relation to metabolic and renal function," *Eur J Endocrinol,* vol. 170, pp. 501-6, Apr 2014.

[138] I. Gouni-Berthold, H. K. Berthold, J. Y. Huh, R. Berman, N. Spenrath, W. Krone, *et al.*, "Effects of lipid-lowering drugs on irisin in human subjects in vivo and in human skeletal muscle cells ex vivo," *PLoS One,* vol. 8, p. e72858, 2013.

[139] Y. Zhang, R. Li, Y. Meng, S. Li, W. Donelan, Y. Zhao, *et al.*, "Irisin stimulates browning of white adipocytes through mitogen-activated protein kinase p38 MAP kinase and ERK MAP kinase signaling," *Diabetes,* vol. 63, pp. 514-25, Feb 2014.

[140] J. Y. Huh, F. Dincer, E. Mesfum, and C. S. Mantzoros, "Irisin stimulates muscle growth-related genes and regulates adipocyte differentiation and metabolism in humans," *Int J Obes (Lond),* Mar 11 2014.

[141] C. Wang, L. Wang, W. Li, F. Yan, M. Tian, C. Wu, *et al.*, "Irisin has no effect on lipolysis in 3T3-L1 adipocytes or fatty acid metabolism in HepG2 hepatocytes," *Endocrine,* Oct 19 2014.

[142] T. Shan, X. Liang, P. Bi, and S. Kuang, "Myostatin knockout drives browning of white adipose tissue through activating the AMPK-PGC1alpha-Fndc5 pathway in muscle," *FASEB J,* vol. 27, pp. 1981-9, May 2013.

[143] Y. Izumiya, H. A. Bina, N. Ouchi, Y. Akasaki, A. Kharitonenkov, and K. Walsh, "FGF21 is an Akt-regulated myokine," *FEBS Lett,* vol. 582, pp. 3805-10, Nov 12 2008.

[144] T. Nishimura, Y. Nakatake, M. Konishi, and N. Itoh, "Identification of a novel FGF, FGF-21, preferentially expressed in the liver," *Biochim Biophys Acta,* vol. 1492, pp. 203-6, Jun 21 2000.

[145] M. K. Badman, P. Pissios, A. R. Kennedy, G. Koukos, J. S. Flier, and E. Maratos-Flier, "Hepatic fibroblast growth factor 21 is regulated by PPARalpha and is a key mediator of hepatic lipid metabolism in ketotic states," *Cell Metab,* vol. 5, pp. 426-37, Jun 2007.

[146] T. Inagaki, P. Dutchak, G. Zhao, X. Ding, L. Gautron, V. Parameswara, *et al.*, "Endocrine regulation of the fasting response by PPARalpha-mediated induction of fibroblast growth factor 21," *Cell Metab,* vol. 5, pp. 415-25, Jun 2007.

[147] T. Lundasen, M. C. Hunt, L. M. Nilsson, S. Sanyal, B. Angelin, S. E. Alexson, *et al.*, "PPARalpha is a key regulator of hepatic FGF21," *Biochem Biophys Res Commun,* vol. 360, pp. 437-40, Aug 24 2007.

[148] E. Hondares, M. Rosell, F. J. Gonzalez, M. Giralt, R. Iglesias, and F. Villarroya, "Hepatic FGF21 expression is induced at birth via PPARalpha in response to milk intake and contributes to thermogenic activation of neonatal brown fat," *Cell Metab,* vol. 11, pp. 206-12, Mar 3 2010.

[149] E. Hondares, R. Iglesias, A. Giralt, F. J. Gonzalez, M. Giralt, T. Mampel, *et al.*, "Thermogenic activation induces FGF21 expression and release in brown adipose tissue," *J Biol Chem,* vol. 286, pp. 12983-90, Apr 15 2011.

[150] D. V. Chartoumpekis, I. G. Habeos, P. G. Ziros, A. I. Psyrogiannis, V. E. Kyriazopoulou, and A. G. Papavassiliou, "Brown adipose tissue responds to cold and adrenergic stimulation by induction of FGF21," *Mol Med,* vol. 17, pp. 736-40, 2011.

[151] A. Suomalainen, J. M. Elo, K. H. Pietilainen, A. H. Hakonen, K. Sevastianova, M. Korpela, *et al.*, "FGF-21 as a biomarker for muscle-manifesting mitochondrial respiratory chain deficiencies: a diagnostic study," *Lancet Neurol,* vol. 10, pp. 806-18, Sep 2011.

[152] A. Kharitonenkov, J. D. Dunbar, H. A. Bina, S. Bright, J. S. Moyers, C. Zhang, *et al.*, "FGF-21/FGF-21 receptor interaction and activation is determined by βKlotho," *Journal of Cellular Physiology,* vol. 215, pp. 1-7, 2008.

[153] Y. Ogawa, H. Kurosu, M. Yamamoto, A. Nandi, K. P. Rosenblatt, R. Goetz, *et al.*, "BetaKlotho is required for metabolic activity of fibroblast growth factor 21," *Proc Natl Acad Sci U S A,* vol. 104, pp. 7432-7, May 1 2007.

[154] J. S. Moyers, T. L. Shiyanova, F. Mehrbod, J. D. Dunbar, T. W. Noblitt, K. A. Otto, *et al.*, "Molecular determinants of FGF-21 activity-synergy and cross-talk with PPARgamma signaling," *J Cell Physiol,* vol. 210, pp. 1-6, Jan 2007.

[155] P. A. Dutchak, T. Katafuchi, A. L. Bookout, J. H. Choi, R. T. Yu, D. J. Mangelsdorf, *et al.*, "Fibroblast growth factor-21 regulates PPARgamma activity and the antidiabetic actions of thiazolidinediones," *Cell,* vol. 148, pp. 556-67, Feb 3 2012.

[156] A. Kharitonenkov, T. L. Shiyanova, A. Koester, A. M. Ford, R. Micanovic, E. J. Galbreath, *et al.*, "FGF-21 as a novel metabolic regulator," *J Clin Invest,* vol. 115, pp. 1627-35, Jun 2005.

[157] D. Cuevas-Ramos, C. A. Aguilar-Salinas, and F. J. Gomez-Perez, "Metabolic actions of fibroblast growth factor 21," *Curr Opin Pediatr,* vol. 24, pp. 523-9, Aug 2012.

[158] T. Coskun, H. A. Bina, M. A. Schneider, J. D. Dunbar, C. C. Hu, Y. Chen, *et al.*, "Fibroblast growth factor 21 corrects obesity in mice," *Endocrinology,* vol. 149, pp. 6018-27, Dec 2008.

[159] J. Xu, S. Stanislaus, N. Chinookoswong, Y. Y. Lau, T. Hager, J. Patel, *et al.*, "Acute glucose-lowering and insulin-sensitizing action of FGF21 in insulin-resistant mouse models--association with liver and adipose tissue effects," *Am J Physiol Endocrinol Metab,* vol. 297, pp. E1105-14, Nov 2009.

[160] F. M. Fisher, J. L. Estall, A. C. Adams, P. J. Antonellis, H. A. Bina, J. S. Flier, *et al.*, "Integrated regulation of hepatic metabolism by fibroblast growth factor 21 (FGF21) in vivo," *Endocrinology,* vol. 152, pp. 2996-3004, Aug 2011.

[161] Y. Hotta, H. Nakamura, M. Konishi, Y. Murata, H. Takagi, S. Matsumura, *et al.*, "Fibroblast growth factor 21 regulates lipolysis in white adipose tissue but is not required for ketogenesis and triglyceride clearance in liver," *Endocrinology,* vol. 150, pp. 4625-33, Oct 2009.

[162] W. L. Holland, A. C. Adams, J. T. Brozinick, H. H. Bui, Y. Miyauchi, C. M. Kusminski, *et al.*, "An FGF21-adiponectin-ceramide axis controls energy expenditure and insulin action in mice," *Cell Metab,* vol. 17, pp. 790-7, May 7 2013.

[163] Z. Lin, H. Tian, K. S. Lam, S. Lin, R. C. Hoo, M. Konishi, *et al.*, "Adiponectin mediates the metabolic effects of FGF21 on glucose homeostasis and insulin sensitivity in mice," *Cell Metab,* vol. 17, pp. 779-89, May 7 2013.

[164] A. L. De Sousa-Coelho, J. Relat, E. Hondares, A. Perez-Marti, F. Ribas, F. Villarroya, *et al.*, "FGF21 mediates the lipid metabolism response to amino acid starvation," *J Lipid Res,* vol. 54, pp. 1786-97, Jul 2013.

[165] M. Wabitsch, R. E. Brenner, I. Melzner, M. Braun, P. Moller, E. Heinze, *et al.*, "Characterization of a human preadipocyte cell strain with high capacity for adipose differentiation," *Int J Obes Relat Metab Disord,* vol. 25, pp. 8-15, Jan 2001.

[166] M. D. Brand, "The efficiency and plasticity of mitochondrial energy transduction," *Biochem Soc Trans,* vol. 33, pp. 897-904, Nov 2005.

[167] A. Subramanian, P. Tamayo, V. K. Mootha, S. Mukherjee, B. L. Ebert, M. A. Gillette, *et al.*, "Gene set enrichment analysis: A knowledge-based approach for interpreting genome-wide expression profiles," *Proceedings of the National Academy of Sciences,* vol. 102, pp. 15545-15550, October 25, 2005 2005.

[168] H. Ogata, S. Goto, K. Sato, W. Fujibuchi, H. Bono, and M. Kanehisa, "KEGG: Kyoto Encyclopedia of Genes and Genomes," *Nucleic Acids Research,* vol. 27, pp. 29-34, 1999.

[169] T. G. O. Consortium, "Creating the Gene Ontology Resource: Design and Implementation," *Genome Research,* vol. 11, pp. 1425-1433, 01/18/received, 05/14/accepted 2001.

[170] E. Y. Chen, C. M. Tan, Y. Kou, Q. Duan, Z. Wang, G. V. Meirelles, *et al.*, "Enrichr: interactive and collaborative HTML5 gene list enrichment analysis tool," *BMC Bioinformatics,* vol. 14, p. 128, 2013.

[171] M. Reich, T. Liefeld, J. Gould, J. Lerner, P. Tamayo, and J. P. Mesirov, "GenePattern 2.0," *Nat Genet,* vol. 38, pp. 500-1, May 2006.

[172] J. D. Bendtsen, H. Nielsen, G. von Heijne, and S. Brunak, "Improved prediction of signal peptides: SignalP 3.0," *J Mol Biol,* vol. 340, pp. 783-95, Jul 16 2004.

[173] T. N. Petersen, S. Brunak, G. von Heijne, and H. Nielsen, "SignalP 4.0: discriminating signal peptides from transmembrane regions," *Nat Methods,* vol. 8, pp. 785-6, 2011.

[174] J. D. Bendtsen, L. J. Jensen, N. Blom, G. Von Heijne, and S. Brunak, "Feature-based prediction of non-classical and leaderless protein secretion," *Protein Eng Des Sel,* vol. 17, pp. 349-56, Apr 2004.

[175] K. Eichelbaum, M. Winter, M. Berriel Diaz, S. Herzig, and J. Krijgsveld, "Selective enrichment of newly synthesized proteins for quantitative secretome analysis," *Nat Biotechnol,* vol. 30, pp. 984-90, Oct 2012.

[176] S. E. Calvo, K. R. Clauser, and V. K. Mootha, "MitoCarta2.0: an updated inventory of mammalian mitochondrial proteins," *Nucleic Acids Research,* vol. 44, pp. D1251-D1257, January 4, 2016 2016.

[177] W. B. Novoa, A. D. Winer, A. J. Glaid, and G. W. Schwert, "Lactic Dehydrogenase: V. INHIBITION BY OXAMATE AND BY OXALATE," *Journal of Biological Chemistry,* vol. 234, pp. 1143-1148, May 1, 1959 1959.

[178] F. G. Schaap, A. E. Kremer, W. H. Lamers, P. L. Jansen, and I. C. Gaemers, "Fibroblast growth factor 21 is induced by endoplasmic reticulum stress," *Biochimie,* vol. 95, pp. 692-9, Apr 2013.

[179] H. G. Crabtree, "Observations on the carbohydrate metabolism of tumours," *Biochem J,* vol. 23, pp. 536-45, 1929.

[180] E. Tanaka, H. Fukuda, K. Nakashima, N. Tsuchiya, H. Seimiya, and H. Nakagama, "HnRNP A3 binds to and protects mammalian telomeric repeats in vitro," *Biochemical and Biophysical Research Communications,* vol. 358, pp. 608-614, 6/29/ 2007.

[181] C. Lee, J. Zeng, Brian G. Drew, T. Sallam, A. Martin-Montalvo, J. Wan, *et al.*, "The Mitochondrial-Derived Peptide MOTS-c Promotes Metabolic Homeostasis and Reduces Obesity and Insulin Resistance," *Cell Metabolism,* vol. 21, pp. 443-454, 3/3/ 2015.

[182] C. Lee, K. Yen, and P. Cohen, "Humanin: a harbinger of mitochondrial-derived peptides?," *Trends in endocrinology and metabolism: TEM,* vol. 24, pp. 222-228, 02/08 2013.

[183] V. Massa, E. Fernandez-Vizarra, S. Alshahwan, E. Bakhsh, P. Goffrini, I. Ferrero, *et al.*, "Severe Infantile Encephalomyopathy Caused by a Mutation in COX6B1, a Nucleus-Encoded Subunit of Cytochrome C Oxidase," *The American Journal of Human Genetics,* vol. 82, pp. 1281-1289, 6/6/ 2008.

[184] P. Bragoszewski, M. Wasilewski, P. Sakowska, A. Gornicka, L. Böttinger, J. Qiu, *et al.*, "Retro-translocation of mitochondrial intermembrane space proteins," *Proceedings of the National Academy of Sciences,* vol. 112, pp. 7713-7718, June 23, 2015 2015.

[185] T. M. Hahn, J. F. Breininger, D. G. Baskin, and M. W. Schwartz, "Coexpression of Agrp and NPY in fasting-activated hypothalamic neurons," *Nat Neurosci,* vol. 1, pp. 271-2, Aug 1998.

[186] M. Zang, A. Zuccollo, X. Hou, D. Nagata, K. Walsh, H. Herscovitz, *et al.*, "AMP-activated Protein Kinase Is Required for the Lipid-lowering Effect of Metformin in Insulin-resistant Human HepG2 Cells," *Journal of Biological Chemistry*, vol. 279, pp. 47898-47905, November 12, 2004 2004.

[187] H. P. Erickson, "Irisin and FNDC5 in retrospect: An exercise hormone or a transmembrane receptor?," *Adipocyte*, vol. 2, pp. 289-93, Oct 1 2013.

[188] P. Lee, J. D. Linderman, S. Smith, R. J. Brychta, J. Wang, C. Idelson, *et al.*, "Irisin and FGF21 are cold-induced endocrine activators of brown fat function in humans," *Cell Metab*, vol. 19, pp. 302-9, Feb 4 2014.

[189] M. Elsen, S. Raschke, and J. Eckel, "Browning of white fat: does irisin play a role in humans?," *J Endocrinol*, vol. 222, pp. R25-38, Jul 2014.

[190] Y. Zhang, C. Xie, H. Wang, R. M. Foss, M. Clare, E. V. George, *et al.*, "Irisin exerts dual effects on browning and adipogenesis of human white adipocytes," *American Journal of Physiology - Endocrinology And Metabolism*, vol. 311, pp. E530-E541, 2016.

[191] S. A. Brooks, "Appropriate glycosylation of recombinant proteins for human use," *Molecular Biotechnology*, vol. 28, pp. 241-255, 2004// 2004.

[192] S.-E. Kim, R. Mori, T. Komatsu, T. Chiba, H. Hayashi, S. Park, *et al.*, "Upregulation of cytochrome c oxidase subunit 6b1 (Cox6b1) and formation of mitochondrial supercomplexes: implication of Cox6b1 in the effect of calorie restriction," *AGE*, vol. 37, pp. 1-17, 2015/05/01 2015.

[193] F. B. Benatti and B. K. Pedersen, "Exercise as an anti-inflammatory therapy for rheumatic diseases-myokine regulation," *Nat Rev Rheumatol*, Nov 25 2014.

[194] K. F. Petersen, D. Befroy, S. Dufour, J. Dziura, C. Ariyan, D. L. Rothman, *et al.*, "Mitochondrial Dysfunction in the Elderly: Possible Role in Insulin Resistance," *Science*, vol. 300, pp. 1140-1142, 2003-05-16 00:00:00 2003.

[195] K. F. Petersen , S. Dufour , D. Befroy , R. Garcia , and G. I. Shulman "Impaired Mitochondrial Activity in the Insulin-Resistant Offspring of Patients with Type 2 Diabetes," *New England Journal of Medicine*, vol. 350, pp. 664-671, 2004.

[196] M. K. Montgomery and N. Turner, "Mitochondrial dysfunction and insulin resistance: an update," *Endocrine Connections*, vol. 4, pp. R1-R15, March 1, 2015 2015.

[197] J. Durieux, S. Wolff, and A. Dillin, "The Cell-Non-Autonomous Nature of Electron Transport Chain-Mediated Longevity," *Cell*, vol. 144, pp. 79-91, 1/7/ 2011.

[198] Q. Zhang, M. Raoof, Y. Chen, Y. Sumi, T. Sursal, W. Junger, *et al.*, "Circulating mitochondrial DAMPs cause inflammatory responses to injury," *Nature*, vol. 464, pp. 104-107, 03/04/print 2010.

[199] Y. Ding, J. Wang, J. Wang, Y. D. Stierhof, D. G. Robinson, and L. Jiang, "Unconventional protein secretion," *Trends Plant Sci*, vol. 17, pp. 606-15, Oct 2012.

[200] F. F. Inagaki, M. Tanaka, N. F. Inagaki, T. Yagai, Y. Sato, K. Sekiguchi, *et al.*, "Nephronectin is upregulated in acute and chronic hepatitis and aggravates liver injury by recruiting CD4 positive cells," *Biochem Biophys Res Commun*, vol. 430, pp. 751-6, Jan 11 2013.

6. Supplementary Material

Supplemental Table 1: Proteins common to the secretomes of C2C12 myotubes and primary muscle fibers. Fold changes by nutrient deprivation and treatment with 100 nM Myxothiazol, respectively, are given with the respective p-values for each protein and represent n=4 experiments. Further, peptide count, peptides used for quantitation and confidence score are given for each protein.

		C2C12 myotubes					Primary muscle fibers - medium fraction					Primary muscle fibers - vesicle fraction					secretion evidence			MitoCarta2.0	
Protein ID	Gene Symbol	Ratio nutrient deprived/control	Anova (p)	Peptide count	Peptides used for quantitation	Confidence score	Ratio Myxothiazol/control	Anova (p)	Peptide count	Peptides used for quantitation	Confidence score	Ratio Myxothiazol/control	Anova (p)	Peptide count	Peptides used for quantitation	Confidence score	SignalP/SecretomeP	Eichelbaum et al, 2012	Secretory protein?	MitoCarta2_score	MitoCarta2_FDR
ENSMUSP00000029955	**1700009N14Rik**	0.699	0.4052	3	2	140.94	6.133	0.0021	3	3	84.31						SecretomeP	no	yes		
ENSMUSP00000031931	**2210010C04Rik**	0.411	0.1930	1	1	67.79	1.056	0.7894	1	1	31.38						SignalP	no	yes		
ENSMUSP00000115672	**Aamdc**	0.017	0.2625	1	1	28.83	10.439	0.0061	1	1	23.80						SignalP	no	yes		
ENSMUSP00000037348	**Acaa2**	1.294	0.9579	1	1	64.37						17.436	0.0001	2	2	79.08	SecretomeP	no	yes	23.3099	0.005
ENSMUSP00000027153	**Acadl**	0.904	0.7425	4	3	156.36						4.952	0.0003	2	2	54.33	SignalP	no	yes	27.6965	0.004
ENSMUSP00000026324	**Acot9**	1.465	0.2625	3	3	61.59						2.897	0.0656	1	1	19.35	SecretomeP	no	yes	5.8393	0.049
ENSMUSP00000106509	**Acp1**	0.635	0.2630	1	1	72.73	5.727	0.0052	4	4	181.62						SecretomeP	no	yes		
ENSMUSP00000034453	**Acta1**	1.309	0.6615	27	2	1893.17	0.387	0.1190	16	1	966.53	3.449	0.0555	33	4	1912.36	SecretomeP	no	yes		
ENSMUSP00000071486	**Actg1**	1.524	0.1258	23	6	1676.24	0.454	0.0389	13	3	575.04	0.527	0.1919	21	4	837.40	SecretomeP	no	yes		
ENSMUSP00000065529	**Adam6b**	0.882	0.7878	1	1	14.61						0.262	0.2882	1	1	25.98	SignalP	no	yes		
ENSMUSP00000023043	**Adsl**	0.588	0.4348	2	2	97.49	7.318	0.0008	7	7	390.85	2.978	0.0013	5	5	191.80	SecretomeP	no	yes		
ENSMUSP00000061851	**Ahcy**	0.899	0.7872	3	3	148.03	3.733	0.0012	7	7	274.79	1.335	0.2222	2	2	88.16	SecretomeP	no	yes		
ENSMUSP00000023583	**Ahsg**	0.490	0.3059	1	1	34.00	0.625	0.3070	1	1	34.21	0.149	0.0296	1	1	27.82	SignalP	yes	yes		
ENSMUSP00000068479	**Ak1**	0.779	0.0295	6	6	375.12	3.103	0.0144	15	15	1262.87	4.387	0.0002	12	12	633.26	SecretomeP	no	yes		
ENSMUSP00000030090	**Alad**	1.416	0.4987	4	4	184.46	65.618	0.0049	1	1	43.99						SecretomeP	no	yes		
ENSMUSP00000031314	**Alb**	0.570	0.6109	4	2	371.15	0.509	0.0010	15	13	839.01	0.306	0.0325	6	4	318.99	SignalP	yes	yes		
ENSMUSP00000031411	**Aldh2**	1.074	0.8292	4	2	126.29						1.163	0.4355	2	2	96.16	SecretomeP	no	yes	21.004	0.004
ENSMUSP00000032934	**Aldoa**	0.692	0.2626	24	19	1561.19	5.022	0.0019	41	34	2676.41	3.720	0.0008	25	25	1312.58	SignalP	no	yes		
ENSMUSP00000025561	**Anxa1**	3.004	0.0021	15	12	913.34						1.231	0.4553	2	2	97.36	SecretomeP	no	yes		
ENSMUSP00000022416	**Anxa11**	1.050	0.8328	1	1	79.97						1.890	0.0147	12	9	520.45	SecretomeP	no	yes		
ENSMUSP00000034756	**Anxa2**	1.642	0.0215	10	9	556.03						0.380	0.0046	3	3	144.64	SecretomeP	yes	yes		
ENSMUSP00000001187	**Anxa4**	1.104	0.9008	3	2	153.53						2.594	0.0047	5	5	289.69	SecretomeP	no	yes		
ENSMUSP00000066035	**Anxa7**	1.025	0.9653	2	1	66.61	2.127	0.0716	1	1	63.11	2.404	0.0063	6	5	384.77	SecretomeP	no	yes		
ENSMUSP00000080058	**Apeh**	0.507	0.1142	3	3	105.06	8.082	0.0011	3	3	128.18						SecretomeP	no	yes		
ENSMUSP00000042602	**Apex1**	0.909	0.7013	4	4	229.78	2.282	0.0272	2	2	43.13						SecretomeP	no	yes		
ENSMUSP00000029708	**Apoa1bp**	0.576	0.0836	3	3	113.71	5.477	0.0150	3	3	168.15						SignalP	yes	yes	18.2289	0.003
ENSMUSP00000035761	**Apob**	0.859	0.6892	1	1	16.21	0.318	0.0325	3	3	112.14						SignalP	yes	yes		
ENSMUSP00000039657	**Atp1a1**	1.768	0.6993	2	1	77.65						1.164	0.5185	17	7	880.61	SecretomeP	no	yes		
ENSMUSP00000032974	**Atp2a1**	1.038	0.8993	8	3	433.69	0.598	0.6777	16	16	1009.60	1.280	0.3269	55	37	3225.12	SecretomeP	no	yes		
ENSMUSP00000119018	**Atp2a1**	1.723	0.2096	1	1	20.35	0.486	0.4867	1	1	19.90	0.535	0.1619	3	2	117.36	SecretomeP	no	yes		
ENSMUSP00000031423	**Atp2a2**	1.676	0.2552	7	2	379.28						0.752	0.7134	18	2	1047.22	SecretomeP	no	yes		
ENSMUSP00000026495	**Atp5a1**	1.014	0.9064	6	6	232.31						1.939	0.0215	16	16	874.74	SecretomeP	no	yes	41.6009	0
ENSMUSP00000026459	**Atp5b**	1.478	0.3667	16	16	1128.95	0.506	0.0058	1	1	24.78	1.936	0.0451	20	20	1086.03	SecretomeP	no	yes	36.4532	0
ENSMUSP00000021197	**Blmh**	0.543	0.0464	6	6	394.71	5.524	0.0015	2	2	64.93						SecretomeP	no	yes		
ENSMUSP00000002064	**Blvra**	0.678	0.3772	1	1	38.75	7.568	0.0009	5	5	201.54						SecretomeP	no	yes		
ENSMUSP00000043092	**Blvrb**	0.116	0.0076	1	1	24.65	1.053	0.8454	1	1	20.58						SecretomeP	no	yes		
ENSMUSP00000070751	**Bsg**	1.114	0.8718	1	1	28.10						2.933	0.0132	5	5	270.47	SignalP	yes	yes		
ENSMUSP00000077612	**C1qbp**	0.661	0.7779	3	3	150.36	3.065	0.0036	1	1	26.77	1.518	0.2636	4	4	108.61	SignalP	no	yes	27.8817	0.004
ENSMUSP00000095270	**Cab39**	0.510	0.3868	1	1	49.00	4.028	0.0022	2	2	99.91						SecretomeP	no	yes		
ENSMUSP00000021065	**Cacng1**	1.435	0.3816	1	1	82.48						3.403	0.0054	1	1	63.66	SignalP	no	yes		
ENSMUSP00000001204	**Calm1**	0.707	0.4316	8	4	389.54	2.682	0.0105	6	4	317.97	2.743	0.0003	4	4	198.17	SecretomeP	no	yes		
ENSMUSP00000003912	**Calr**	0.312	0.0721	17	16	987.83	0.243	0.0152	2	2	40.42	0.456	0.0038	1	1	22.21	SignalP	yes	yes		
ENSMUSP00000031779	**Calu**	0.875	0.6664	16	3	1065.86						1.983	0.1325	1	1	35.82	SignalP	yes	yes		

ENSMUSP00000071720	**Camk2g**	0.600	0.3479	2	1	120.61						2.225	0.0802	3	1	122.17	SecretomeP	no	yes		
ENSMUSP00000020637	**Canx**	1.302	0.3905	4	4	172.11						1.593	0.1393	1	1	17.79	SignalP	yes	yes		
ENSMUSP00000025891	**Capn1**	0.274	0.0507	3	2	103.39	9.245	0.0002	6	5	274.88	3.175	0.0025	16	16	709.35	SecretomeP	no	yes		
ENSMUSP00000001845	**Capns1**	0.466	0.0973	2	2	140.12	4.467	0.0005	2	2	100.97	4.779	0.0008	4	4	190.68	SecretomeP	no	yes		
ENSMUSP00000030518	**Capzb**	1.077	0.8173	4	4	152.81	5.757	0.0021	1	1	13.90						SecretomeP	no	yes		
ENSMUSP00000003554	**Casq1**	2.167	0.0531	6	4	348.20	1.332	0.7397	1	1	86.94	1.376	0.3380	8	8	509.05	SignalP	yes	yes		
ENSMUSP00000029454	**Casq2**	4.079	0.0048	7	6	422.59						1.205	0.5283	1	1	28.78	SignalP	yes	yes		
ENSMUSP00000031402	**Cct6a**	1.260	0.3498	11	10	382.97	3.280	0.0254	1	1	18.84	10.380	0.0004	1	1	71.18	SecretomeP	no	yes		
ENSMUSP00000026704	**Cct8**	1.259	0.3682	15	14	708.69						2.796	0.0105	2	2	61.75	SecretomeP	no	yes		
ENSMUSP00000054634	**Cdc42**	1.004	0.9137	3	3	132.01						3.932	0.0033	1	1	19.04	SecretomeP	no	yes		
ENSMUSP00000113527	**Cdh13**	0.745	0.4745	6	5	258.74	5.050	0.0000	4	4	133.86	1.953	0.0386	3	3	123.59	SignalP	yes	yes		
ENSMUSP00000077262	**Cfl2**	0.626	0.1580	7	6	365.19	5.009	0.0005	12	11	669.54	4.057	0.0001	4	4	224.04	SecretomeP	no	yes		
ENSMUSP00000072538	**Col18a1**	0.869	0.7847	11	10	618.15	0.495	0.0035	6	6	272.75						SignalP	yes	yes		
ENSMUSP00000001547	**Col1a1**	1.368	0.7925	57	55	3994.89	0.498	0.1926	4	4	200.14						SignalP	yes	yes		
ENSMUSP00000085192	**Col3a1**	1.238	0.8728	57	53	3361.72	0.431	0.1584	2	2	60.00						SignalP	yes	yes		
ENSMUSP00000033898	**Col4a1**	0.670	0.2679	2	2	214.50	0.889	0.6355	2	2	152.28	0.128	0.0015	3	2	136.83	SignalP	yes	yes		
ENSMUSP00000033899	**Col4a2**	0.409	0.1151	4	3	129.84	0.494	0.0079	3	3	122.50	0.139	0.0132	1	1	15.94	SignalP	yes	yes		
ENSMUSP00000001147	**Col6a1**	1.542	0.5245	24	22	1968.91	2.809	0.2072	9	9	488.05	2.098	0.3786	9	9	334.50	SignalP	yes	yes		
ENSMUSP00000001181	**Col6a2**	1.534	0.3227	14	13	501.55	4.880	0.0841	5	5	212.09	4.504	0.2047	1	1	61.90	SignalP	yes	yes		
ENSMUSP00000057131	**Col6a3**	3.908	0.0006	43	40	2018.29	4.174	0.1432	13	13	630.21	3.126	0.2406	5	5	223.86	SignalP	yes	yes		
ENSMUSP00000019517	**Cops3**	0.929	0.8578	1	1	60.62	13.279	0.0010	1	1	28.80						SecretomeP	no	yes		
ENSMUSP00000048416	**Cops4**	0.772	0.3681	2	2	111.32	6.184	0.0006	4	4	155.50	11.177	0.0008	2	2	76.23	SecretomeP	no	yes		
ENSMUSP00000075150	**Cox6b1**	2.590	0.0258	1	1	30.52	32.375	0.0011	2	2	50.49						SecretomeP	no	yes	28.1988	0.004
ENSMUSP00000003714	**Cp**	0.820	0.5724	18	18	789.85	0.324	0.0002	3	3	89.19						SignalP	yes	yes		
ENSMUSP00000048555	**Cpe**	0.849	0.6866	6	6	231.26						0.014	0.0003	1	1	31.45	SignalP	yes	yes		
ENSMUSP00000034562	**Cryab**	0.791	0.6036	5	5	252.23	0.305	0.0079	4	4	154.92	1.312	0.2324	7	7	289.93	SecretomeP	no	yes		
ENSMUSP00000005826	**Cs**	0.920	0.9861	6	2	192.43	4.413	0.0003	3	3	153.67	1.595	0.0728	4	4	158.65	SecretomeP	no	yes	33.5076	0
ENSMUSP00000032658	**Csrp3**	0.671	0.4455	3	3	97.99	4.558	0.0000	5	5	282.59	2.906	0.0153	3	3	109.17	SecretomeP	no	yes		
ENSMUSP00000005185	**Cstb**	0.766	0.4104	1	1	15.70	6.628	0.0082	1	1	13.21						SecretomeP	no	yes		
ENSMUSP00000018186	**Cyb5r3**	1.311	0.3584	5	5	239.18						6.121	0.0195	1	1	15.42	SecretomeP	no	yes	2.1933	0.167
ENSMUSP00000001242	**D10Jhu81e**	0.686	0.2402	1	1	62.41	1.984	0.0867	1	1	19.20	5.144	0.0011	2	2	48.30	SignalP	yes	yes	29.2236	0.005
ENSMUSP00000079294	**Dag1**	0.998	0.8803	12	12	566.50	6.316	0.0015	4	4	199.61	11.241	0.0059	1	1	52.13	SignalP	yes	yes		
ENSMUSP00000027634	**Dbi**	0.872	0.9543	2	2	157.24	4.953	0.0016	2	2	94.78						SecretomeP	no	yes	8.4322	0.029
ENSMUSP00000025649	**Ddb1**	0.551	0.0371	16	14	714.36	8.357	0.0021	5	5	207.93						SecretomeP	no	yes		
ENSMUSP00000070682	**Ddx39b**	1.055	0.6011	7	1	178.29	7.527	0.0033	4	4	137.66	3.347	0.0157	1	1	46.85	SecretomeP	no	yes		
ENSMUSP00000027409	**Des**	0.893	0.6195	32	23	1843.22	3.334	0.0020	19	16	945.11	1.296	0.0411	25	21	1022.39	SecretomeP	no	yes		
ENSMUSP00000106481	**Dld**	0.711	0.5798	6	6	195.09	4.553	0.0058	3	3	113.10	2.851	0.0579	3	3	154.57	SecretomeP	no	yes	31.4471	0
ENSMUSP00000060346	**Dlst**	1.252	0.4216	1	1	34.00						4.037	0.0174	3	3	165.05	SecretomeP	no	yes	38.04	0
ENSMUSP00000003612	**Dusp3**	0.854	0.7217	1	1	117.24						8.958	0.0001	1	1	28.21	SecretomeP	no	yes		
ENSMUSP00000018851	**Dync1h1**	1.070	0.9506	22	18	892.18						0.413	0.0043	6	6	227.66	SecretomeP	no	yes		
ENSMUSP00000024946	**Eci1**	0.404	0.0393	2	2	73.74	5.636	0.0001	3	3	195.75						SecretomeP	no	yes	18.6394	0.003
ENSMUSP00000116492	**Eef1b2**	0.707	0.1724	3	2	227.62	6.048	0.0054	4	4	221.71	7.234	0.1176	3	2	121.59	SecretomeP	no	yes		
ENSMUSP00000028668	**Eif3j1**	1.040	0.8699	3	3	115.48	12.175	0.0000	7	7	266.37	2.613	0.0679	2	2	76.02	SignalP	no	yes		
ENSMUSP00000127034	**Eif4a1**	0.916	0.9709	9	4	591.74	4.036	0.1111	5	1	213.43						SecretomeP	no	yes		
ENSMUSP00000023599	**Eif4a2**	0.826	0.6062	7	2	524.69	5.342	0.0038	5	1	252.37	1.866	0.0100	3	3	138.74	SecretomeP	no	yes		
ENSMUSP00000029803	**Eif4e**	0.819	0.7467	3	2	87.77	Infinity	0.0000	1	1	38.83						SecretomeP	no	yes		
ENSMUSP00000048833	**Eif4h**	1.261	0.2975	1	1	26.27	33.973	0.0425	1	1	13.99						SecretomeP	no	yes		
ENSMUSP00000029142	**Eif6**	1.066	0.6677	5	5	192.10	2.175	0.0123	1	1	24.54						SecretomeP	no	yes		
ENSMUSP00000021559	**Erh**	0.760	0.3435	3	3	169.65	4.455	0.0058	1	1	52.49						SecretomeP	no	yes		
ENSMUSP00000022573	**Esd**	0.798	0.6121	1	1	15.30	2.403	0.0687	6	6	263.77	1.145	0.5496	2	2	51.44	SecretomeP	no	yes		
ENSMUSP00000054583	**Fbln1**	0.505	0.0966	10	1	572.30	0.472	0.0058	17	2	1117.85	0.244	0.0849	11	1	495.93	SignalP	yes	yes		
ENSMUSP00000105058	**Fbln1**	1.100	0.9042	10	1	567.03	0.468	0.0231	18	3	1136.85	0.088	0.0012	11	1	485.73	SignalP	yes	yes		
ENSMUSP00000028633	**Fbn1**	2.066	0.0716	61	59	3399.17						17.362	0.4226	6	6	203.22	SignalP	yes	yes		
ENSMUSP00000027810	**Fh1**	0.489	0.0028	6	6	249.14	10.424	0.0016	5	5	153.59	2.625	0.0092	4	4	124.28	SecretomeP	no	yes	36.4148	0
ENSMUSP00000023854	**Fhl1**	0.982	0.8142	9	9	481.08	6.554	0.0018	19	19	1319.24	3.065	0.0033	11	11	604.33	SecretomeP	no	yes		
ENSMUSP00000040150	**Fhl3**	0.608	0.1348	7	7	413.96	1.718	0.1558	6	6	296.57	1.641	0.1322	3	3	140.78	SecretomeP	no	yes		
ENSMUSP00000037206	**Fkbp1a**	0.603	0.2046	3	3	225.22	5.033	0.0010	5	5	345.89						SecretomeP	no	yes		
ENSMUSP00000021332	**Fkbp3**	1.549	0.1801	2	2	67.53	7.017	0.0002	4	3	166.15	14.084	0.0020	2	2	35.04	SecretomeP	no	yes		
ENSMUSP00000035489	**Fmod**	1.102	0.8928	7	6	466.77	0.217	0.7946	1	1	29.32						SignalP	yes	yes		
ENSMUSP00000054499	**Fn1**	1.856	0.0445	115	103	10394.98	0.280	0.0009	14	14	451.74	0.064	0.0005	6	6	187.25	SignalP	yes	yes		
ENSMUSP00000025563	**Fth1**	0.144	0.0047	2	2	43.13	8.595	0.0025	2	2	57.62						SecretomeP	no	yes	6.1372	0.046
ENSMUSP00000023684	**Gart**	0.498	0.2521	2	2	59.33	5.200	0.0049	2	2	58.05	10.977	0.0003	2	2	73.71	SecretomeP	no	yes		
ENSMUSP00000017430	**Glod4**	0.685	0.1435	5	5	178.46	9.277	0.0008	3	3	128.71						SecretomeP	no	yes	12.4632	0.013
ENSMUSP00000066621	**Glrx3**	0.896	0.8493	3	3	135.39	4.865	0.0187	2	2	141.52	9.137	0.0003	3	3	47.78	SecretomeP	no	yes		

ENSMUSP00000071686	**Gm10123**	1.257	0.3209	12	10	517.81	3.337	0.0050	5	5	209.72						SecretomeP	no	yes		
ENSMUSP00000132590	**Gm20390**	0.726	0.2713	11	3	534.79	5.244	0.0017	11	11	504.36						SignalP	no	yes		
ENSMUSP00000036849	**Gm5884**	0.779	0.4108	3	3	106.11						5.540	0.0019	2	1	35.20	SecretomeP	no	yes		
ENSMUSP00000072775	**Gm8991**	2.151	0.0432	5	5	228.60	5.339	0.0016	3	3	106.52						SecretomeP	no	yes		
ENSMUSP00000084807	**Gm9396**	0.630	0.4796	6	6	304.68						7.094	0.0088	2	2	44.34	SecretomeP	no	yes		
ENSMUSP00000034097	**Got2**	0.800	0.5496	10	9	577.78	3.207	0.0002	8	8	403.69	1.324	0.1599	7	7	272.98	SignalP	no	yes	11.1028	0.018
ENSMUSP00000049355	**Gpi1**	0.503	0.0372	16	16	834.11	4.667	0.0036	25	25	1530.39	3.468	0.0052	16	16	642.36	SecretomeP	yes	yes	10.7637	0.019
ENSMUSP00000028239	**Gsn**	1.077	0.5286	17	13	712.27	0.340	0.0251	2	2	137.90	0.808	0.5663	1	1	13.88	SignalP	yes	yes		
ENSMUSP00000033992	**Gsr**	0.939	0.8691	4	4	102.21	4.782	0.0063	7	7	424.87	26.199	0.0116	1	1	82.67	SecretomeP	no	yes	17.3498	0.003
ENSMUSP00000078630	**Gss**	0.536	0.0619	8	8	342.71	11.533	0.0058	1	1	31.35						SecretomeP	no	yes		
ENSMUSP00000026050	**Gsto1**	0.463	0.0325	7	6	288.28	7.207	0.0034	6	6	258.65						SecretomeP	no	yes	8.8844	0.029
ENSMUSP00000114019	**Gyg**	0.755	0.1083	3	3	145.74	5.501	0.0042	10	10	472.88	2.445	0.0088	2	2	50.71	SignalP	no	yes		
ENSMUSP00000137309	**H1f0**	2.485	0.0772	1	1	73.78						1.340	0.2555	1	1	37.82	SecretomeP	no	yes		
ENSMUSP00000029610	**Hadh**	0.637	0.4363	3	2	111.58	6.286	0.0038	2	2	58.95						SecretomeP	no	yes	28.9761	0.005
ENSMUSP00000024974	**Hagh**	0.515	0.0621	4	4	117.21	8.471	0.0042	4	4	159.09						SecretomeP	yes	yes	21.3661	0.004
ENSMUSP00000005017	**Hdgf**	0.491	0.2040	6	6	350.63	79.577	0.0039	1	1	52.22						SecretomeP	no	yes		
ENSMUSP00000026485	**Hdhd2**	0.469	0.0449	3	3	117.31	5.487	0.0085	1	1	14.74	44.457	0.0034	1	1	28.22	SignalP	no	yes		
ENSMUSP00000020504	**Hint1**	0.851	0.7590	1	1	57.36	7.251	0.0021	2	2	197.75	23.427	0.0008	2	2	65.41	SecretomeP	no	yes	5.5326	0.052
ENSMUSP00000082459	**Hrc**	0.768	0.9722	9	9	800.39						1.174	0.6120	2	2	149.15	SignalP	yes	yes		
ENSMUSP00000028222	**Hspa5**	0.581	0.1031	19	16	1336.98	0.563	0.0401	7	4	388.90	6.412	0.0043	9	7	441.78	SignalP	yes	yes		
ENSMUSP00000005077	**Hspb1**	1.085	0.8556	10	10	464.63						3.938	0.0016	7	7	232.87	SecretomeP	no	yes		
ENSMUSP00000099544	**Hspb7**	0.357	0.0311	1	1	50.28	11.819	0.0003	7	7	370.81	2.876	0.0023	6	6	259.70	SecretomeP	no	yes	6.4897	0.044
ENSMUSP00000068174	**Impa1**	0.649	0.4259	1	1	51.25	13.595	0.0017	4	4	124.80						SecretomeP	no	yes		
ENSMUSP00000032898	**Ipo5**	0.841	0.6391	11	10	467.71	5.650	0.0027	9	9	302.15	9.840	0.0002	1	1	26.79	SecretomeP	no	yes		
ENSMUSP00000096712	**Itga7**	0.930	0.9608	9	9	314.84						6.600	0.0120	4	3	109.44	SignalP	yes	yes		
ENSMUSP00000087457	**Itgb1**	0.742	0.4450	7	5	215.81						5.164	0.0056	4	4	141.92	SignalP	yes	yes		
ENSMUSP00000034426	**Kars**	0.570	0.1147	2	2	97.45						10.282	0.0414	1	1	30.32	No evidence	yes	yes	10.0889	0.022
ENSMUSP00000029353	**Kpna4**	0.768	0.6536	2	2	67.02	5.804	0.0050	1	1	45.92	19.475	0.0013	1	1	56.35	SecretomeP	no	yes		
ENSMUSP00000001479	**Kpnb1**	0.621	0.2563	6	6	330.78	2.472	0.0561	2	2	101.38	8.133	0.0034	4	4	190.51	SecretomeP	no	yes		
ENSMUSP00000017270	**Krt42**	6.097	0.4152	13	2	521.51						0.218	0.0609	8	2	269.47	SecretomeP	no	yes		
ENSMUSP00000027071	**Lactb2**	0.336	0.0035	1	1	27.35	10.302	0.0015	1	1	16.46						SecretomeP	no	yes	6.9782	0.038
ENSMUSP00000015791	**Lama5**	1.753	0.2151	4	3	166.84	0.564	0.0996	24	22	1114.42	0.151	0.0018	9	8	369.00	SignalP	yes	yes		
ENSMUSP00000002979	**Lamb1**	1.071	0.7943	2	2	45.71	0.519	0.0100	106	100	7039.28	0.200	0.0001	93	89	4483.22	No evidence	yes	yes		
ENSMUSP00000027752	**Lamc1**	3.164	0.0228	6	4	156.27	0.548	0.0131	123	120	8253.05	0.190	0.0001	118	116	6169.37	SignalP	yes	yes		
ENSMUSP00000036386	**Ldha**	0.257	0.0128	15	11	842.79	5.841	0.0003	17	14	832.56	2.970	0.0116	15	13	648.84	SecretomeP	no	yes		
ENSMUSP00000032373	**Ldhb**	0.427	0.1160	4	2	129.35	4.112	0.0032	7	5	418.73	2.009	0.4991	8	6	319.36	SecretomeP	no	yes		
ENSMUSP00000086795	**Lgals1**	0.776	0.4713	11	10	887.77	5.714	0.0034	7	7	344.07	6.730	0.0650	1	1	21.24	No evidence	yes	yes		
ENSMUSP00000114350	**Lgals3**	1.233	0.2960	5	5	285.17	0.609	0.0093	4	4	276.74						SecretomeP	yes	yes		
ENSMUSP00000016033	**Lta4h**	0.858	0.5884	8	7	261.87	8.832	0.0006	9	9	453.79						SecretomeP	no	yes		
ENSMUSP00000040877	**Lum**	0.476	0.4773	3	3	75.97	0.365	0.0223	1	1	75.77						SignalP	yes	yes		
ENSMUSP00000030842	**Lzic**	0.779	0.3943	2	2	38.31	6.464	0.0000	1	1	42.13						SecretomeP	no	yes		
ENSMUSP00000045432	**Mamdc2**	3.377	0.0262	1	1	16.26						0.006	0.5154	1	1	20.99	SignalP	yes	yes		
ENSMUSP00000019037	**Mb**	0.425	0.0495	8	8	580.28	5.353	0.0038	17	17	1465.16	2.422	0.0134	10	10	901.03	SecretomeP	no	yes		
ENSMUSP00000041149	**Mif**	0.702	0.4655	2	2	93.43	7.033	0.0021	2	2	102.30						SecretomeP	yes	yes		
ENSMUSP00000034856	**Mpi**	0.352	0.0064	4	4	218.37	9.047	0.0014	6	6	332.48	0.858	0.9827	2	1	129.87	SecretomeP	no	yes		
ENSMUSP00000113071	**Msn**	0.550	0.0428	32	22	1757.41	9.834	0.0004	7	3	276.18	14.340	0.0582	1	1	43.32	SecretomeP	no	yes		
ENSMUSP00000030033	**Murc**	1.150	0.5477	4	4	255.51	13.654	0.0032	1	1	36.00	2.321	0.0068	6	6	210.16	SecretomeP	no	yes		
ENSMUSP00000042195	**Mybph**	1.034	0.6184	7	6	350.94	3.960	0.0003	1	1	13.93	6.280	0.0025	2	2	57.16	SecretomeP	no	yes		
ENSMUSP00000027151	**Myl1**	1.123	0.6445	13	5	671.29	5.861	0.0000	14	9	706.83	2.428	0.0313	21	17	1101.35	SecretomeP	no	yes		
ENSMUSP00000026428	**Myl6b**	1.446	0.3148	6	4	256.83	2.280	0.0148	4	2	123.00	2.477	0.0091	10	8	485.57	SecretomeP	no	yes		
ENSMUSP00000034349	**Nae1**	0.533	0.3851	3	3	119.95	6.370	0.0026	3	3	108.30						SecretomeP	no	yes		
ENSMUSP00000110120	**Ncam1**	1.007	0.9027	22	20	1874.26	6.263	0.0083	1	1	13.83						No evidence	yes	yes		
ENSMUSP00000005532	**Nid1**	0.710	0.2080	25	22	1457.94	0.527	0.0061	71	68	5292.26	0.252	0.0004	59	59	3147.59	SignalP	yes	yes		
ENSMUSP00000022340	**Nid2**	0.615	0.7188	37	34	2352.99	0.388	0.0042	24	22	1303.18	0.222	0.0005	7	6	243.58	SignalP	yes	yes		
ENSMUSP00000023432	**Nit2**	0.492	0.0222	1	1	35.96	7.113	0.0036	3	3	103.12						SignalP	no	yes	19.2218	0.003
ENSMUSP00000001480	**Npepps**	0.497	0.0103	10	10	374.09	5.186	0.0047	15	15	484.88	2.612	0.1217	1	1	17.65	SignalP	no	yes		
ENSMUSP00000075067	**Npm1**	1.244	0.5847	4	4	251.16						1.320	0.6137	1	1	35.50	SecretomeP	no	yes		
ENSMUSP00000008594	**Nutf2**	0.497	0.0010	1	1	66.62	3.728	0.0180	2	2	125.20						SecretomeP	no	yes		
ENSMUSP00000026122	**P4hb**	0.572	0.1358	17	16	1097.96						0.999	0.8417	3	3	176.98	SignalP	yes	yes	0.1296	0.303
ENSMUSP00000030765	**Padi2**	1.680	0.0550	1	1	13.92						2.787	0.0442	4	4	154.03	SecretomeP	no	yes		
ENSMUSP00000030805	**Park7**	0.739	0.2696	7	7	205.27	4.590	0.0022	16	16	820.98	2.997	0.0002	10	10	436.04	SecretomeP	no	yes	1.6908	0.204
ENSMUSP00000023072	**Parvb**	0.725	0.0742	1	1	59.39						2.449	0.0718	1	1	42.99	SecretomeP	no	yes		
ENSMUSP00000054863	**Pcbp1**	0.984	0.9917	3	2	177.60	8.005	0.0018	2	2	30.10						SecretomeP	no	yes		
ENSMUSP00000113761	**Pdcd5**	0.729	0.3208	2	2	123.22	22.658	0.0009	2	2	86.59						SecretomeP	no	yes		

ENSMUSP00000033662	**Pdha1**	0.532	0.0648	2	2	48.48						2.183	0.0272	2	2	101.96	SecretomeP	no	yes	42.9867	0
ENSMUSP00000052912	**Pdia6**	1.290	0.1007	6	5	361.99						0.674	0.1019	3	3	105.48	SignalP	yes	yes		
ENSMUSP00000034053	**Pdlim3**	0.959	0.9709	4	4	167.08	6.053	0.0024	12	11	535.63	5.490	0.0010	5	5	182.94	SecretomeP	no	yes		
ENSMUSP00000018437	**Pfn1**	0.980	0.9659	9	9	464.88	3.822	0.0089	8	7	349.29						SecretomeP	no	yes		
ENSMUSP00000020768	**Pgam2**	0.469	0.0592	9	5	389.86	4.961	0.0017	17	13	938.17	3.414	0.0022	13	13	562.03	SecretomeP	no	yes		
ENSMUSP00000034264	**Pgls**	0.424	0.0091	6	5	156.81	5.058	0.0101	1	1	39.56						SecretomeP	no	yes		
ENSMUSP00000034834	**Pkm**	1.298	0.4855	31	3	2388.96	7.043	0.0021	42	1	3161.47						SignalP	no	yes		
ENSMUSP00000128770	**Pkm**	0.386	0.0455	31	3	2234.14	4.145	0.0067	47	6	3607.31	3.354	0.0033	43	43	2471.44	SignalP	no	yes		
ENSMUSP00000102724	**Plaa**	0.699	0.3679	5	5	228.01						34.556	0.0055	1	1	15.14	SecretomeP	no	yes		
ENSMUSP00000014578	**Plg**	1.422	0.3260	1	1	32.46	0.626	0.2834	1	1	17.31	0.136	0.0342	1	1	14.36	SignalP	yes	yes		
ENSMUSP00000072773	**Postn**	3.341	0.0526	24	23	1790.18	0.249	0.0790	1	1	54.87						SignalP	yes	yes		
ENSMUSP00000015100	**Ppp1cb**	0.562	0.3125	5	1	207.69	1.188	0.6299	6	6	214.72	3.508	0.0002	2	2	97.33	SecretomeP	no	yes		
ENSMUSP00000007708	**Ppp2r1a**	0.804	0.5736	5	4	194.26	3.328	0.0039	9	9	399.77	4.799	0.0092	4	4	171.79	SecretomeP	no	yes		
ENSMUSP00000086640	**Ppp2r2a**	0.376	0.0148	2	1	71.52						9.384	0.0148	2	2	58.25	SecretomeP	no	yes		
ENSMUSP00000099944	**Ppp3r1**	0.673	0.0880	1	1	82.17	4.661	0.0020	2	2	87.50						SecretomeP	no	yes		
ENSMUSP00000102078	**Prdx1**	0.900	0.8566	12	11	500.50	4.097	0.0009	10	10	503.61	2.881	0.0030	6	6	225.21	SecretomeP	no	yes		
ENSMUSP00000005292	**Prdx2**	1.069	0.6894	5	5	310.79	5.250	0.0020	6	5	345.97	3.567	0.0007	4	4	184.45	SecretomeP	no	yes	3.1813	0.123
ENSMUSP00000025961	**Prdx3**	1.161	0.4757	6	5	195.73	2.886	0.0067	2	2	52.63	2.067	0.1050	3	3	76.73	SecretomeP	no	yes	29.4366	0.006
ENSMUSP00000025904	**Prdx5**	1.197	0.2749	4	3	182.04	6.768	0.0013	4	4	159.63	1.774	0.2038	1	1	13.68	SecretomeP	no	yes		
ENSMUSP00000097444	**Prep**	0.738	0.0637	14	14	770.28	4.106	0.0040	13	13	722.41	3.563	0.0052	4	4	165.14	SecretomeP	no	yes	30.7783	0
ENSMUSP00000056500	**Prkar1a**	0.683	0.4116	2	2	55.21						7.530	0.0028	1	1	32.24	SecretomeP	no	yes		
ENSMUSP00000035220	**Prkar2a**	0.771	0.4835	1	1	41.87	6.442	0.0009	5	5	267.54	3.078	0.0004	3	3	159.01	SecretomeP	no	yes		
ENSMUSP00000023629	**Pros1**	0.551	0.0034	4	4	166.15	0.559	0.3677	1	1	41.54						SignalP	yes	yes		
ENSMUSP00000031910	**Prss1**	0.314	0.0926	1	1	23.21	1.134	0.4400	1	1	22.48	0.432	0.0026	3	1	63.49	SignalP	yes	yes		
ENSMUSP00000015855	**Prune**	0.797	0.6688	2	2	60.07						1.938	0.0609	1	1	36.68	SecretomeP	no	yes		
ENSMUSP00000005923	**Psmb4**	0.341	0.0088	5	5	317.17	4.725	0.0039	3	3	141.90						SecretomeP	no	yes		
ENSMUSP00000022803	**Psmb5**	0.320	0.0205	4	4	236.99	5.520	0.0020	5	4	282.69						SecretomeP	no	yes		
ENSMUSP00000018430	**Psmb6**	0.304	0.0205	4	4	221.67	8.676	0.0071	3	3	167.30						SecretomeP	no	yes		
ENSMUSP00000028083	**Psmb7**	0.326	0.0322	5	4	228.14	7.247	0.0011	1	1	60.26						SecretomeP	no	yes		
ENSMUSP00000021595	**Psmc1**	0.671	0.3398	1	1	83.11						7.012	0.0016	3	3	220.01	SecretomeP	no	yes		
ENSMUSP00000032824	**Psmc4**	1.550	0.1448	1	1	135.73						6.133	0.0021	2	2	68.10	SecretomeP	no	yes		
ENSMUSP00000022380	**Psmc6**	0.907	0.8506	5	5	159.47						3.066	0.0006	1	1	23.33	SecretomeP	no	yes		
ENSMUSP00000026560	**Psmd13**	1.060	0.7633	3	3	56.81						5.282	0.0008	2	2	79.40	SecretomeP	no	yes		
ENSMUSP00000098295	**Psmd9**	0.655	0.0900	4	4	142.27	18.107	0.0565	1	1	22.40						SecretomeP	no	yes		
ENSMUSP00000050292	**Ptges3**	1.461	0.3098	4	4	146.13						9.305	0.0120	1	1	15.14	SecretomeP	no	yes		
ENSMUSP00000058321	**Ptrf**	1.282	0.2831	3	2	154.68						1.897	0.0084	9	9	465.25	SecretomeP	no	yes		
ENSMUSP00000113703	**Pxdn**	1.639	0.1230	28	27	1468.12	0.496	0.0179	15	15	703.68	0.364	0.0237	11	11	442.80	SignalP	yes	yes		
ENSMUSP00000032510	**Pzp**	0.487	0.1425	1	1	44.76	0.332	0.0227	1	1	57.36	0.127	0.0094	1	1	25.85	SignalP	no	yes		
ENSMUSP00000018156	**Rac3**	0.412	0.0304	1	1	28.64						4.055	0.0317	1	1	43.14	SecretomeP	no	yes		
ENSMUSP00000066238	**Rap1b**	1.597	0.0524	1	1	14.68						5.643	0.0043	1	1	63.78	SecretomeP	no	yes		
ENSMUSP00000006128	**Rcn1**	0.972	0.8715	6	6	207.39	0.357	0.1569	1	1	34.35						SignalP	yes	yes		
ENSMUSP00000002303	**Rhoc**	1.425	0.9080	2	1	39.41						1.481	0.0993	1	1	31.90	SecretomeP	no	yes		
ENSMUSP00000101651	**Rnh1**	0.809	0.2012	14	13	677.55	3.607	0.0219	8	7	499.51	2.646	0.0346	3	3	153.11	SecretomeP	no	yes		
ENSMUSP00000008826	**Rpl10**	1.680	0.1953	2	1	152.61						0.722	0.2022	1	1	76.68	SecretomeP	no	yes		
ENSMUSP00000048469	**Rpl10a**	0.846	0.4024	3	3	167.81	1.260	0.7170	1	1	30.22	1.694	0.0048	2	2	45.40	SecretomeP	no	yes	2.37	0.154
ENSMUSP00000115722	**Rpl13a**	1.798	0.1326	3	3	69.99						2.209	0.0250	1	1	15.33	SecretomeP	no	yes		
ENSMUSP00000073581	**Rps12**	1.819	0.0041	6	6	235.49						7.731	0.0962	1	1	37.64	SecretomeP	no	yes	27.47	0.004
ENSMUSP00000025511	**Rps14**	0.875	0.6602	2	2	112.32						1.956	0.1575	2	2	36.73	SecretomeP	no	yes	2.0102	0.18
ENSMUSP00000069004	**Rps15**	3.305	0.0243	1	1	16.26						4.832	0.0131	1	1	44.46	SecretomeP	no	yes		
ENSMUSP00000102198	**Rps15a**	1.869	0.1023	4	4	127.81						3.472	0.0049	2	2	56.78	SecretomeP	no	yes	2.4596	0.152
ENSMUSP00000103940	**Rps16**	2.559	0.0046	1	1	44.76						2.511	0.1171	1	1	26.05	SignalP	no	yes		
ENSMUSP00000079628	**Rps17**	1.151	0.6061	2	2	181.56						2.508	0.0287	2	2	70.91	SecretomeP	no	yes		
ENSMUSP00000092502	**Rps2**	2.067	0.0327	5	5	163.52						4.385	0.0051	2	2	45.87	SecretomeP	no	yes		
ENSMUSP00000120528	**Rps20**	1.878	0.0764	3	3	128.61						16.160	0.0351	1	1	36.05	SecretomeP	no	yes		
ENSMUSP00000099908	**Rps27a**	2.338	0.0976	5	1	221.23						2.779	0.0015	3	3	104.50	SecretomeP	no	yes		
ENSMUSP00000029722	**Rps3a1**	2.179	0.0376	3	3	138.42						2.353	0.0234	1	1	67.78	SignalP	no	yes		
ENSMUSP00000004554	**Rps5**	1.689	0.0179	4	4	185.68	2.116	0.1873	1	1	39.27	2.640	0.0027	1	1	83.94	SecretomeP	no	yes		
ENSMUSP00000073880	**Rps7**	3.116	0.0167	3	3	76.64						15.799	0.0540	1	1	13.25	SecretomeP	no	yes		
ENSMUSP00000035105	**Rpsa**	1.460	0.2109	6	5	350.79	2.362	0.0455	4	4	142.40	2.355	0.0406	1	1	67.06	SecretomeP	no	yes		
ENSMUSP00000028059	**Rsu1**	1.753	0.1365	3	3	74.40	7.731	0.0007	3	3	50.63						SecretomeP	no	yes		
ENSMUSP00000047737	**S100a13**	0.359	0.0257	3	3	107.45	21.342	0.0008	2	2	44.43						SecretomeP	yes	yes		
ENSMUSP00000068971	**Serpinc1**	0.729	0.9278	1	1	60.18	0.477	0.0782	5	5	229.34	0.429	0.0082	2	2	51.39	SignalP	yes	yes		
ENSMUSP00000000769	**Serpinf1**	1.207	0.9611	19	16	1353.18	0.396	0.0420	2	2	114.39	0.290	0.0213	2	2	85.19	SignalP	yes	yes		
ENSMUSP00000091706	**Serpinh1**	1.774	0.0924	5	5	238.61	0.451	0.0011	1	1	36.83	0.541	0.0676	3	3	95.44	SignalP	yes	yes		

ENSMUSP00000005067	**Sgta**	0.667	0.1227	4	4	242.98						22.373	0.0262	1	1	31.97	SecretomeP	no	yes		
ENSMUSP00000038744	**Skp1a**	0.825	0.1960	6	5	125.89	9.165	0.0000	4	4	180.33	6.578	0.0724	1	1	48.99	SecretomeP	no	yes		
ENSMUSP00000048522	**Smpx**	0.588	0.3292	1	1	73.45	103.344	0.0086	1	1	25.72						SecretomeP	no	yes		
ENSMUSP00000073911	**Smyd1**	0.991	0.8172	1	1	16.64	0.583	0.0948	1	1	21.28	2.532	0.0260	5	5	234.92	SecretomeP	no	yes		
ENSMUSP00000023707	**Sod1**	0.840	0.6981	5	4	291.90	4.541	0.0027	5	4	365.45	10.843	0.0027	5	5	177.71	SecretomeP	no	yes	5.9256	0.046
ENSMUSP00000018737	**Sparc**	1.056	0.8613	13	5	1255.08	0.371	0.0001	7	7	221.49	0.108	0.0015	4	4	105.31	SignalP	yes	yes		
ENSMUSP00000023161	**Srl**	0.829	0.3555	5	5	153.96	0.156	0.0052	2	1	50.12	1.805	0.0821	17	17	866.74	SignalP	yes	yes		
ENSMUSP00000023039	**St13**	1.144	0.6053	5	5	282.92	0.516	0.1545	3	3	143.73	0.369	0.2328	1	1	23.20	SecretomeP	no	yes		
ENSMUSP00000052942	**Sugt1**	0.382	0.1648	1	1	59.44						4.989	0.0138	1	1	66.93	SecretomeP	no	yes		
ENSMUSP00000006254	**Tbcb**	1.131	0.8013	1	1	42.99	25.973	0.0002	1	1	36.95						SecretomeP	no	yes		
ENSMUSP00000044903	**Thbs1**	2.063	0.0535	30	27	1414.39	0.319	0.0206	5	5	182.51	0.144	0.0691	3	3	117.25	SignalP	yes	yes		
ENSMUSP00000099384	**Tnnc2**	0.904	0.8444	7	6	426.04	3.973	0.0003	13	13	1028.42	1.737	0.1102	14	14	836.38	SecretomeP	no	yes		
ENSMUSP00000119848	**Tnni1**	1.489	0.2475	7	7	243.57	1.569	0.1295	3	3	183.95	1.104	0.6442	6	6	208.68	SecretomeP	no	yes		
ENSMUSP00000101591	**Tnni2**	1.071	0.7061	5	4	204.35	4.135	0.0003	10	10	473.20	3.356	0.0053	9	9	326.85	SecretomeP	no	yes		
ENSMUSP00000109315	**Tpm1**	0.638	0.1508	19	1	870.18	4.522	0.0000	17	5	841.01	1.888	0.1055	24	10	967.90	SecretomeP	no	yes		
ENSMUSP00000014990	**Tppp3**	1.741	0.1747	3	3	149.29	4.953	0.0004	4	4	155.26						SecretomeP	no	yes		
ENSMUSP00000035158	**Trf**	1.160	0.6131	4	2	60.18	0.523	0.1921	1	1	22.43	0.278	0.2596	1	1	20.45	SignalP	yes	yes		
ENSMUSP00000049243	**Tspan8**	0.316	0.7277	1	1	91.64						7.225	0.2858	1	1	41.86	SignalP	no	yes		
ENSMUSP00000078429	**Tuba4a**	0.906	0.8119	13	2	785.80	0.409	0.0463	5	2	233.93	3.635	0.0024	6	2	276.73	SecretomeP	no	yes		
ENSMUSP00000042342	**Tubb4b**	0.809	0.8166	13	1	877.18	0.517	0.1372	6	6	242.93	3.822	0.0012	12	1	522.16	SecretomeP	no	yes		
ENSMUSP00000030051	**Txn1**	0.958	0.8815	3	2	207.75	4.237	0.0011	2	2	166.95						SecretomeP	yes	yes		
ENSMUSP00000001989	**Uba1**	0.961	0.9893	17	17	959.18	0.712	0.4156	4	4	146.71	3.509	0.0029	11	11	481.76	SecretomeP	no	yes		
ENSMUSP00000087658	**Ube2l3**	0.879	0.4982	3	3	102.38	4.443	0.0092	4	4	268.02						SecretomeP	no	yes		
ENSMUSP00000005714	**Ube2m**	1.167	0.7152	1	1	14.59	20.092	0.0001	3	3	78.96						SecretomeP	no	yes		
ENSMUSP00000096932	**Ube2n**	0.893	0.8023	4	3	150.06	6.809	0.0007	2	2	54.93	5.004	0.0008	2	2	42.46	SecretomeP	no	yes		
ENSMUSP00000104830	**Ube2v1**	0.792	0.6752	4	3	197.17	9.906	0.0054	5	2	235.14	7.587	0.0006	1	1	46.01	SecretomeP	no	yes		
ENSMUSP00000002289	**Uchl3**	0.703	0.3862	4	4	246.60	3.651	0.0107	2	2	101.92						SecretomeP	no	yes		
ENSMUSP00000026743	**Uqcrc1**	1.678	0.3293	1	1	38.78						3.180	0.0158	7	7	284.47	SecretomeP	no	yes	42.6144	0
ENSMUSP00000045284	**Uqcrfs1**	1.407	0.4829	1	1	28.20						3.360	0.0062	2	2	59.83	SecretomeP	no	yes	41.8598	0
ENSMUSP00000089728	**Usp14**	0.837	0.9142	4	3	129.48	2.825	0.0316	2	2	63.15	2.418	0.0165	1	1	33.12	SecretomeP	no	yes		
ENSMUSP00000020673	**Vdac1**	1.521	0.4239	2	2	71.83						7.312	0.0002	5	4	224.82	SignalP	no	yes	28.1988	0.004
ENSMUSP00000022293	**Vdac2**	1.602	0.3248	2	2	141.28						7.111	0.0010	3	3	145.89	SecretomeP	no	yes	25.489	0.003
ENSMUSP00000028062	**Vim**	1.061	0.7652	30	22	2170.82	0.759	0.3357	18	14	847.47	0.256	0.0160	23	18	969.73	SecretomeP	no	yes		
ENSMUSP00000113345	**Vps29**	0.607	0.7495	1	1	31.26	5.865	0.0152	1	1	13.60						SecretomeP	no	yes		
ENSMUSP00000001544	**Vwa5a**	0.779	0.5643	3	3	146.81	166.270	0.0018	1	1	29.96						SecretomeP	no	yes		
ENSMUSP00000070946	**Xpnpep1**	0.676	0.1648	5	5	184.46	6.437	0.0069	3	3	84.53						SecretomeP	no	yes		
ENSMUSP00000020538	**Xpo1**	0.781	0.5279	1	1	14.76	5.020	0.0019	2	1	57.55						SecretomeP	no	yes		
ENSMUSP00000001365	**Yars**	1.034	0.7937	7	5	190.45	1.778	0.0281	1	1	36.80						SecretomeP	no	yes		
ENSMUSP00000032309	**Ybx3**	0.993	0.7944	8	5	471.56	17.618	0.0010	3	3	142.32	2.247	0.1724	2	2	63.22	SecretomeP	no	yes		

Appendix

List of Figures

List of Tables

Acknowledgements

I would like to thank Prof. Dr. Matthias Tschöp for being my supervisor and giving me the opportunity to work on my PhD project at his institute, Prof. Dr. Martin Klingenspor for supervising this thesis project and Dr. Martin Jastroch for being my supervisor and mentor throughout the project. Further, I would like to thank Dr. Stefanie Hauck and Dr. Christine von Törne for performing the mass spectrometric analyses for this project and for their advice, and Daniel Lamp for isolation of primary muscle fibers as well as his general help in the lab, Dr. Susanne Keipert for her scientific input and support, Maria Kutschke for her assistance in the lab, Prof. Dr. Richard DiMarchi and his team for providing synthesized Irisin and Cox6b1, and the HELENA graduate school for funding my PhD. Further, I would like to thank Michaela Bauer, Dr. Sara Brandt, Dr. Christoffer Clemmensen, Dr. Brian Finan, Ingrid Fischer, Dr. Simone Hausmann, Uma Kabra, Dr. Petra Kotzbeck, Dr. Beata Legutko, Dr. Dominik Lutter, Dr. Carola Meyer, Dr. Timo Müller, Christina Neff, Katrin Pfuhlmann, Ines Pramme, Dr. Sonja Schriever, Lisa Suwandhi, Elma Stapic, Dr. Siegfried Ussar, Marina Wimmer, and Dr. Fabio Zani. Last but not least, I thank my parents, my brothers, Dani, Tanja, and Basti!